REACTIVE OXYGEN SPECIES AND TRANSIENT RECEPTOR POTENTIAL CATION CHANNEL VANILLOID 1 (TRPV1) AS MEDIATORS OF WALLERIAN DEGENERATION

by

Bradley James Kievit

B.Sc., The University of Calgary, 2016

A THESIS SUBMITTED IN PARTIAL FUFILLMENT OF

THE REQUIREMENTS FOR THE DEGREE OF

MASTER OF SCIENCE

in

THE COLLEGE OF GRADUATE STUDIES

(Biology)

THE UNIVERSITY OF BRITISH COLUMBIA

(Okanagan)

January 2019

The following individuals certify that they have read, and recommend to the College of Graduate Studies for acceptance, a thesis/dissertation entitled:

REACTIVE OXYGEN SPECIES AND TRANSIENT RECEPTOR POTENTIAL CATION CHANNEL VANILLOID 1 (TRPV1) AS MEDIATORS OF WALLERIAN DEGENERATION

submitted by Bradley James Kievit in partial fulfillment of the requirements of

the degree of Master of Science.

Dr. Philip Barker, Biology, Irving K. Barker School of Arts and Sciences

Supervisor

Dr. Andis Klegeris, Biology, Irving K. Barker School of Arts and Sciences

Supervisory Committee Member

Dr. Frederic Menard, Chemistry, Irving K. Barker School of Arts and Sciences

Supervisory Committee Member

Dr. Miranda Hart, Biology, Irving K. Barker School of Arts and Sciences

University Examiner

Dr. Cheryl Wellington, Faculty of Medicine

External Examiner

Abstract

Axons that are physically separated from their cell soma undergo degradation through a process termed "Wallerian degeneration" (WD). This process, typically induced by acute injury, was initially thought to occur as a result of axons passively "wasting away" since they are no longer receiving nutrient supply from the soma. However, subsequent discoveries revealed that axons degenerate by activation of a prodegenerative signalling pathway and that inhibition of key elements of this pathway can protect axons. Furthermore, inhibiting WD in various disease models such as glaucoma, Parkinson's disease and motor neuron disease protects axons from degeneration. One key element of WD is an intra-axonal calcium rise that occurs just before axons begin to fragment. Preventing this calcium rise delays the onset of axon fragmentation. To date, the full complement of ion channels responsible for this calcium influx have not been identified. Furthermore, the mechanism by which these calcium channels are activated is unknown. WD can be modeled *in vitro* by transecting axons of dorsal root ganglia (DRG), which separates them from their soma. We have used this model along with the Ca^{2+} sensor dye Fluo-4-AM to show that Ca^{2+} influx is reduced in axons treated with capsazepine (CPZ), an antagonist of the transient receptor potential cation channel vanilloid 1 (TRPV1), as well as in *Trpv1*$^{-/-}$ axons. Furthermore, CPZ-treated sensory neurons and DRGs of a *Trpv1*$^{-/-}$ background were partially rescued from degeneration after transection, indicating a prodegenerative role for TRPV1. We found that reactive oxygen species (ROS) mediate the activation of TRPV1 in this setting and, consistent with this, ROS-scavengers abolished Ca^{2+} influx in transected axons. Furthermore, we found that mitochondrial depolarization, a phenomenon that is known to occur during WD, triggers a ROS-dependent calcium influx through TRPV1 when initiated by the mitochondrial poison carbonyl cyanide m-chlorophenyl hydrazine (CCCP). CCCP also induces degeneration in cultured sensory

neurons but is protected by Ca^{2+} chelation, ROS scavenging and inhibition of TRPV1 with CPZ. This thesis shows for the first time that TRPV1 is involved in WD and suggests that mitochondrial ROS are responsible for initiating calcium rise by sensitization of calcium channels.

Lay Summary

Axons are threadlike projections from neurons used for signalling with other cells. When axons are physically separated from their cell body, they degrade by a process called “Wallerian degeneration” (WD). WD is an active process therefore it requires activation of various signals within the axon for degeneration to occur. One of these signals is a rise in the concentration of calcium in the axons just before fragmentation. If this calcium is removed, then degeneration is delayed. Calcium has been found to enter axons through channels bound to the plasma membrane however only a few of these channels have been identified. Furthermore, the mechanism by which these channels are activated, which thereby allows calcium to pass through them, is unknown. In this thesis, I showed that a specific calcium channel, termed TRPV1, is responsible for some of this calcium influx and I determine a mechanism by which it is activated.

Preface

I conducted the research presented in this thesis, including all experimental data, analysis and writing. Genevieve Dorval and Svetlana Simtchouk performed molecular cloning and mutagenesis of TRPV1-GECO constructs. Aaron Johnstone contributed essential discussions. Julien Gibon and Philip Barker contributed essential discussions, provided direction for experiments and edits to text.

All animal use was approved by UBC Animal Care Committee (protocol # A16-0138).

Table of Contents

List of Figures

List of Abbreviations

ADP	= adenosine diphosphate
ADPR	= adenosine diphosphate ribose
AM	= acetylmethoxyester
ANOVA	= analysis of variance
AP-1	= activator protein 1
ATP	= adenosine triphosphate
Bax	= Bcl-2-associated X protein
Bak	= Bcl-2 homologous antagonist/killer
Bcl-2	= B-cell lymphoma 2
cADPR	= cyclic adenosine diphosphate ribose
Cap	= capsaicin
CCCP	= carbonyl cyanide m-chlorophenyl hydrazine
CNS	= central nervous system
CPZ	= capsazepine
CRMP2	= collapsin response mediator protein 2
DAG	= diacylglycerol
DLK	= dual leucine zipper kinase
DMEM	= Dulbecco's modified eagle serum
DMSO	= dimethyl sulfoxide
DPI	= diphenyleneiodonium
DRG	= dorsal root ganglia
Duox	= dual oxidase

ect4 = ectoderm-expressed 4

EDTA = ethylenediaminetetraacetic acid

EGFR = epidermal growth factor receptor

EGTA = ethylene glycol-bis(β-aminoethyl ether)-N,N,N’,N’-tetraacetic acid

ER = endoplasmic reticulum

ETC = electron transport chain

FBS = fetal bovine serum

FDU = 5-fluoro-2’-deoxyuridine

FIJI = Fiji is just ImageJ

GECO = genetically-encoded calcium indicator for optical imaging

GSK3β = glycogen synthase kinase-3β

HEK = human embryonic kidney

HBSS = Hank’s balanced salt solution

HEPES = 4-(2-hydroxyethyl)-1-piperazineethanesulfonic acid

HSV = herpes simplex virus

IMM = inner mitochondrial membrane

IP_3R = inositol triphosphate receptor

JNK = c-jun N-terminal kinase

MAPK = mitogen activated protein kinase

MAPKK = mitogen activated protein kinase kinase

MAP3K = mitogen activated protein kinase kinase kinase

MKK = mitogen activated protein kinase kinase

MOI = multiplicity of infection

mPTP = mitochondrial permeability transition pore

NAC = N-acetyl-L-cysteine

NAD^+/NADH = nicotinamide adenine dinucleotide

$NADP^+$/NADPH = nicotinamide adenine dinucleotide phosphate

Nam = nicotinamide

NCX = Na^+/Ca^{2+} exchanger

NGF = nerve growth factor

Nif = nifedipine

NMN = nicotinamide mononucleotide

NMNAT = nicotinamide mononucleotide adenylyltransferase

Nox = NADPH oxidase

PARP = poly-ADP-ribose polymerase

PBS = phosphate buffered saline

PDL = poly-D-lysine

PFA = paraformaldehyde

PKC = protein kinase C

PNS = peripheral nervous system

PMA = phorbol 12-myristate 13-acetate

P/S = penicillin-streptomycin

R-GECO = red GECO

RIRR = ROS-induced ROS release

ROI = region of interest

RNA = ribonucleic acid

RNAi = RNA interference

roGFP = reduction-oxidation sensitive green fluorescent protein

ROS = reactive oxygen species

RyR = ryanodine receptor

SAM = sterile alpha motif

SARM1 = sterile alpha and toll/interleukin receptor motif-containing 1

SCG10 = superior cervical ganglion 10

SEM = standard error of the mean

shRNA = short hairpin RNA

siRNA = small interfering RNA

TBS-T = tris-buffered saline – Tween 20

TIR = toll/interleukin receptor

TLR = toll-like receptor

TMRE = tetramethylrhodamine ethyl ester

Tm1Jul = targeted mutation 1, David Julius

TrkA = tropomyosin receptor kinase A

TRP = transient receptor potential

TRPA1 = transient receptor potential cation channel ankyrin 1

TRPM8 = transient receptor potential cation channel menthol 8

TRPV1 = transient receptor potential cation channel vanilloid 1

UBE4B = ubiquitin conjugation factor E4 B

WD = Wallerian degeneration

WldS = Wallerian degeneration slow

ZNRF1 = zinc and ring finger 1

Acknowledgements

I would sincerely like to thank Dr. Phil Barker for guiding and supervising my thesis work. I thank you for not giving up on me, even though I'm sure at times it would have been very easy to do so. You have been a steady supply of help and encouragement, but you have also pushed me to fight my own battles and it is in these moments that I really think I learned the most. I am extremely fortunate to have been granted this opportunity to work with you and it was an experience that I will look back on fondly. I would also like to the members of my supervisory committee, Dr. Andis Klegeris and Dr. Frederic Menard for very helpful suggestions and thoughtful dialogue in meetings that I am grateful to have had.

I thank Dr. Julien Gibon for truly rising above and beyond in all of the help that he has provided me and the lab as a whole. I really appreciate the meaningful discussions that we have had and the optimistic demeanor that you maintain; it has kept me sane more times than I can count. I would also like to thank Dr. Aaron Johnstone for everything that he has taught me in the areas of dissection, cell culture, microscopy, image analysis and science in general. You showed me the value of not cutting corners or settling for "good enough" and without you, I wouldn't have any data to write a thesis about.

Lastly, I would like to thank my family. To my parents, thank you for putting a roof over my head and food in my stomach over these last years. Your love and support has set me straight and has helped me make it through. To my sister, thank you loving me and making me laugh after long nights of work. And to Laura Hulstein, I don't even know what I can say. Without you, I wouldn't have made it to this point. Thank you for your unwavering love, your continuous patience, your uplifting encouragement and your endless sacrifice. You have contributed more to this thesis than you can possibly imagine.

For my parents and my fiancé,

Chapter 1: Introduction

1.1. Wallerian Degeneration (WD)

Neurons are unique cells for many reasons. One of which is that they possess protrusions called axons that can extend upwards of one meter in humans. These are attached to cell bodies that are only 10 - 50 μm in diameter, giving a cell body to axon length ratio of 1:20,000 – 1:100,000[1]. This makes axons especially susceptible to damage by any number of phenomena such as nerve transection, crush or stretch. Since adult neurons are non-dividing by nature, these events lead to axon degeneration which can cause permanent disability to an organism. Axon loss is prominent in a number of neurological disorders including hereditary and acquired neuropathies[2,3], Alzheimer's disease[4], Parkinson's disease[5], amyotrophic lateral sclerosis[6], multiple sclerosis[7] and traumatic brain injury[8]. This suggests a prominent role for axonal degeneration in many diseases and stopping or even delaying axon destruction may provide therapeutic benefit in treating a diverse range of pathologies.

The degeneration of damaged axons was first observed and documented over 150 years ago by Augustus Volney Waller[9] and was termed "Wallerian degeneration" (WD). Wallerian degeneration pertains to the auto-destruction of axons that is typically induced by acute injury. This is both functionally and biochemically different from other forms of neurite loss such as those that occur during embryonic development. The intracellular pathways and mechanisms employed in axons undergoing WD remains uncertain.

1.1.1. Wallerian degeneration slow (WldS) and nicotinamide adenine dinucleotide (NAD^+)

During Wallerian degeneration, it was thought that the cut axons passively "wasted away" as they no longer received nutrient supply from the soma. This idea was challenged when Lunn and colleagues came upon the "Wallerian Degeneration Slow" (WldS) mouse that possesses an autosomal dominant allele causing a profound delay in Wallerian degeneration[10]. WldS mice that undergo sciatic nerve transection maintained distal axon structure and function up to two weeks after the transection event whereas distal axons in wildtype mice lasted no longer than two days (Figure 1.1)[10,11]. This discovery revolutionized the understanding of axon degeneration at the time because it indicated that axons undergo an active form of degeneration that can be altered by genetic manipulation. The *WldS* gene has since been demonstrated to protect axons from degeneration in disease models such as glaucoma[12], Parkinson's disease[13] and motor neuron disease[14], associating the WldS gene product and Wallerian degeneration with neurological disorders that involve axon loss.

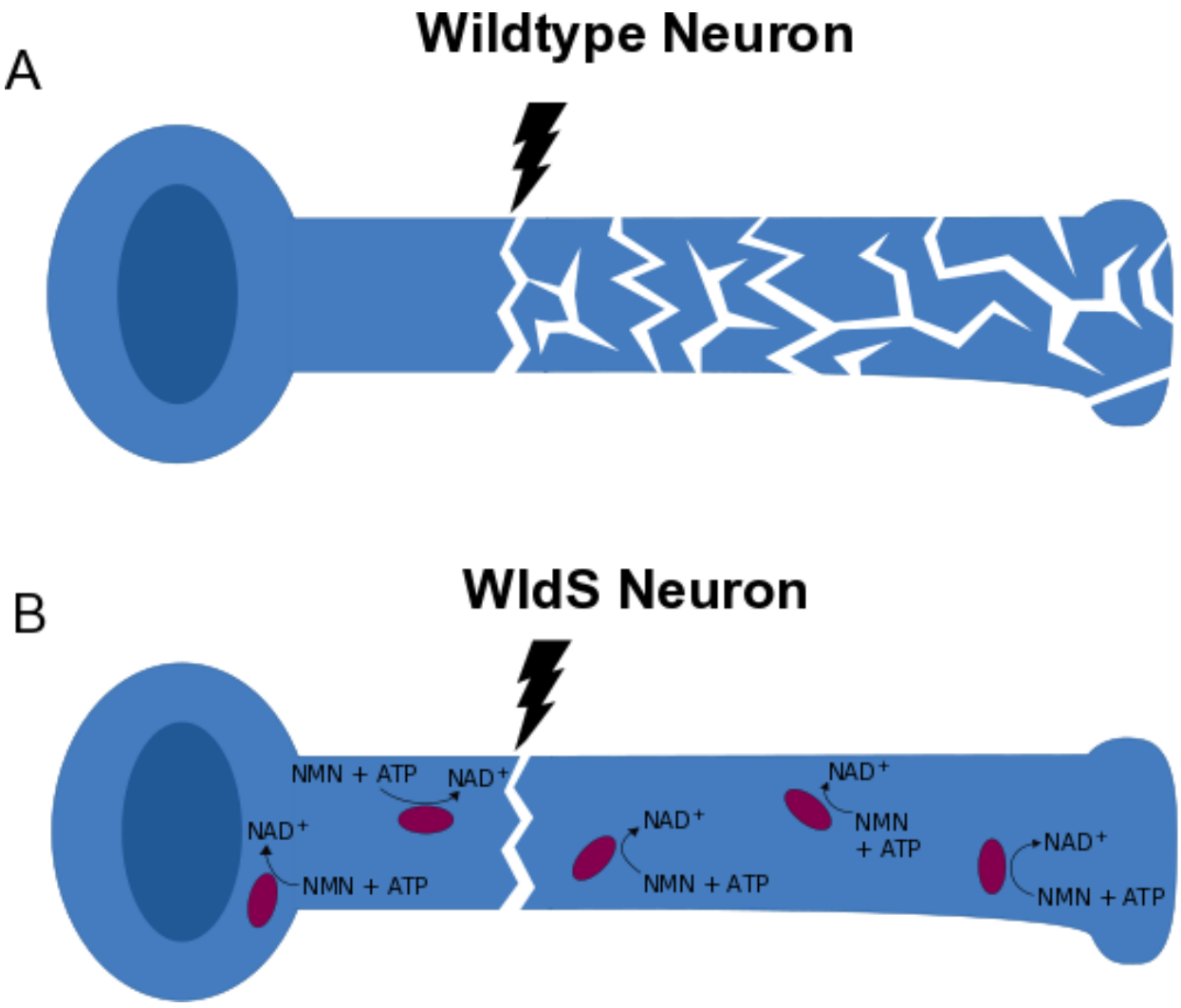

Figure 1.1. The effect of nerve transection in wildtype and WldS neurons. Wildtype neurons that undergo axotomy experience a loss of function and structure (A). Neurons expressing the mutant WldS protein show profound protection for upwards of weeks by providing newly synthesized NAD^+ (B). NAD^+ = nicotinamide adenine dinucleotide, NMN = nicotinamide mononucleotide, ATP = adenine triphosphate.

The *WldS* gene consists of a chimeric fusion protein containing the nicotinamide adenine dinucleotide (NAD^+) synthesizing enzyme, nicotinamide mononucleotide adenylyltransferase (NMNAT1), which produces NAD^+ from nicotinamide mononucleotide (NMN) and ATP (Figure

1.1B), and a fragment of the ubiquitination factor UBE4B[15]. The current understanding of the function of this mutant protein with respect to axon protection is that it aberrantly localizes NMNAT1, normally a nuclear NMNAT isoform, to the axon where it remains active. This has been supported by the finding that exogenous overexpression of WldS, NMNAT1, or other NAD^+-synthesizing isoforms, in the axonal compartment causes WldS-like axon protection after axotomy[16,17]. This form of axon protection after injury is evolutionarily conserved as NMNAT enzymatic activity within the WldS protein can also delay axon degeneration in *Drosophila*[18]. Since NMNAT1 is not normally expressed in axons, the WldS protein appears to function as a gain of function allele for the axonal protein, NMNAT2. In healthy neurons, NMNAT2 undergoes constitutive proteasomal degradation and is replenished by continual anterograde transport of newly synthesized NMNAT2 from the soma[19]. After acute nerve injury, NMNAT2 levels are rapidly depleted because the connection to the cell body is lost (Figure 1.2). In the WldS mouse, ectopic NAD^+-synthesizing activity via WldS in the axon is able to maintain NMNAT functionality in the separated axon[19].

NAD^+ is a ubiquitous metabolite that serves important roles in cell signaling and energy metabolism[20]. NAD^+ consists of an adenine nucleotide connected to a nicotinamide-ribose moiety by two phosphate groups. After it has donated an electron to the electron transport chain in mitochondria (NADH → NAD^+), NAD^+ is considered a cation due to the charge on a key nitrogen atom. However, NAD^+ is actually anionic while the reduced NADH has a net charge of "-2". Besides its canonical role as an energy substrate in glycolysis and the electron transport chain, NAD^+ donates its ADP-ribose moiety to proteins in a posttranslational modification termed ADP-ribosylation. Poly(ADP-ribose) structures have prominent regulatory roles in processes such as DNA repair and telomere maintenance. Inhibition of the catalyzing poly-ADP-ribose polymerase

(PARP) enzyme has shown promise in treatment of various cancers as well as stroke, myocardial infarction and neurological conditions such as Parkinson's disease[21]. NAD^+ also serves as a precursor for cyclic ADP-ribose (cADPR), a molecule that regulates intracellular Ca^{2+} levels[22].

NAD^+ levels do not rise after axotomy in WldS axons indicating that the NMNAT-dependent protection of axons does not result from an increase in steady state levels of NAD^+[23,24]. Rather, available data suggests that NMNAT2 is rapidly depleted after acute injury and a resulting NAD^+ drop leads to energetic failure in wildtype axons (Figure 1.2). In this scheme, WldS acts as a gain of function mutation that prevents this drop. Consistent with this model, NAD^+ levels plummet in transected axons but supplementation with NAD^+ or overexpression of NMNAT preserves the axon[25].

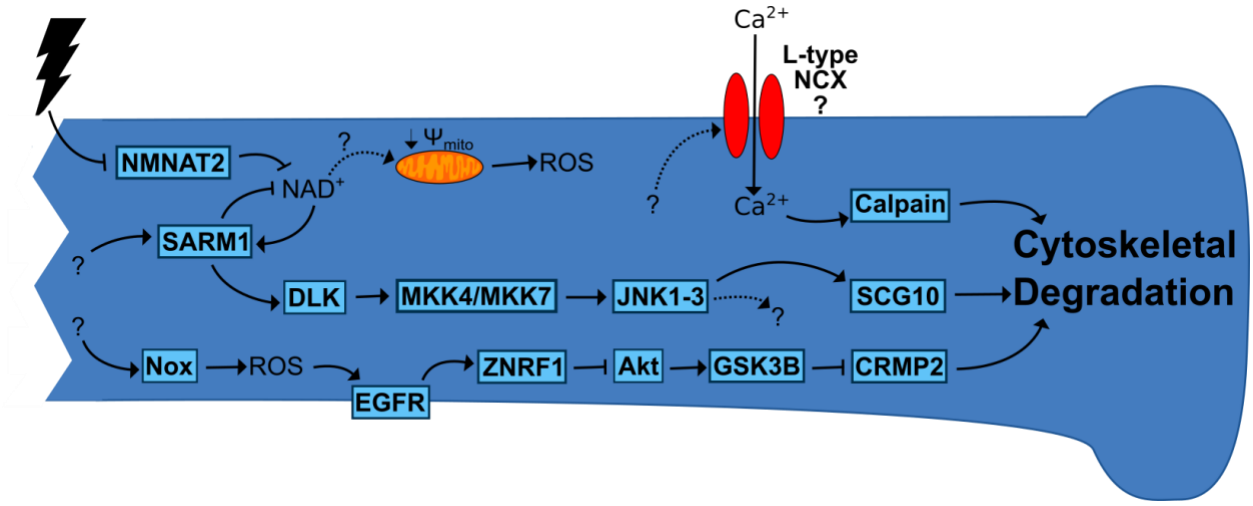

Figure 1.2. The initiators of Wallerian degeneration. Upon axon transection, NMNAT2 can no longer be supplied to axons and NAD^+ can therefore no longer be replenished. SARM1 is also dimerized and activated, possibly from an initial NAD^+ drop, causing enzymatic depletion of NAD^+. The exact mechanism of SARM1 activation is unknown in WD. SARM1 activation also triggers the DLK pathway which culminates in SCG10 activation and likely other undiscovered targets. Mitochondrial failure is also observed which releases ROS into the axoplasm. This has been hypothesized to occurs as a result of NAD^+ loss however no definitive mechanism has been established. Ca^{2+} influx occurs through a suite of channels such as the Na^+ - Ca^{2+} exchanger and L-type channels and causes downstream calpain activation. Other channels are likely activated as well. The mechanism by which calcium influx is initiated is unknown. The Nox complex is also activated via unknown mechanisms to trigger another degenerative pathway which culminates in CRMP2 deactivation. Altogether, calpain activation, SCG10 activation and CRMP2 loss cause a loss of cytoskeletal stability and structure, contributing to axon fragmentation. NMNAT2 = nicotinamide mononucleotide adenylyltransferase 2, NAD^+ = nicotinamide adenine dinucleotide, SARM1 = sterile alpha and TIR motif-containing 1, ROS = reactive oxygen species, NCX = Na^+/Ca^{2+} exchanger, DLK = dual leucine zipper kinase, MKK = mitogen activated protein kinase kinase, JNK1-3 = c-jun n-terminal kinase 1-3, SCG10 = superior cervical ganglion 10, Nox = NADPH oxidase, EGFR = epidermal growth factor receptor, ZNRF1 = zinc and ring finger 1, GSK3B = glycogen synthase kinase-3B, CRMP2 = collapsing response mediator protein 2.

1.1.2. Sterile alpha and TIR motif-containing 1 (SARM1)

Another important component of the WD mechanism is SARM1 (for sterile alpha and toll/interleukin receptor (TIR) motif-containing 1) protein. A potential role for SARM1 in WD

was first discovered in a large-scale genetic screen in *Drosophila* which demonstrated that a *dSarm* (the *Drosophila* analog of SARM1, also called *ect4*) loss of function delayed axon degeneration in olfactory neurons after axotomy[26]. This effect was confirmed in mice using an RNAi screen where knockdown of SARM1 lead to delayed degeneration of injured sensory axons[27]. The same phenomenon was also demonstrated in a SARM1$^{-/-}$ mouse where injured axons were preserved for up to 14 days[27]. Thus, SARM1 is an important pro-degenerative element in WD.

SARM1 is predominantly located at the outer mitochondrial membrane in neurons although mitochondrial localization is not necessary for its role in WD[27]. SARM1 loss does not impair the function of toll-like receptors (TLRs), suggesting that it is distinct from other TIR-containing proteins, which serve as TLR scaffolds[28]. SARM1 promotes neuron death as a result of hypoxia[28] and viral infection[29]. SARM1 homologs *tir-1* and *dSarm* also play a role in the immune response in *C. elegans*[30] and *Drosophila*[31] respectively. Whether SARM1 exerts its role in stress responses in the same way as in axon degeneration remains unresolved.

SARM1 is made of two sterile alpha motif (SAM) domains, a C-terminal TIR domain and an auto-inhibitory N-terminal domain, which includes a mitochondrial localization sequence. Full length SARM1 expression has no effect on degeneration in healthy axons but expression of an N-terminus-lacking SARM1 mutant causes axon degeneration and neuron death in both *Drosophila* and mouse models[27] hence its assumed auto-inhibitory role. The SAM domain multimerizes SARM1, creating SARM1-SARM1 homodimers which must be formed for SARM1 to become active (Figure 1.2)[27]. The TIR domain is the active downstream effector which was recently found to be the first TIR domain with enzymatic properties[32]. Multimerization by the SAM domains must occur in order to bring TIR domains in proximity to initiate their enzymatic effect[27].

Essuman and colleagues recently discovered that the SARM1 TIR domain catalyzes the degradation of NAD^+ into ADP-ribose (ADPR), cADPR and nicotinamide (Figure 1.2)[32]. Since NAD^+ levels and axon integrity are maintained in $SARM1^{-/-}$ injured axons both *in vivo* and *in vitro*[27], it would appear that the rapid loss of NAD^+ that occurs after axotomy reflects the NADase activity of SARM1. Whether this SARM1-dependent NAD^+ degradation causes or results from initiation of axon degeneration is not yet known. Nevertheless, this supports the role of NAD^+ metabolism as a central point in WD.

Recently, lifelong *in vivo* axon rescue was observed in $SARM1^{-/-}$ null mice with axonopathy whereas WldS mice developed neuromuscular defects by 3 months of age[33] suggesting that SARM1-centered models, as opposed to WldS, reflect a more physiologically accurate depiction of WD.

1.1.3. Dual leucine zipper kinase (DLK)

This now raises the following question: Do pro-degenerative pathways function downstream of NMNAT and SARM1? Loss-of-function genetic screens have identified dual leucine zipper kinase (DLK/MAP3K12) as a member of such a pathway[34]. DLK-deficient axons were protected from degeneration after axotomy in mouse and *Drosophila* models[34]. DLK is a mitogen activated protein kinase kinase kinase (MAP3K) that operates upstream of c-jun-n-terminal kinase (JNK), a kinase previously shown to be activated following axonal injury (Figure 1.2)[35]. DLK/JNK inhibition also protects axons from chemotherapy-induced neuropathy[36], suggesting that this pathway initiates a degeneration program in several circumstances. The axon protection offered by DLK loss is not as profound as that of $SARM1^{-/-}$ or WldS perhaps due to a

functional redundancy with two other MAP3Ks, MAP3K4 and MAP3K10 however combined knockdown of all three MAP3Ks leads to axon protection that is WldS-like.[36]. There is also redundancy downstream of the MAP3Ks, which activate two MAPKKs, MKK4 and MKK7. These two MAPKKs in turn activate the 3 JNK MAPKs (JNK1-3)[36].

JNKs typically affect cell processes by altering the transcription factor AP-1 but, since WD occurs independent of transcriptional dynamics, due to its inability to access the nucleus from which it has been physically separated, other targets must be responsible. Currently, only one such axonal target, stathmin 2 (SCG10 in humans), has been identified (Figure 1.2)[37]. SCG10 is a binding protein for microtubules that is degraded upon JNK activation, possibly causing a cytoskeletal fragmentation mechanism for JNK/SCG10[37]. Other as of yet undiscovered axonal JNK targets may also participate in WD (Figure 1.2).

Dimerization of the SARM1-TIR domain and injury to wild-type axons activates MAPK signaling[36] implying that both NAD^+ depletion and MAPK activation are downstream of SARM1. A recent study however determined that MAPK signalling is required downstream of injury-dependent NAD^+ loss and upstream of axon degeneration but is not required for the same phenomena induced by SARM1-TIR dimerization[38]. This observation suggests that MAPK may operate upstream of SARM1 to promote its activation. This remains to be resolved but it seems likely that the order of activation in WD is more complex than a simple linear pathway. Further studies will be crucial to determine the relative role of NMNAT, SARM1 and DLK as the axon degenerates.

1.2. Calcium Effects in WD

A long recognized phenomenon in WD is an increase in intra-axonal calcium[39]. NMNAT, SARM1 and DLK activity have previously been placed in an "initiation phase" of WD whereas the Ca^{2+} rise, subsequent protease activation and microtubule and cytoskeletal depolymerization characterize what is considered to be an "execution phase"[40]. Ca^{2+} is integral to WD progression and degeneration is significantly delayed in neurons cultured in media with reduced levels of calcium[41]. Furthermore, calcium-supplemented media that is treated with ethylene glycol-bis(β-aminoethyl ether)-N,N,N',N'-tetraacetic acid (EGTA), a calcium chelator, delays degeneration of transected axons[41]. The entry of Ca^{2+} was assumed to occur by either a passive influx through a compromised axon membrane or from passive entrance into the opened axon at the cut site which diffuses distally over time. This idea was challenged when it was shown that non-specific calcium channel blockers cobalt and manganese, L-type channel antagonists nifedipine and nimodipine and a sodium-calcium exchanger antagonist bepridil all delay degeneration of cut sensory axons (Figure 1.2)[39]. This suggested that the membrane maintains structural integrity until late in the degenerative process and that the influx of Ca^{2+} occurs through ion channels[39]. More recently, sensory neurons in zebrafish that were transgenic with GCaMP, a genetically based calcium indicator[42], displayed two distinct phases of intra-axonal calcium increase in their axons after transection[43], suggesting that calcium influx after axotomy may occur through more than one mechanism. Notably, axotomy first causes an immediate and transient wave of calcium influx proximal to the cut site that is unaltered in WldS mice. This initial wave causes rapid destruction of mitochondria near the cut site due to calcium overload and mitochondrial permeabilization[44]. This is later followed by a second wave throughout the entire distal axon that immediately precedes fragmentation. Interestingly, only this second phase is blocked in WldS axons suggesting that this

later phase relies on the intra-axonal elements of WD discussed above[43]. This reduced calcium influx during the second wave but not the first wave in WldS axons was also confirmed mice[45].

The functional effect of Ca^{2+} influx in WD is largely tied to the activation of a group of calcium-dependent cysteine proteases called calpains[39]. Addition of pharmacological calpain inhibitors to wildtype primary neurons[39] and transgenic mice overexpressing the endogenous calpain inhibitor calpastatin[46,47] displayed significant levels of protection from WD-mediated axon degeneration. Furthermore, introduction of exogenous calpain (m-calpain) to primary neurons exacerbates axon disintegration during WD[48]. In wild-type mice, axotomized axons have continually decreasing levels of endogenous calpastatin as axon fragmentation progresses[47].

To date, L-type calcium channels and sodium-calcium exchangers are the only channels that have been definitively implicated in the second calcium wave that occurs in WD[39]. Inhibition of these channels delays the progression of WD but does not protect axons nearly to the degree that WldS or $SARM1^{-/-}$ transgenic neurons do[49]. Therefore, there likely remain other neuronally-expressed calcium channels that are activated along with L-type channels and sodium-calcium exchangers that have not yet been identified for their role in WD (Figure 1.2). Furthermore, the mechanism by which L-type channels and sodium-calcium exchangers are activated in WD has not been elucidated.

1.2.1. The TRPV1 channel

The transient receptor potential cation channel vanilloid 1 (TRPV1) is a nonselective cation channel that is expressed in sensory neurons of the peripheral nervous system (PNS) and in the central nervous system (CNS)[50]. This protein typically forms as a homotetrameric complex to

create its ion pore[51]. It is a member of the TRP family, a large group of ion channels that serve diverse functions. These include sensation of physical stimuli such as osmotic pressure[52], stretch[53] and vibration[54], sensation of taste[55] and sensation of both noxious[56] and non-noxious temperatures[57].

TRPV1 can be activated by numerous stimuli, including capsaicin (the spicy compound found in hot chili peppers)[58] heat (above 43 °C)[59], acidic conditions[60], allicin (the burning compound in garlic)[61] and isothiocyanate compounds present in wasabi and mustard[62]. TRPV1 is sensitized by inflammatory elements such as prostaglandins[63] which increase activation from noxious stimuli and allow activation from previously non-noxious stimuli to occur. This manifests in the organism as hyperalgesia[63] and allodynia[64] respectively. TRPV1 displays a desensitizing effect from prolonged activation by capsaicin or noxious heat and is regulated by negative feedback through TRPV1 calcium influx, causing activation of Ca^{2+}-dependent elements such as calmodulin and subsequent inhibition of the channel[65]. TRPV1 has been a prime target for analgesic treatment due its role in pain and its effect on pain tolerance.

TRPV1 antagonists have proven effective for analgesic treatment of inflammatory and neuropathic pain in rats[66]. Prolonged topical application of TRPV1 agonists such as capsaicin causes desensitization[67]. Consequently, capsaicin patches and ointments can be purchased over the counter as topical analgesics. The analgesic effect of prolonged capsaicin treatment has been shown to occur through the reversible ablation of TRPV1-expressing sensory nerve terminals[68], suggesting a role of TRPV1 in sub-apoptotic neuron degeneration. This process requires Ca^{2+} influx through TRPV1 and nerve terminal ablation is decreased by calpain inhibition[68].

TRPV1 is also sensitized by reactive oxygen species (ROS). Similar to prostaglandins, ROS does not directly open the ion pore but rather lowers its threshold of activation, causing calcium influx as a result of a normally innocuous stimuli[69]. Treatment of mice with an intraplantar injection of H_2O_2 caused thermal hyperalgesia along with increased nociceptive behaviour such as paw licking and both of these effects were reduced in *Trpv1*$^{-/-}$ mice[70]. Multiple studies suggest that ROS-induced TRPV1 sensitization is the result of modification of reactive cysteine residues on the channel. The oxidizing molecule present in garlic, allicin, has been found to activate TRPV1 solely through the N-terminal cysteine 157 in mice (cysteine 158 in humans) while still allowing normal activation by capsaicin[71,72]. It has been postulated that cysteine 157 is important for proper formation of the TRPV1 complex since mutations to this residue cause a relative increase in monomeric TRPV1[73]. This occurs as ROS covalently modifies the thiol groups on TRPV1 cysteine residues, which alters the tertiary and quaternary structure of the TRPV1 complex[73]. ROS either reacts directly with the cysteine residues on the protein or indirectly by oxidizing lipids which then go on to alter TRPV1[74]. Altogether, TRPV1 fits the model for a potential role in WD-mediated calcium influx since it has already been shown to cause nerve terminal degeneration and it has a sensitivity to ROS, which are produced in large amount during WD as described below (Figure 1.2)[75].

Another finding that strongly supports a potential role for TRPV1 in WD is the recent discovery of its role in developmental degeneration by trophic factor deprivation (Johnstone et al, in preparation). It is well established that removal of nerve growth factor (NGF) causes axon degeneration and eventually cell death in dorsal root ganglia (DRG). However, the Barker lab found that treatment of NGF-deprived DRGs with capsazepine (CPZ), a TRPV1 antagonist, blocks this effect. NGF-withdrawal-induced degeneration is similarly blocked in DRG neurons from

Trpv1$^{-/-}$ mice. Unlike WD, the NGF deprivation pathway has a clear dependence on the intrinsic apoptotic pathway, which is initiated by mitochondrial dysfunction. During this process, mitochondria are depolarized and the mitochondrial permeability transition pore (mPTP) is formed. This leads to release of cytochrome C and cleavage of caspase-3, the central executioner of the apoptotic pathway. Altogether, this suggests that NGF-deprivation causes TRPV1 activation leading to a feed forward cascade of calcium influx, mPTP formation and apoptosis in sensory neurons.

The role of TRPV1 in WD has been incompletely described. In rats, an upregulation of TRPV1 expression occurs in axons proximal to an injury on the side connected to the cell soma and interestingly, TRPV1 inhibition using AMG517 caused increased nerve regeneration after injury[76]. It was also shown in mice that after axotomy, siRNA-mediated inhibition of TRPV1 reduced nerve regeneration, an effect that was negated after TRPV1 protein levels were recovered[77]. The first of these two studies suggests that TRPV1 inhibits regrowth of proximal axons after injury whereas the second suggests the opposite. The role of TRPV1 in axons distal to the injury site (the side separated from the cell soma) has not been reported and is a focus of this thesis.

1.3. Reactive Oxygen Species (ROS) in WD

Reactive oxygen species (ROS) are oxygen-containing molecules that are most commonly produced by the reduction of molecular oxygen (O_2) into superoxide radical ($^{\bullet}O_2^-$) which in turn generates hydroxyl radical ($^{\bullet}OH$) and hydrogen peroxide (H_2O_2) usually before being converted into water[78]. Of the three, the hydroxyl radical is considered to be the most highly "active" however

because superoxide and H_2O_2 participate closely in its formation, all three are referred to as ROS. These intermediates, although experiencing short half-lives[79], can be very damaging. ROS can quickly and irreversibly oxidize proteins, lipids, nucleic acids and low molecular mass metabolites to significantly alter or completely abolish their function[78,80].

WD induces ROS production in a variety of model organisms (Figure 1.2). In zebrafish, axotomy caused rapid oxidation of the ROS-sensitive biosensor roGFP and this was prevented by WldS overexpression[81]. In murine sensory axons, axotomy caused an increase in fluorescence of the ROS-sensitive dye CellROX[82]. In rat dorsal root ganglia, axotomy causes a significant increase in ROS levels and overexpression of either NMNAT1 or NMNAT3 reduces ROS accumulation and blocks axon degeneration[83]. Further, in an *in vivo* model, mice experience significant axon death in the sciatic nerve 8 – 13 weeks after it has been transected however axon survival is increased by continuous infusion with the ROS scavenger N-acetyl-L-cysteine (NAC)[84]. Excessive ROS accumulation and oxidative stress have also been observed in traumatic brain injury, a condition characterized by widespread Wallerian degeneration in the CNS[85]. The prime candidates for this observed ROS accumulation are the nicotinamide adenine dinucleotide phosphate (NADPH) oxidase (Nox) complex and/or mitochondria. It has never however been shown definitively that ROS release after axotomy causes calcium influx (Figure 1.2).

1.3.1. Nicotinamide adenine dinucleotide phosphate (NADPH) oxidase (Nox) complex-derived ROS

Nox complexes are membrane-associated protein complexes that oxidize NADPH to generate superoxide from O_2[86]. They have been found to be a source of ROS for multiple signaling

purposes in the CNS and PNS. These include immune response and activation of neutrophils[87] as well as plasticity, where Nox activation promotes neuronal development and axonal growth[88,89]. Nox complexes are comprised of seven known catalytic subunits in the mammal: Nox 1 – 5 and Duox 1 and 2[86].

The Nox complex may be a ROS source in WD. Inhibition of the Nox complex by two Nox inhibitors, diphenyleneiodonium (DPI) or apocynin, delayed axon degeneration and reduced ROS accumulation after axotomy in mice (Figure 1.2)[82]. Furthermore, this same study tested the effect of downregulation of each of the Nox complex subunits by short hairpin RNA (shRNA) and found that Nox 2, 3, 4 and Duox 2 downregulation significantly protected axons after transection.

It has been found that direct activation of the Nox complex by phorbol 12-myristate 13-acetate (PMA), an analog of the endogenous activator diacylglycerol (DAG), produces a ROS burst[90]. This mirrors the known endogenous activation by protein kinase C (PKC)[90]. PMA treatment causes Ca^{2+} influx that is reduced in $Nox1^{-/-}$ neurons, suggesting that ROS derived from the Nox complex might activate calcium channels[91]. The Barker lab has recently shown that PMA-induced calcium influx is reduced by NAC and is completely abolished in *Trpv1*$^{-/-}$ neurons (Johnstone et al, in preparation). After neurotrophic factor deprivation, murine sensory axons that were treated with VAS2870, another Nox complex inhibitor, or apocynin saw significant axon protection as well as a remarkable reduction in Ca^{2+} influx (Johnstone et al, in preparation). Furthermore, treatment of axons with Gö6976 or Gö6983, inhibitors of the upstream Nox activator PKC, prior to trophic factor deprivation has the same protective effects. Altogether this suggests that PKC-dependent ROS production induces Ca^{2+} influx and subsequent degeneration by activating TRPV1.

1.3.2. Mitochondria-derived ROS

In the mitochondria, ROS are produced as a byproduct of the electron transport chain (ETC) where electrons travel from a high energy state electron donor to a low energy state electron acceptor through a series of redox reactions. This final electron donation occurs at complex IV of the ETC where O_2 is converted to H_2O under controlled conditions. However, there is also a small leakage of electrons primarily at complex I and complex III which leads to premature or incomplete reduction of O_2 into superoxide[92]. This happens with 0.2% to 2.0% of all O_2 in the mitochondria[93] and is not only tolerable but is important for normal cell function[94]. To keep ROS levels, as well as cations and other solutes, tolerable in the mitochondria, they can be released into the cytosol by a rapid opening and closing of the mPTP in a process termed mPTP "flickering"[95]. This allows for release of extra mitochondrial metabolites and ions without causing full depolarization of the inner mitochondrial membrane (IMM).

ROS can be produced in excess under abnormal mitochondrial conditions, such as when ATP-synthase activity is inadequate or when the $NADH/NAD^+$ ratio is especially high[96]. The latter condition is characteristic of transected axons due to loss of NMNAT-mediated NAD^+ synthesis and active SARM1-mediated NAD^+ depletion[19,32]. This can lead to extended mPTP opening, beyond just a "flickering", which causes IMM depolarization and mitochondrial destruction in a process termed ROS-induced ROS release (RIRR)[97,98]. RIRR does not just release excess ROS from individual mitochondria but completely empties all its free-floating contents into the cytosol[99]. This mitochondrial collapse leads to a transient increase in ROS generation in the ETC causing even further release which can subsequently cause oxidative stress to neighbouring mitochondria, triggering another RIRR event[99,100]. This spread of RIRR events from one

mitochondria to the next can lead to widespread mitochondrial depolarization and massive ROS production and release in a cell[100,101].

Another common mitochondrial insult that can lead to mitochondrial ROS release is Ca^{2+} overload. In healthy cells, mitochondria can act as a Ca^{2+} buffer, using the potential of the IMM to actively engage in Ca^{2+} uptake from the cytosol and endoplasmic reticulum (ER)[102]. However, during periods of high Ca^{2+} in the ER or cytosol, Ca^{2+} accumulates in the mitochondria which in turn leads to prolonged mPTP opening and depolarization[103]. This is exacerbated by oxidative stress and leads to ROS release from the mitochondria[104].

Mitochondrial failure is a well-known event in WD (Figure 1.2). Axon transection quickly triggers a termination of mitochondrial movement[81,105] and causes a decline in glycolysis and mitochondrial respiration in the later stages[106]. Axotomy also causes an increase in mitochondrial ROS production [81], an increase in mPTP opening[107] and a profound loss in mitochondrial potential[108]. Furthermore, mitochondrial movement, glycolysis, respiration, increased ROS and mPTP opening were all close to normal in WldS axons, placing these event downstream of WldS protection.

Mitochondrial failure has also been shown to cause downstream TRPV1 activation. In a study using vagal neurons, mitochondrial dysfunction was experimentally induced using either the complex I inhibitor antimycin A, the complex III inhibitor rotenone or the IMM depolarizer carbonyl cyanide m-chlorophenyl hydrazine (CCCP); all three caused a significant calcium rise that was abolished in *Trpv1*$^{-/-}$, *Trpa1*$^{-/-}$ double-null mice[109]. Furthermore, antimycin A and CCCP caused a significant increase in mitochondrial ROS levels, as demonstrated by an increase in the mitochondrial superoxide dye MitoSOX. Antimycin A and rotenone have also been demonstrated

to cause axon degeneration and cytotoxicity at a later stage, an effect that is reduced in WldS axons[110].

Despite unanimous agreement that mitochondria are lost after axotomy, the role of mitochondrial dysfunction in downstream axon death in WD is still an area of contention (Figure 1.2). One hypothesis suggests that mitochondrial depolarization is the central initiator of SARM1-dependent axon degeneration[75]. This follows the logic that loss of mitochondrial depolarization causes imminent death in neurons and that NAD^+, an important substrate for effective energy metabolism and therefore proper mitochondrial function[111], is heavily depleted after axon transection. In $SARM1^{-/-}$ neurons, CCCP caused mitochondrial depolarization, ROS accumulation and calcium influx however the axon remained structurally intact[75]. Further, inhibition of mPTP formation and opening by either pharmacological or genetic means reduces axon degeneration after transection[107]. This places mitochondrial dysfunction and calcium influx upstream of SARM1 and suggests that mitochondrial loss is a key initiator of WD.

Another research group has proposed the NMN hypothesis[112] which attributes axon degeneration to rising levels of the NAD^+ precursor NMN. NMN accumulation during WD is required for calcium influx and axon degeneration[113] and is not observed in $SARM1^{-/-}$ mice[113]. While SARM1 deletion protects the axon as a whole, axotomized $SARM1^{-/-}$ axons still experience mitochondrial depolarization and dysfunction, suggesting that mitochondrial dynamics operate in a different pathway. This is further supported by the finding that CCCP does not significantly alter the progression of WD in mice[113] and that axons containing no mitochondria in *C. elegans* degenerate normally after laser axotomy[114]. In a *Drosophila* line that contains no axonal mitochondria, axon transection causes unimpeded degeneration and is even protected by WldS and NMNAT overexpression[115]. Whereas the first hypothesis places mitochondria and calcium influx

upstream of SARM1, the second indicates that calcium influx is downstream of SARM1 and places mitochondrial dysfunction in a pathway parallel to degenerative mechanisms.

1.4. Cell Lines and Experimental Models

In this study, human embryonic kidney (HEK) 293T cells were used for experimentation with viral vectors and embryonic day 13.5 (e13.5) murine dorsal root ganglia (DRG) were used for all other experiments. HEK293T cells were originally isolated from tissue with neuron-like qualities from the kidney of a legally aborted fetus[116-118]. HEK293T cells are widely used for experimentation involving recombinant proteins due to their consistent growth rate and high transfection and infection efficiencies. Furthermore these cells do not express TRPV1 natively, which allows a blank slate to study TRPV1 if expressed exogenously[119,120].

DRGs are clusters of neurons located on the dorsal roots on spinal nerves. The axons of DRGs extend throughout the body to relay sensory information into the CNS. When cultured *in vitro* the axons of embryonic DRGs grow in large abundance and extend outward from the central explant. This creates areas that are rich with axons but contain very few cell somas. For this reason, DRGs are widely used in the field of WD since these axon-rich areas can be physically separated from the ganglion using various methods such as a scalpel blade or a laser[27,32,43,44,75,121]. Importantly, DRGs are pseudounipolar meaning they do not have dendrites and instead adapt the functions of a dendrite into the single branched axon of each cell[122]. The means that the extended axon network *in vitro* does indeed contain only axons.

The *Trpv1* cation channel has functional and structural similarities to many other members of the TRP family[123]. Furthermore, pharmacological TRPV1 manipulation always runs the risk of

having confounding off-target effects. In order to analyze the effects of TRPV1 alone, *Trpv1* knockout mice were generated[124]. In short, the mouse *Trpv1* gene was disrupted by deleting an exon encoding segments of transmembrane domains 5 and 6 along with the pore-loop region in between. This produced mice that were viable and fertile.

1.5. Research Overview and Hypothesis

Since pharmacological inhibition or genetic ablation of calcium channels that are known to be involved in WD has significantly delayed the onset of distal axon degeneration, identifying the key channels involved is crucial for elucidating this pathway further and identifying other targets for therapeutic intervention[12-14]. Previous studies have revealed that axoplasmic calcium rise is due primarily to influx from the extracellular environment as opposed to depletion of intracellular stores[39,113,125,126] confirming the importance of identifying this full suite of membrane-bound ion channels. The TRPV1 channel is a strong candidate due to its prominence in other modes of axon degeneration and its ability to be sensitized by ROS.

The manner in which the calcium cascade is initiated in the execution phase of WD is still unknown. ROS accumulation has been strongly implicated in this[81-83,85], either through activation of the Nox complex[82] or through production and release of ROS from mitochondrial stores[75,107,108]. The relative role of these two sources as well as their importance in initiating calcium influx and axonal degeneration has not been fully elucidated. Furthermore, the steps connecting ROS accumulation to calcium influx have been implied[43,127] but not demonstrated directly[75]. This again brings TRPV1 to the forefront because it has been shown to be activated by both the Nox

complex[91,128] and by mitochondrial ROS[109,129] a mechanism of ROS-dependent TRPV1 sensitization is established[71-73].

The **central hypothesis** of this thesis proposes that TRPV1 is activated during WD by ROS and that this causes calcium influx and downstream axon death. To study the role of ROS and calcium channels in axotomy *in vitro*, several techniques were employed to simulate WD in primary E13.5 murine dorsal root ganglia and in the HEK293T cell line. Results were generated using a combination of axonal dyes and immunostaining techniques through fluorescence microscopy.

The two main **research objectives** addressed in this thesis are:

1. To determine the contribution of TRPV1 to Wallerian degeneration.
    a. Investigate the role of TRPV1 in axotomy-induced calcium rise.
    b. Investigate the role of TRPV1 in axotomy-induced axon degeneration.
2. To determine the mechanism of calcium channel activation in Wallerian degeneration.
    a. Investigate the role of ROS in axotomy-induced calcium rise.
    b. Investigate the role of the Nox complex in axotomy-induced calcium rise.
    c. Determine the effect of axotomy on mitochondria.
    d. Elucidate the effect of mitochondrial depolarization on calcium influx and axon degeneration.

e. Investigate the role of cysteine 157 on TRPV1 sensitization by mitochondrial ROS.

Chapter 2: Materials and Methods

2.1. Chemicals and Reagents

The following reagents were obtained from Sigma Aldrich (Oakville, ON, Canada): Poly-D-Lysine (PDL), 2,2,2-tribromoethanol (avertin reagent), 2-methyl-2-butanol (avertin reagent), 5-fluoro-2'-deoxyuridine (FDU), dimethyl sulfoxide (DMSO), NAD^+, paraformaldehyde (PFA), fluoroshield, nifedipine, NAC, CCCP and capsaicin.

The following reagents were obtained from Wisent Bioproducts (Saint-Jean-Baptiste, QC, Canada): Hank's balanced salt solution (HBSS), penicillin-streptomycin solution (P/S), L-glutamine, phosphate buffered saline (PBS), 0.53 mM ethylenediaminetetraacetic acid (EDTA) solution and Dulbecco's modified eagle medium (DMEM) with phenol red.

The following reagents were obtained from ThermoFisher Scientific (Ottawa, ON, Canada): Type I bovine collagen (PureCol), 4-(2-hydroxyethyl)-1-piperazineethanesulfonic acid (HEPES), ethanol, calcium chloride dihydrate, Neurobasal medium, B-27 serum-free supplement, the mitochondrial dye tetramethylrhodamine ethyl ester (TMRE) and Ca^{2+} dye Fluo-4-AM.

The following reagents were obtained from VWR (Radnor, PA, USA): Sterile water, Tween 20, EGTA, sodium chloride, glycerol and fetal bovine serum (FBS).

Laminin, in the form of laminin/entactin complex, and 0.05% trypsin/ EDTA solution were purchased from Corning (Corning, NY, USA). Tris, skim milk powder and sucrose were purchased from BioShop Canada (Burlington, ON, Canada). CPZ, VAS2870, apocynin and DPI were obtained from Tocris Bioscience (Oakville, ON, Canada). Mouse NGF 2.5S was ordered from Alomone Labs (Jerusalem, Israel). Triton X-100 was purchased from Millipore EMD (Burlington,

MA, USA). The axonal marker dye Calcein-AM was obtained from AAT Bioquest (Sunnyvale, CA, USA).

The primary mouse antibody for tubulin subtype β-III (tuj1, catalogue # MAB5564) was purchased from Millipore EMD (Burlington, MA, USA) and the secondary goat anti-mouse Alexa 488 antibody was purchased from Jackson Laboratories (West Grove, PA, USA).

2.2. Equipment and Supplies

Dissection of murine embryos, extraction of dorsal root ganglia and seeding of explants for cell culture were completed in a unidirectional flow clean bench table top workstation (Envirco Corporation, Sanford, NC, USA). All other aspects of cell culture were performed in a class II type A2 biological safety cabinet (Labconco, Kansas City, MO, USA) and cells were kept in an air-jacketed CO_2 incubator (VWR). All experiments were conducted using either 4-chamber glass bottom dishes (Cellvis, Mountain View, CA, USA), 6-well cell culture plates (VWR), 10 cm cell culture plates (Corning) or 1 μm pore-containing filter inserts (Falcon, Corning, NY, USA) inside of 6-well companion plates (Falcon). The 4-chamber glass bottom dishes were used for Fluo-4, TMRE and Calcein imaging in axons as well as TRPV1-R-GECO imaging in HEK293T cells. The 6-well culture plates were used for fixation and tuj1 staining of DRGs after CCCP treatment. The filter inserts and their accompanying companion plates were used for fixation and tuj1 staining of DRGs after axotomy. The 10 cm plates were used as a carry plate for HEK293T cells.

Dissections were performed under a Leica MZ16 stereomicroscope (Leica Biosystems, Concord, ON, Canada). Blade axotomy was completed using an Olympus CKX53 inverted

microscope (Olympus Canada, Richmond Hill, ON, Canada). All imaging was completed using Zeiss AxioObserver.Z1 inverted epifluorescence microscope (Carl Zeiss, Toronto, ON, Canada) equipped with ZEN2 image acquisition software (Carl Zeiss).

2.3. Cells, Animal Models and Viruses

HEK293T cells were purchased from ATCC (Manassas, VA, USA). Cells were frozen in 50% FBS, 40% DMEM and 10% glycerol. For culturing, cells were quickly thawed by immersion in a 37 °C water bath and grown in DMEM basal media supplemented with 10% FBS and 1% P/S. Cells were removed from plates for seeding and carrying purposes by washing plates in 0.53 mM EDTA solution then incubating plates in 0.53 mM EDTA/0.05% Trypsin solution for 5 minutes at 37 °C. The trypsin solution, containing suspended cells, was centrifuged to pellet the cells. The supernatant was aspirated and replaced with DMEM basal media. These cells were then counted using a cell counter and seeded at the desired density.

Experiments with primary cell cultures were conducted *in vitro* using embryonic mouse neurons. To harvest these, pregnant E13.5 CD1 (Charles River, Sherbrooke, QC, Canada) or c57Bl/6 (Jackson Laboratories, Bar Harbor, ME, USA) mice were first anaesthetized by intraperitoneal injection of 200 μL avertin (35 mM 2,2,2-tribromoethanol and 0.62% (v/v) 2-methyl-2-butanol) and then sacrificed by cervical dislocation. Embryos were harvested and dissected in cold HBSS under a dissecting microscope. All animal procedures were approved by the Canadian Council of Animal Care and the University of British Columbia (UBC) animal care committee. Efforts were made to minimize the number of animals used.

Plasmids for wildtype and C157A TRPV1 conjugated to a red genetically-encoded calcium

indicator for optical imaging (R-GECO) were constructed by molecular cloning and site-directed mutagenesis. Final copies were adapted into herpes simplex virus (HSV) vectors by the Viral Core Facility at the McGovern Institute for Brain Research (Massachusetts Institute of Technology, Cambridge, MA, USA). For storage, viruses were flash frozen using pre-chilled 70% ethanol at -80 °C. Viruses were stored in PBS supplemented with 10% sucrose and 25 mM HEPES buffer.

2.4. Dissection and Culturing of Primary Embryonic Murine Dorsal Root Ganglion Explants

Dorsal root ganglia were harvested from E13.5 CD1 or c57Bl/6 embryos and grown on either glass plates, plastic plates or filter inserts. All plating surfaces were coated overnight with PDL (1 mg/ml) dissolved in water, the plates were then washed once with water then left to dry. Following this, the plates were coated with laminin (10 g/ml) dissolved in water for a minimum of 1 hour and then collagen (0.1 mg/ml, PureCol) dissolved in water for a minimum of 1 hour. Plates were washed once again with water and were filled with basal culture media at 37 °C. Basal culture media consisted of Neurobasal supplemented with 2% B-27, 1% L-glutamine, 1% penicillin/streptomycin (50 units/mL penicillin, 50 μg/mL streptomycin final) , 20 μM FDU and 12.5 ng/ml NGF. Cells were grown in a humidified 37 °C incubator with 5% CO_2.

2.5. Experimental Methods

2.5.1. End-point Ca^{2+} imaging with Fluo-4

Calcium levels were assessed using Fluo-4-AM in axons after axotomy under various conditions. DRG explants were plated on 4-chamber glass culture plates and incubated in basal media for 3 – 5 days. During this time, axons projected outward up to 4 mm away from cell bodies in the ganglia. Using a surgical blade (no. 20, Integra Miltex, Plainsboro, NJ, USA), cuts were made just next to the explant on only one side of the DRG. Thus, in the same culture, some DRG neurons underwent degeneration while others remained intact. The culture dishes were returned to the incubator after axotomy for 2 hours and 30 minutes. The partially axotomized DRGs were then incubated in 1 μM Fluo-4-AM in DMSO for 15 minutes (final DMSO concentration did not exceed 0.1% v/v), a membrane permeable dye that exhibits an increase in fluorescence when bound to Ca^{2+} at 506 nm when excited at 488 nm. After incubation, cells were washed once in warm HBSS then immersed for 15 minutes in HBSS supplemented with 12.5 ng/ml NGF and 2 mM $CaCl_2$. The incubation period allowed the dye to enter the axon after which endogenous esterases cleaved the acetylmethoxyester (AM) group off the dye, rendering the dye impermeable to the membrane and trapping it within the axon. The cells were then washed and re-immersed in NGF- and calcium-containing HBSS before being imaged. HBSS is used because it is able to buffer the culture, keeping it at physiological pH without supplemention with 5% CO_2. Live-imaging of axons was done 3 hours after axotomy, a time that has been previously found to display maximal Ca^{2+} effects with minimal fragmentation. Images of axons on both the axotomized side and the intact side of the DRG using a Zeiss AxioObserver Z1 were captured using a 40x objective and was captured and analyzed using the Zen 2 software.

Axon intensity was calculated using ImageJ software (FIJI build, National Institute of Health, Bethesda, MD, USA). First, background intensity was calculated as the mean intensity of 4 selected axon-free regions of interest (ROIs) on a given image. A threshold was then made based on individual pixel intensities in order to separate the axonal area from the background, which had lower intensity values than axons even in field with low intra-axonal Ca^{2+}. The mean intensity of this now thresholded image, containing only area occupied by axons, was recorded and the previously calculated background intensity was subtracted from it. Each plotted fluorescence value was the average of at least 4 fields taken from the same explant and was divided by the mean intensity of the intact untreated control for the entire experiment, which was assigned an arbitrary value of 1, normalizing the data.

2.5.2. Fixation, cytoskeletal immunostaining and imaging of filter cultures

Axonal degeneration was assessed after axotomy by immunostaining entire DRGs and quantifying axon density under various conditions. DRG cultures were grown on cell culture filter inserts containing 1 μm pores for 72 hours, allowing axons to grow both above and below the filter while keeping soma on top of the filter (Figure 2.1A). Using a previously established method[130], axotomy was achieved by scraping the top side of the filters, thus detaching all axons from their cell bodies above and initiating degeneration in the axons below. The filters were then returned to the incubator for 6 hours, a time that was previously determined to show degeneration without losing the axons altogether. An intact control that was not scraped was also included in every experiment. After 6 hours, the filters were washed once with PBS and fixed in a PBS solution containing 4% w/v PFA for 20 minutes at room temperature. The filters were then washed again

with PBS and blocked in a blocking solution made of 5% skim milk and 0.2% Triton X-100 in TBS-T for 30 minutes. Filters were then incubated at 4 ℃ overnight with antibodies against β-III tubulin, diluted 1:10,000 (100μg/L) in blocking solution containing 0.02% Triton X-100. The next day, filters were washed 3 times for 15 minutes each in PBS then incubated hidden from light for 1 h at room temperature in Alexa 488-conjugated goat anti-mouse secondary antibodies diluted 1:2000 in blocking solution with no Triton X-100. Filters were then washed hidden from light three times for 15 minutes each in PBS. Filters were then cut out of their inserts and carefully mounted on Superfrost Plus slides (Fisher Scientific) using Fluoroshield (Sigma-Aldrich) and microscope cover glass (Fisher Scientific).

Imaging was performed using the Zeiss AxioObserverZ1 inverted epifluoresence microscope at 5x magnification with an automated, motorized stage. Tiled images were stitched automatically with Zen 2 software to produce master images of entire filters on microscope slides (Figure 2.1B). Regions of interest made of a quarter of a DRG, with the former location of the soma at the corner of the image and with axons projecting outward from this corner, were selected from these master images and saved separately. These images had their axon abundance quantified using Axoquant 2.0, an algorithm designed in R studio[131]. Essentially, the algorithm first masks the image, creating a binary image denoting presence of axon of lack thereof. The algorithm then draws concentric quarter-circles, with the center being the former location of the soma in the corner of the image, of increasing radial size every 100 μm away from the corner. It then determines the axon density, or the proportion of pixels occupied by axon to those that are not, of bins between each concentric circle. This creates an axon density curve with respect to distance from the soma. Each replicate in a curve is made up a minimum of 6 quarter DRG images selected from at least 3 different explants on the filter.

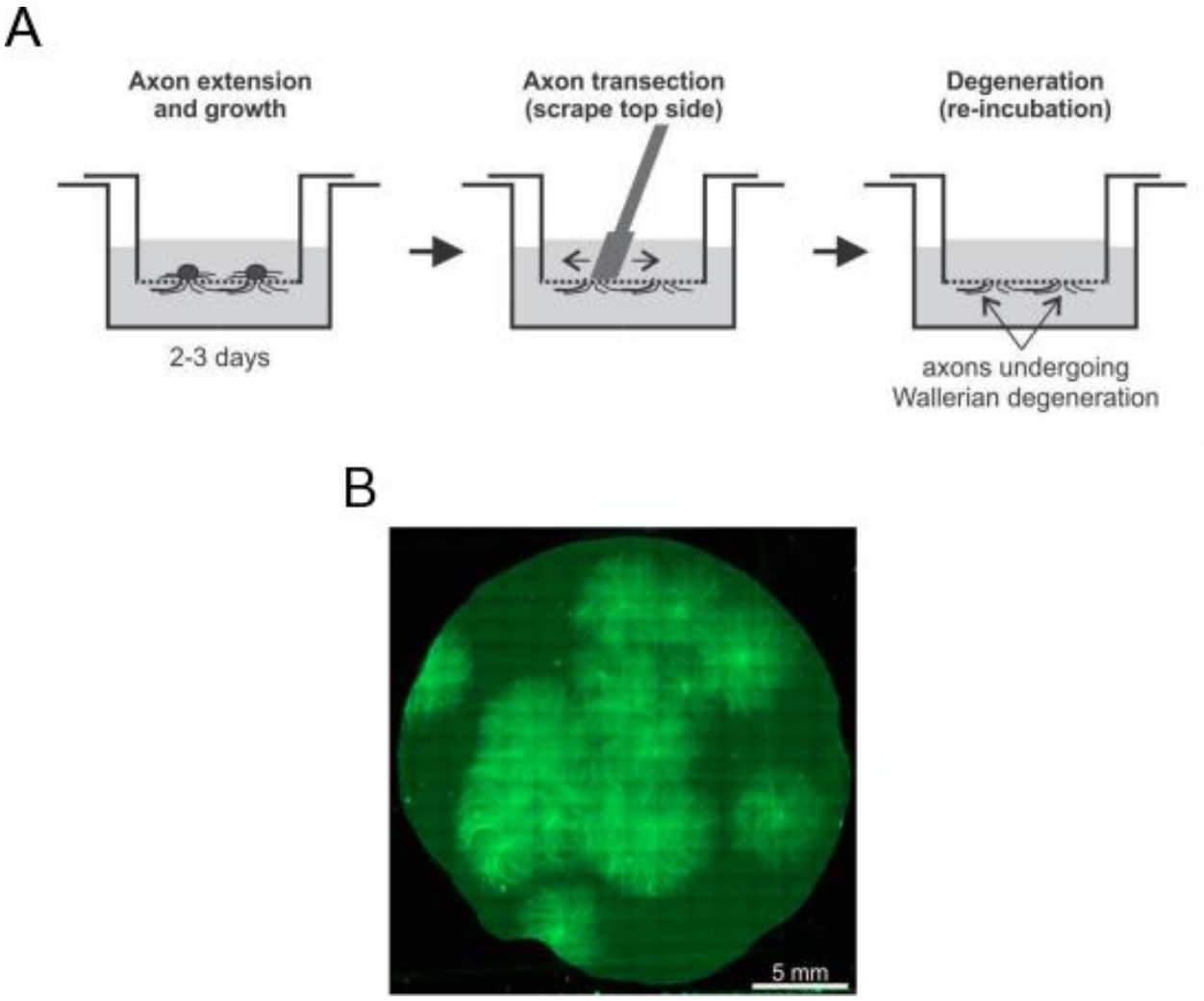

Figure 2.1. Scraping filters containing DRG explants yields uniformly degenerating axons for imaging. (A) Schema outlining a typical axotomy experiment. After sufficient re-incubation time, axons are immunostaining and filters are mount for imaging (B; scale bar indicates 5 mm). Images adapted from Unsain et al. 2014[130].

2.5.3. Live Ca^{2+} and mitochondria imaging with Fluo-4 and tetramethylrhodamine, ethyl ester (TMRE)

The acute effects of mitochondrial loss on calcium influx were assessed in axons under various conditions. DRG explants were plated on 4-chamber glass culture plates and incubated in basal media for 3 – 5 days. Thirty minutes prior to imaging, cultured neurons were incubated with 1 μM Fluo-4 dissolved in DMSO and 100 nM TMRE in DMSO (final DMSO concentration did not exceed 0.2% v/v), a dye with an excitation peak at 540 nm and an emission peak at 590 nm that accumulates in mitochondria based on the potential of the inner membrane, for 15 minutes at 37 °C and then washed in HBSS and allowed to equilibrate in fresh, room-temperature HBSS supplemented with 12.5 ng/ml NGF and 2 mM $CaCl_2$. Imaging was performed in fresh HBSS supplemented with 12.5 ng/ml NGF and 2 mM $CaCl_2$ with a Zeiss AxioObserver Z1 and Zen software with a 488 nm laser for Fluo-4 excitation and 540 nm laser for TMRE excitation and with a 40x objective. Images were captured every 5 seconds for a total of 500 seconds. After a baseline was established (t = 0 – 100s), CCCP, a potent mitochondrial poison that renders the inner mitochondrial membrane leaky to protons, was added directly to the plate, at a final concentration of 50 μM.

Each individual time course generated 100 Fluo-4 images and 100 TMRE images. For all images, background was removed by subtracting the average intensity of 4 selected axon-free areas (done individually for Fluo-4 and TMRE) from the average intensity of the entire image. This background was calculated and applied on a frame-by-frame basis for the entire time course. The intensity of an entire time course was normalized to the intensity level of the first image (t = 0s; done individually for Fluo-4 and TMRE). The mean of all three time courses done in a given experiment day for each condition was generated to create single replicates. Fluo-4 peak values

were determined by taking the maximum normalized intensity value from t = 100 – 150s (frame 20 – frame 30), which is the time immediately following CCCP treatment, from the averaged time course of an experiment day.

2.5.4. Fixation, cytoskeletal immunostaining and imaging of plated cultures

The long-term effect of mitochondrial loss on axon degeneration was assessed by applying CCCP then immunostaining entire DRGs and quantifying axon density under various conditions. DRG cultures were grown on 6-well culture plates for 72 hours. 50 μM CCCP, dissolved in DMSO (final concentration did not exceed 0.1% v/v) and suspended in an aliquot of basal media, was added to each well and incubated for 5 hours, a time previously determined to display maximal axon loss without losing the axons altogether. After 5 hours, plates were washed in PBS and fixed in 4% PFA in PBS solution for 20 minutes at room temperature. Plates were then immunostained with tuj1 and Alexa488 as described in **2.5.2**. For imaging, the 6-well plates were imaged directly at 5x magnification using the Zeiss AxioObserver Z1. Adjacent images of the entire plate were tiled to produce a master image of all conditions. Quarter DRGs were selected and analyzed using Axoquant 2.0 as described in **2.5.2**[131].

2.5.5. Endpoint mitochondrial abundance imaging with TMRE and Calcein-AM

Mitochondrial abundance in axons was assessed after axotomy using a combination of TMRE and Calcein staining. DRG explants were grown on 4-chamber glass plates for 3 – 5 days. Axotomy was accomplished by cutting next to explants on one side, leaving the other intact. The

plates were then returned to the incubator for 2 hours and 30 minutes. 160 nM Calcein-AM, a green dye that crosses into cells based on their passive plasma membrane potential, dissolved in DMSO (0.1% v/v) was added to the plates which were then returned to the incubator for 30 minutes. 100 nM TMRE dissolved in DMSO (final DMSO concentration did not exceed 0.2% v/v) was then added to the plates which were returned to the incubator for 15 minutes. After incubation, cells were washed once in warm HBSS then immersed for 15 minutes in HBSS supplemented with 12.5 ng/ml NGF and 2 mM $CaCl_2$. This, along with the incubation before, allowed the AM group from the Calcein to be cleaved so that the dye would remain in the axon. The cells were then washed and re-immersed in NGF- and calcium-containing HBSS before being imaged. In summary, explants were axotomized 3 hours and 30 minutes, Calcein was added 1 hour and TMRE was added 30 minutes prior to imaging.

Fluorescent images of axons were taken with excitation at 488 nm and 540 nm and emission at 506 nm and 590 nm respectively on both the axotomized side and the intact side of the DRG using a Zeiss AxioObserver Z1 with a 40x objective and were captured using the Zen 2 software. For both the Calcein and TMRE images, a manual threshold mask based on pixel intensity was established to create a binary image that displays cross-sectional axon area and cross-sectional mitochondria area respectively using ImageJ (FIJI build). The mitochondrial abundance readout was generated by dividing the area of positive TMRE signal (total mitochondrial area) by the area of positive Calcein signal (total axon area). Each replicate was an average of at least four images of the same DRG explant which were normalized to the intact control over the whole experiment.

2.5.6. Ca^{2+} imaging with TRPV1-R-GECO fusion proteins

HEK293T cells were infected with herpes simplex virus (HSV)-expressing vectors for wildtype TRPV1-R-GECO or TRPV1-R-GECO mutants that have cysteine 157 replaced with an alanine (C157A) to examine the effect of specific cysteine mutation on the ROS sensitivity of TRPV1. Cells were seeded in 4-chamber glass culture plates at a density of 2.27×10^3 cell per cm^2 (50,000 cells per well) and grown in DMEM basal media supplemented with 10% FBS and 1% P/S. 24 hours later, an aliquot of WT or C157A TRPV1-R-GECO was quickly thawed in a 37 °C water bath, suspended in PBS and applied directly to the culture wells at a multiplicity of infection (MOI) of 1. 48 hours later, cells were switched to fresh HBSS supplemented with 2 mM $CaCl_2$. Cells were imaged at 590 nm and excited at 540 nm at 5 second intervals for a total of 360 seconds (6 minutes; 72 frames). After a two-minute baseline was established (t = 0 – 120s), solution containing CCCP (final concentration of 50 μM) dissolved in DMSO (0.1% v/v) and suspended in fresh HBSS with 2 mM $CaCl_2$ was added in addition to the initial solution without disrupting the imaging time course. Another two minutes later (t = 120 – 240s), solution containing capsaicin (final concentration of 1 μM) dissolved in DMSO (final DMSO concentration did not exceed 0.2% v/v) and suspended in fresh HBSS with 2 mM $CaCl_2$ was added in addition to the previous solutions. Following this, images were collected for another two minutes (t = 240 – 360s).

Image analysis was completed using ImageJ (FIJI build). ROIs were drawn individually around every bright cell still present in the final frame, therefore occluding cells that were lifted off the plate, cells that were not infected and cells that were unresponsive to capsaicin. Each ROI was traced back to ensure that the region traced accounted for any cell movement throughout the time course. Background correction was performed by obtaining the mean pixel intensity of 4 background regions; this value was subtracted from the mean intensity of each cell region of

interest on a frame-by-frame basis. Cells were then sorted based on minimum cell intensity. Cells that, at any point in the time course, reached an intensity less than 1 intensity unit (out of 255 for grayscale 8-bit images) above background were occluded from the analysis. GECO responses were then standardized as fold-change from the average GECO intensity of each cell over the two minutes of baseline (t = 0 – 120s). From this, average maximum cell value from the period of CCCP treatment (t = 120 – 240s) were recorded for each independent experiment.

2.6. Generation of Mixed-Genotype Trpv1$^{+/-}$ DRG Cultures

Trpv1$^{-/-}$ C57BL6 mice carrying the Trpv1^{tm1Jul} (targeted mutation 1, David Julius) allele in homozygosity were obtained from Jackson Laboratories. These alleles contain a truncated and poreless and dysfunctional TRPV1. The mutant mice were crossed with wild-type C57BL6 mice to generate Trpv1$^{-/+}$ animals, and these heterozygotes were bred in timed pregnancies to produce mixed-genotype litters of Trpv1$^{+/+}$, Trpv1$^{-/+}$ and Trpv1$^{-/-}$ E13.5 embryos.

2.7. Methods of Pharmacological Manipulation

2.7.1. Calcium withdrawal and calcium chelation

The effect of Ca^{2+} removal on endpoint Fluo-4 intensity after axotomy was assessed by incubating plates in prewarmed Ca^{2+}-free HBSS supplemented with 12.5 ng/ml NGF 1 hour after axotomy. Furthermore, washes and fresh HBSS incubations were performed with room

temperature Ca^{2+}-free HBSS supplemented with 12.5 ng/ml NGF. Control plates that instead used HBSS supplemented with 12.5 ng/ml NGF and 2 mM $CaCl_2$ were included in each experiment.

For live Ca^{2+} imaging with CCCP, plates were incubated in prewarmed Ca^{2+}-free HBSS supplemented with 12.5 ng/ml NGF 30 minutes prior to imaging. Furthermore, washes, aliquots for CCCP delivery and fresh HBSS incubations were performed with room temperature Ca^{2+}-free HBSS supplemented with 12.5 ng/ml NGF. Control plates that instead used HBSS supplemented with 12.5 ng/ml NGF and 2 mM $CaCl_2$ were included in each experiment.

In long-term CCCP experiments assessing axon degeneration, calcium withdrawal was accomplished by incubating wells in prewarmed basal media supplemented with 6 mM EGTA 30 minutes prior to scraping filters and applying CCCP respectively.

2.7.2. NAD^+ supplementation

For filter experiments involving NAD^+, fresh warm basal media was supplemented with 5 mM NAD^+ and added to cultures 30 minutes prior to filter scraping. Control filters had fresh warm untreated basal media (0 mM NAD^+) added to culture instead.

For Fluo-4 and mitochondrial abundance experiments, HBSS supplemented with 12.5 ng/ml NGF, 2 mM $CaCl_2$ and 5 mM NAD^+ was used for all washes and fresh HBSS incubations. Controls using HBSS supplemented with just 12.5 ng/ml NGF and 2 mM $CaCl_2$ were included in each experiment.

2.7.3 Reactive oxygen species scavenging by N-acetyl-L-cysteine

For long term CCCP-induced degeneration experiments assessing the effects of ROS scavenging, fresh warm basal media was supplemented with 20 mM NAC and added to cultures 30 minutes prior to CCCP treatment. Control wells had fresh warm unaltered basal media (0 mM NAC) added to culture instead.

For Fluo-4 (axotomy and CCCP) and mitochondrial abundance experiments, HBSS supplemented with 12.5 ng/ml NGF, 2 mM $CaCl_2$ and 20 mM NAC was used for all washes, aliquots for drug delivery and fresh HBSS incubations. Controls using HBSS supplemented with just 12.5 ng/ml NGF and 2 mM $CaCl_2$ (0 mM NAC) were included in each experiment.

2.7.4 Pharmacological TRPV1, L-type channel and Nox complex inhibitors

TRPV1 inhibitor capsazepine, L-type inhibitor nifedipine and Nox complex inhibitors VAS2870, apocynin and DPI were all added to cell cultures at a final concentration of 10 μM. All inhibitors were prepared in DMSO (final DMSO concentration of 0.1% v/v) and were in all cases applied 30 minutes prior to beginning experiments. All inhibitors were supplemented into HBSS washes, fresh incubations and aliquots for CCCP application. Control experiments included media and HBSS treated with an empty DMSO (0.1% v/v) vehicle instead.

2.8. Statistical Analyses

GraphPad Prism software (version 7.0, GraphPad Software Inc., La Jolla, CA, USA) was used to conduct statistical analyses. Data obtained from quantified Fluo-4, TMRE, Calcein and R-GECO images were always normalized. In endpoint experiments values were normalized to the mean of all intact controls over the whole experiment, allowing for accurate representation of variability across different days.

All experiments, other than the R-GECO experiments, were analyzed using a two-way analysis of variance (ANOVA). In endpoint experiments, the two factors were axotomy vs intact and the presence vs absence of a reagent. In time course experiments, the two factors were CCCP vs DMSO vehicle addition and the presence vs absence of a reagent. These were all followed by Tukey's post-hoc comparison so that differences both within and across conditions could be compared. In Axoquant 2.0 experiments, the two factors were distance from soma (taken in repeated measures) and the presence vs absence of a reagent. Axoquant 2.0 experiments were all followed by Dunnett's post-hoc analysis compared to the axotomized control in filter experiments or the CCCP control in CCCP-induced degeneration experiments. In R-GECO experiments, a Mann-Whitney U test was used to compare the two columns due to their lack of normality (Shapiro – Wilk test for normality, $p = 0.0099$).

Normalized data are presented as boxplots displaying median, 25%, 75% percentile and minimum/maximum. Data from Axoquant 2.0 experiments were displayed as means ± standard error of the mean (S.E.M.). Significance was established at $P < 0.05$.

Chapter 3: Results

3.1. Determine the Contribution of TRPV1 to Wallerian Degeneration

Calcium rise occurs in two waves after axon transection: There is an immediate wave occurring proximal to the cut site that is thought to occur by passive influx through the opened axon[43,44] and a late second wave which occurs after a lag phase that acts throughout the entire distal axon[39,41,43,45]. This later wave requires extracellular calcium and activation of ion channels[39].

Before introducing pharmacological or genetic manipulations, we wanted to confirm the presence of a late-stage calcium event by imaging axons far from the cut site. We therefore initiated WD by blade axotomy in DRG axons. An hour later, we changed to Ca^{2+}-free media. We loaded the cells with Fluo-4 and imaged three hours after axotomy (Figure 3.1A). We confirm that axotomy causes a late stage calcium rise in axons that is abolished by removal of extracellular calcium (Figure 3.1B)[41,45].

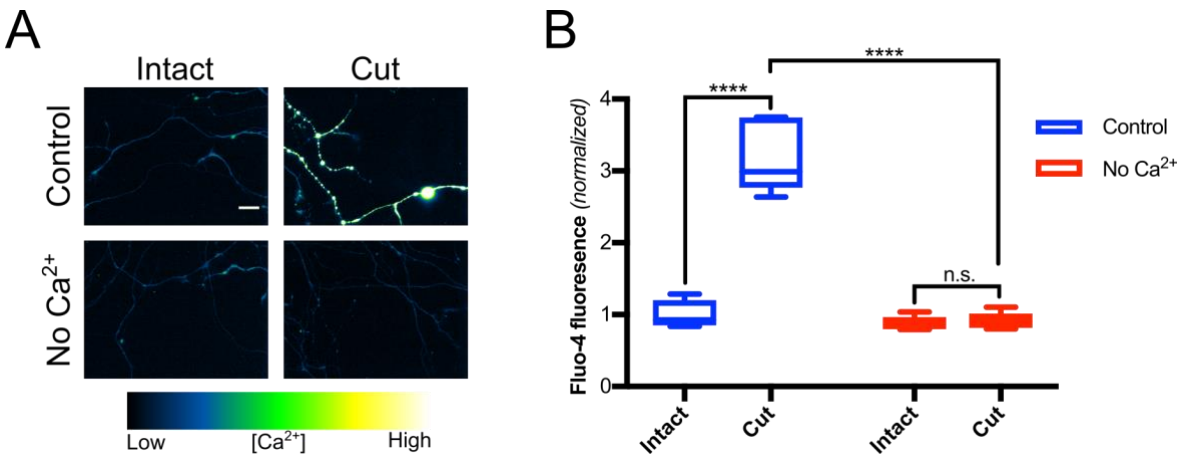

Figure 3.1. Axotomy increases axoplasmic calcium levels. Cultured DRG neurons were either transected, separating the distal axons from the cell soma, or left intact. One hour later, the media was changed to Ca^{2+}-containing HBSS (Control) or Ca^{2+}-free HBSS (No Ca^{2+}). Neurons were loaded with the fluorescent Ca^{2+} sensor dye fluo-4 and imaged (See Materials and Methods) (A; scale bar indicates 25 μm). Intra-axonal [Ca^{2+}] was assessed through fluorescence microscopy by determining fluo-4 intensity (B). Data from DRGs of n = 6 embryos per condition are presented (boxplots indicate median, 25%, 75% percentile and min/max). ****P<0.0001 (two-factor ANOVA, $F_{axotomy}$ (1, 20) = 100.3, P<0.0001, $F_{treatment}$ (1, 20) = 115.3, P<0.0001, followed by Tukey's post-hoc comparison).

Despite the prominent role of calcium in WD, the mechanism of initiation of the later calcium wave is unknown and the full suite of calcium channels activated during this process have yet to be identified[43,132]. Since TRPV1 has been shown to cause axon death in different degeneration contexts (Johnstone et al, in preparation)[68] we hypothesized that TRPV1 contributes to the late-stage calcium rise in WD. We therefore pretreated DRGs with either capsazepine (CPZ), which blocks TRPV1, or nifedipine (Nif), which blocks L-type calcium channels, and initiated WD by blade axotomy. Three hours after transection, we imaged Fluo-4-loaded axons (Figure 3.2A). We confirm that inhibition of L-type channels, a group of calcium channels previously shown to be involved in this process[39], significantly reduces axotomy-induced calcium rise and we

show, for the first time, that inhibition of TRPV1 causes a reduction in axotomy-induced calcium rise as well (Figure 3.2B).

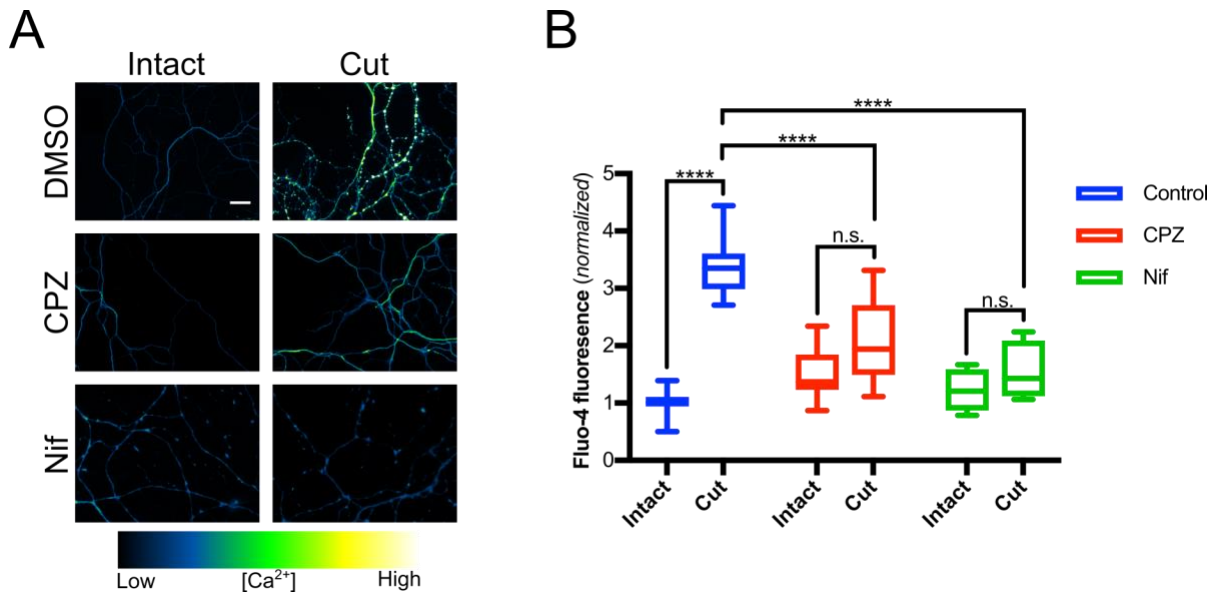

Figure 3.2. Pharmacological inhibition of TRPV1 and L-type channels reduces calcium influx after axotomy. Cultured DRG neurons were either transected or left intact. Thirty minutes prior to transection, neurons were treated with capsazepine (CPZ), nifedipine (Nif) or DMSO (DMSO). Neurons were loaded with the fluorescent Ca^{2+} sensor dye fluo-4 and imaged (See Materials and Methods) (A; scale bar indicates 25 μm). Intra-axonal [Ca^{2+}] was assessed through fluorescence microscopy by determining fluo-4 intensity (B). Data from control DRGs of n = 10 embryos, CPZ-treated DRGs of n = 8 embryos and Nif-treated DRGs of n = 6 embryos are presented (boxplots indicate median, 25%, 75% percentile and min/max). ****P<0.0001 (two-factor ANOVA, $F_{axotomy}$ (1, 42) = 57.46, P<0.0001, $F_{treatment}$ (2, 42) = 9.909, P=0.0003, followed by Tukey's post-hoc comparison).

Since TRPV1 inhibition reduces calcium influx, we hypothesized that this would therefore protect axons from degeneration. To test this, we grew cells on porous membranes and pretreated them with either capsazepine (CPZ) or nifedipine (Nif). We initiated WD by scraping away the

soma and processed axons for tubulin immunostaining six hours later (Figure 3.3A). We then recorded axon density traces with respect to distance from the center of the explant (Figure 3.3B and 3.3C). We confirm that inhibition of L-type channels significantly reduces axotomy-induced axon degeneration as expected[39] and we show, for the first time, that inhibition of TRPV1 significantly protects axons from degeneration after axotomy.

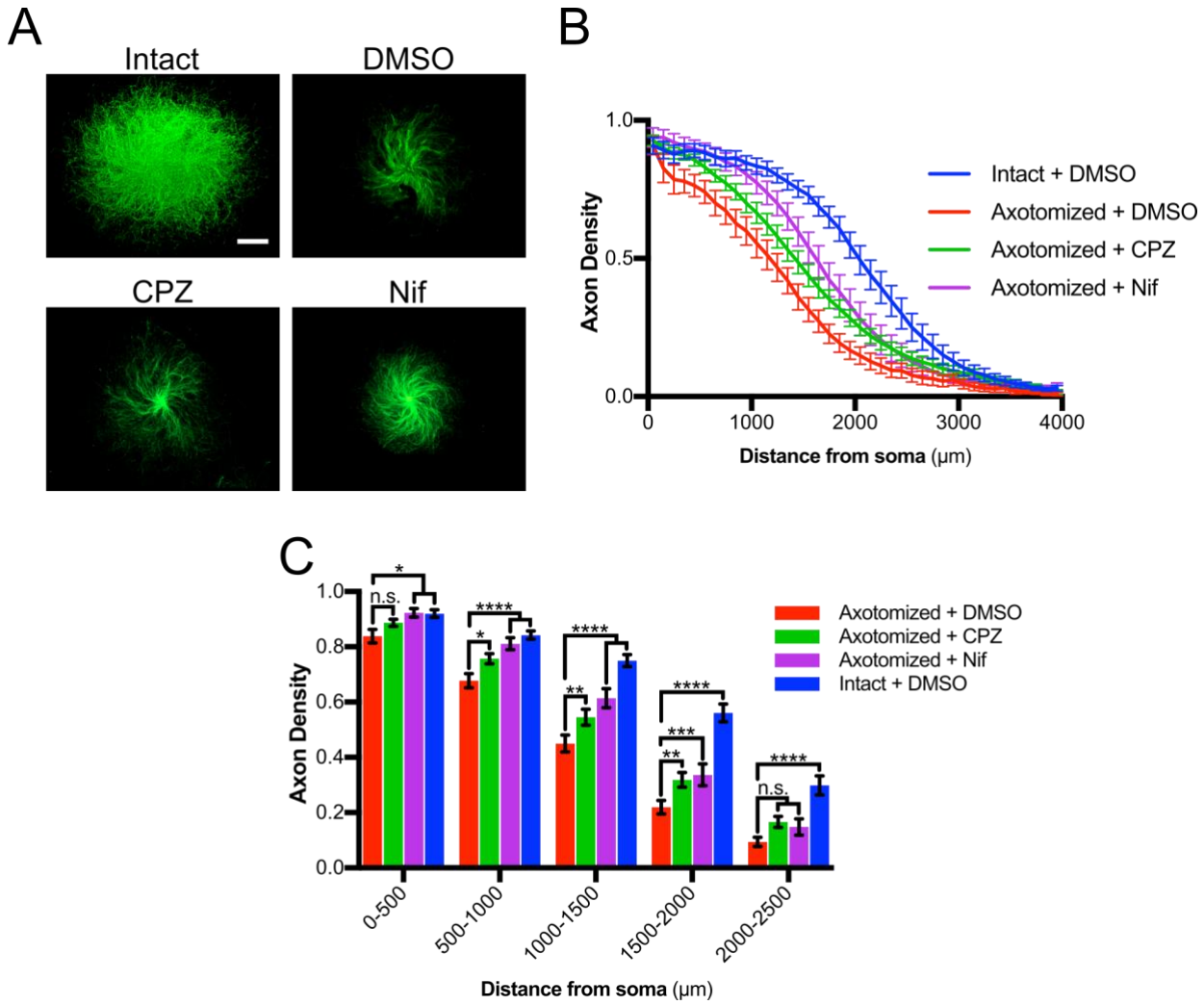

Figure 3.3. Pharmacological inhibition of TRPV1 and L-type channels reduces axotomy-induced degeneration. DRG neurons cultured on porous filters were either left intact and treated with DMSO (Intact + DMSO) or scraped on the side of the filter with cell soma in the presence of DMSO (Axotomized + DMSO), capsazepine (Axotomized + CPZ) or nifedipine (Axotomized + Nif). Filters were fixed after 6 hours of treatment and the axon sides were processed for tubulin immunostaining and imaged (A; scale indicates 1 mm). Axon density was assessed in 100 µm bins to generate a curve (B) or in 500 µm bins for statistical analysis (C). Data from axotomized + CPZ-treated DRGs of n = 17 embryos, intact + DMSO-treated as well as axotomized + Nif-treated DRGs of n = 16 embryos and axotomized + DMSO-treated DRGs of n =13 embryos are presented (means ± S.E.M.). ****P<0.0001, ***P<0.001, **P<0.01, *P<0.05 relative to Axotomized + DMSO (two-factor ANOVA with repeated measures on distance from soma, $F_{distance}$ (4, 232) = 990.1, P<0.0001, $F_{treatment}$ (3, 58) = 20.56, P<0.0001, followed by Dunnett's post-hoc analysis). Statistical analysis was completed on the entire curve (0 – 4000 µm from soma) however only 0 – 2500 µm from soma are presented in C.

We next evaluated the effects of TRPV1 inhibition on transected axons using a genetic knockout model. We initiated WD in *Trpv1*$^{+/+}$ and *Trpv1*$^{-/-}$ DRG cultures by blade axotomy and imaged using Fluo-4 three hours later (Figure 3.4A). Here we demonstrate that genetic knockout of *Trpv1* significantly reduces calcium rise in transected axons (Figure 3.4B).

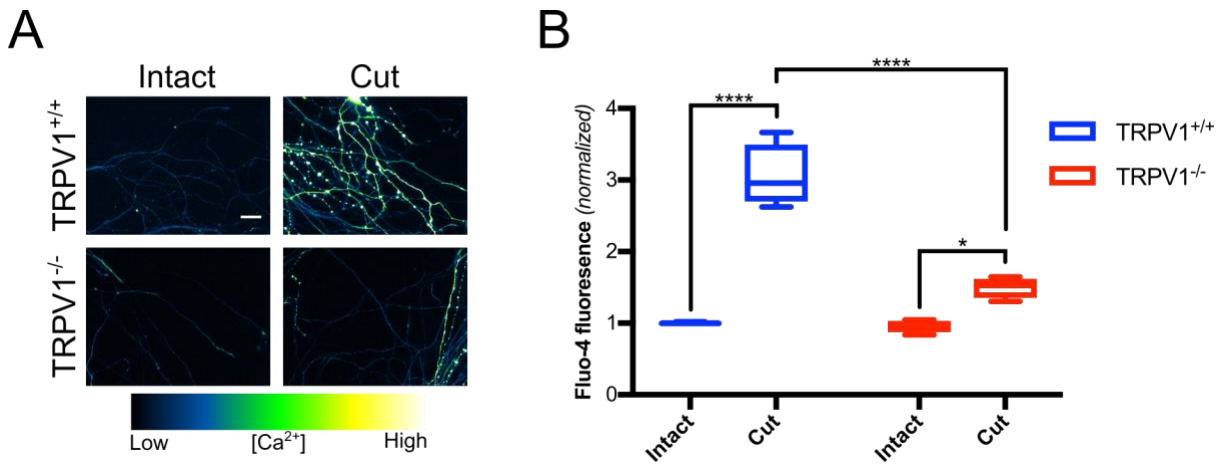

Figure 3.4. Axotomy induces calcium influx through TRPV1. Cultured DRG neurons from mixed-genotype litters of *Trpv1* knockout mice were either transected or left intact. Neurons were loaded with the fluorescent Ca^{2+} sensor dye fluo-4 and imaged (See Materials and Methods) (A; scale bar indicates 25 μm). Intra-axonal [Ca^{2+}] was assessed through fluorescence microscopy by determining fluo-4 intensity (B). Data from DRGs of n = 4 embryos per condition are presented (boxplots indicate median, 25%, 75% percentile and min/max). ****P<0.0001, *P<0.05 (two-factor ANOVA, $F_{axotomy}$ (1, 12) = 121.2, P<0.0001, $F_{treatment}$ (1, 12) = 45.5, P<0.0001, followed by Tukey's post-hoc comparison).

We also hypothesized that transected axons of a *Trpv1* knockout background would be protected from degeneration. To evaluate this, we grew *Trpv1*$^{+/+}$ and *Trpv1*$^{-/-}$ DRGs on porous filters and scraped away the cell soma to initiate WD. Six hours later, we processed axons for tubulin immunostaining (Figure 3.5A). Here we show that genetic knockout of *Trpv1* partially protects axons from degeneration after transection (Figure 3.5B), confirming the involvement of TRPV1 in WD.

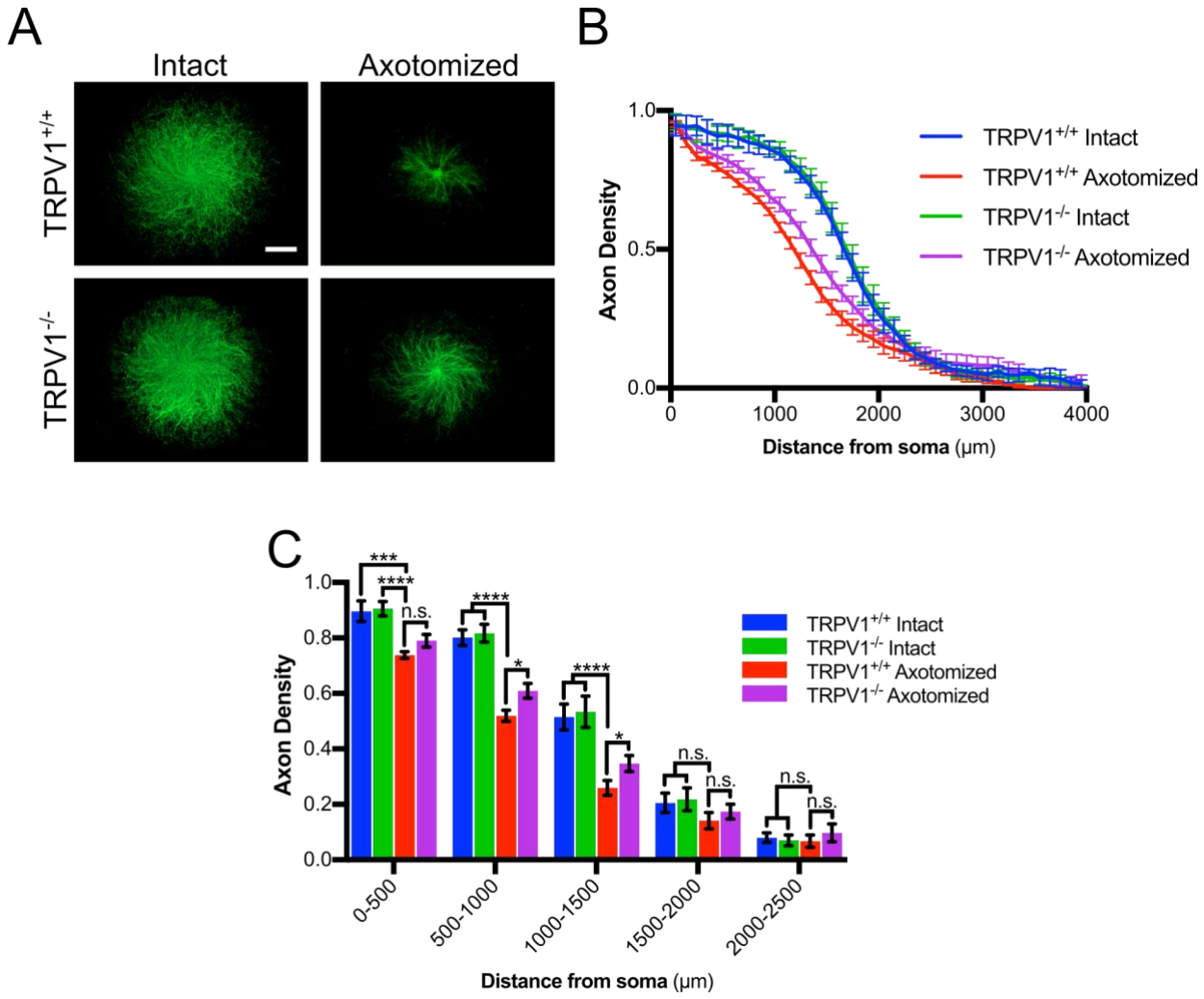

Figure 3.5. *Trpv1* knockout reduces axotomy-induced degeneration. DRG neurons from mixed-genotype litters of *Trpv1* knockout mice were cultured on porous filters were either left intact on both sides (*Trpv1*$^{+/+}$ Intact, *Trpv1*$^{-/-}$ Intact) or scraped on the side with cell soma (*Trpv1*$^{+/+}$ Axotomized, *Trpv1*$^{-/-}$ Axotomized). Filters were fixed after 6 hours of treatment and the axon sides were processed for tubulin immunostaining and imaged (A; scale indicates 1 mm). Axon density was assessed in 100 μm bins to generate a curve (B) or in 500 μm bins for statistical analysis (C). Data from axotomized *Trpv1*$^{+/+}$ and *Trpv1*$^{-/-}$ DRGs of n = 6 embryos or intact *Trpv1*$^{+/+}$ and *Trpv1*$^{-/-}$ DRGs of n = 3 embryos are presented (means ± S.E.M.). ****P<0.0001, *P<0.05 relative to *Trpv1*$^{+/+}$ Axotomized (two-factor ANOVA with repeated measures on distance from soma, $F_{distance}$ (4, 56) = 880.2, P<0.0001, $F_{treatment}$ (3, 14) = 10.96, P=0.0006, followed by Dunnett's post-hoc analysis). Statistical analysis was completed on the entire curve (0 – 4000 μm from soma) however only 0 – 2500 μm from soma are presented in C.

3.2. Determine the Mechanism of Calcium Channel Activation in Wallerian Degeneration

3.2.1. Investigate the role of ROS in axotomy-induced calcium rise

The mechanism of late stage calcium channel activation after axotomy is unknown. However now that a role for TRPV1, a ROS-sensitive channel, has been established, we hypothesized that ROS are required for axotomy-induced calcium influx. To evaluate this, we pretreated DRGs with NAC, a ROS scavenger that is commonly used to study the role of ROS in axons[82,133,134] and initiated WD by blade axotomy. Three hours later, we imaged Fluo-4-loaded axons (Figure 3.6A). Here we observe that scavenging ROS completely abolishes axotomy-induced calcium rise in axons (Figure 3.6B), confirming a central role for ROS in Wallerian degeneration[81-84].

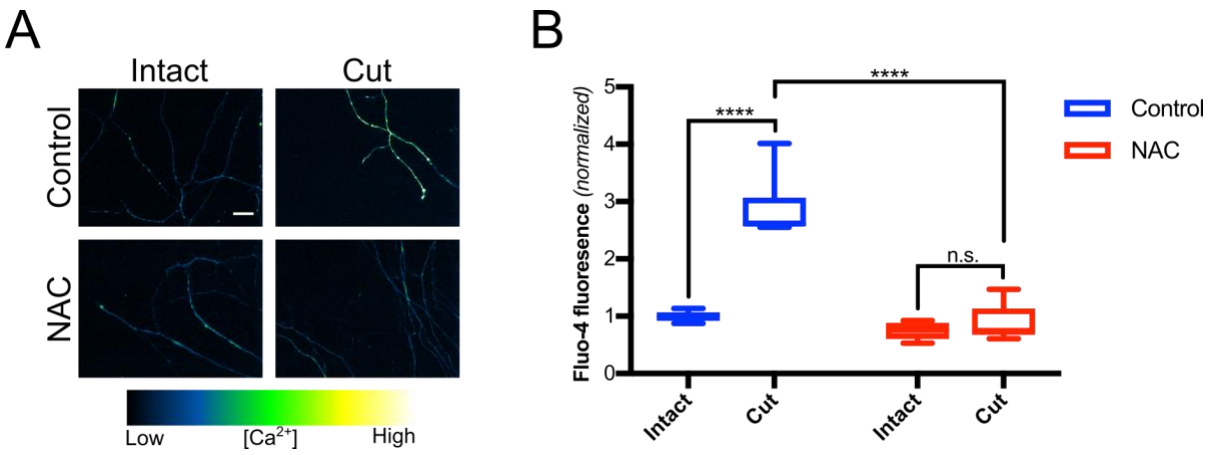

Figure 3.6. ROS scavenging prevents calcium influx after axotomy. Cultured DRG neurons were either transected or left intact in the presence of untreated media (Control) or NAC-supplemented media (NAC). Neurons were loaded with the fluorescent Ca^{2+} sensor dye fluo-4 and imaged (See Materials and Methods) (A; scale bar indicates 25 μm). Intra-axonal [Ca^{2+}] was assessed through fluorescence microscopy by determining fluo-4 intensity (B). Data from control DRGs of n = 6 embryos and NAC-treated DRGs of n = 5 embryos are presented (boxplots indicate median, 25%, 75% percentile and min/max). ****P<0.0001 (two-factor ANOVA, $F_{axotomy}$ (1, 18) = 43.22, P<0.0001, $F_{treatment}$ (1, 18) = 54.88, P<0.0001, followed by Tukey's post-hoc comparison).

Pharmacological inhibition of the Nox complex and shRNA-mediated knockdown of various Nox complex subunits has been shown to decrease ROS accumulation and protect axons after transection[82]. We therefore hypothesize that the Nox complex supplies ROS to induce calcium influx after axotomy. We pretreated DRG neurons with three well-known pharmacological Nox complex inhibitors, VAS2870, apocynin or DPI[82,135-137] then initiated WD by blade axotomy and imaged three hours later (Figure 3.7A). In contrast to previous results cited above, we observe that, at three hours after axotomy, calcium rise is not reduced by any of the three Nox complex inhibitors (3.7B).

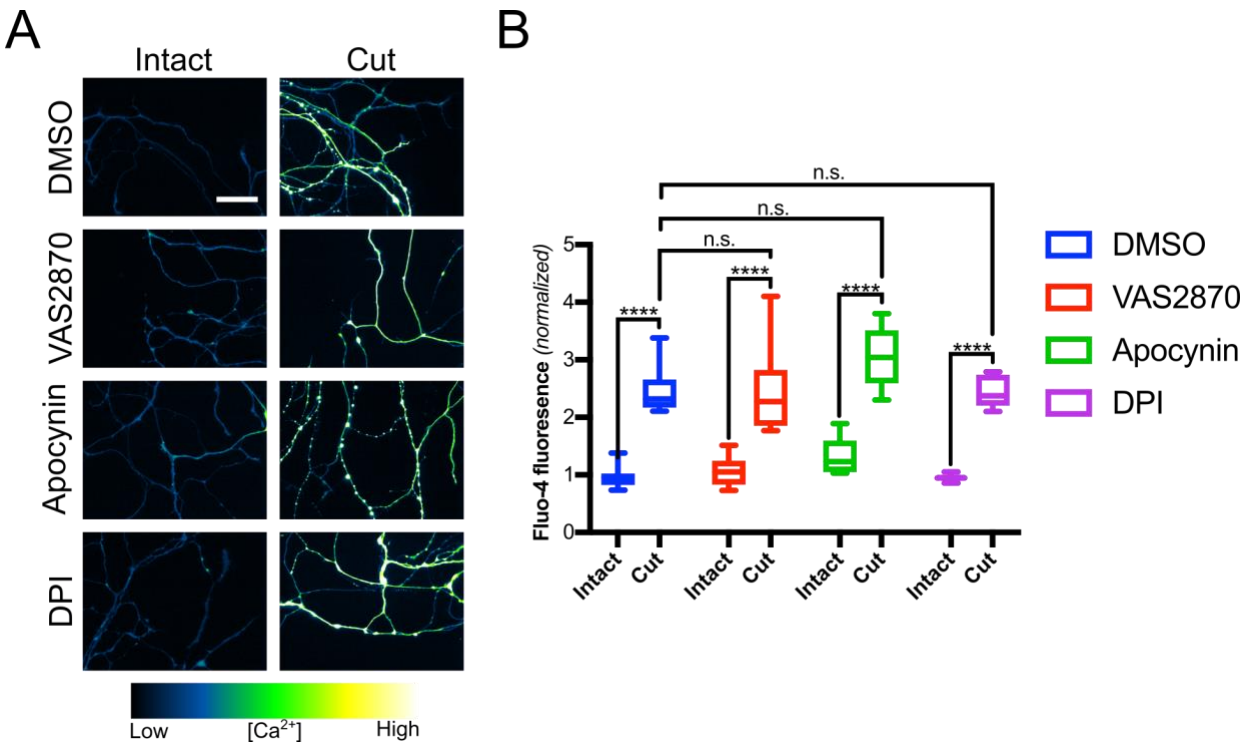

Figure 3.7. Nox complex inhibition does not reduce calcium influx following axotomy. Cultured DRG neurons were either transected or left intact in media containing VAS2870 (VAS2870), apocynin (Apocynin), diphenyleneiodonium (DPI) or DMSO (DMSO). Neurons were loaded with the fluorescent Ca^{2+} sensor dye fluo-4 and imaged (See Materials and Methods) (A; scale bar indicates 25 μm). Intra-axonal [Ca^{2+}] was assessed through fluorescence microscopy by determining fluo-4 intensity (B). Data from DMSO-treated and VAS2870-treated DRGs of n = 11 embryos as well as apocynin-treated and DPI-treated DRGs of n = 5 embryos are presented (boxplots indicate median, 25%, 75% percentile and min/max; bars indicate median and min/max). ****P<0.0001, ***P<0.001 (two-factor ANOVA, $F_{axotomy}$ (1, 56) = 185.2, P<0.0001, $F_{treatment}$ (3, 56) = 3.121, P=0.0331, followed by Tukey's post-hoc comparison).

3.2.2. Determine the effect of axotomy on mitochondria

Because the Nox complex does not appear to be responsible for the ROS-induced calcium rise three hours after axotomy, we turned our attention instead to mitochondria which are well established ROS generators[92,93,96]. It is known that axotomy causes widespread mitochondrial failure in distal axons[81,105,106,108] so we set out to establish the timing of this event relative to other

events in WD. Clarifying the temporal arrangement of mitochondrial loss, NAD^+ drop and ROS accumulation is an important investigative step because the execution phase of WD begins concurrently with a sharp drop in intra-axonal NAD^+ levels and this is considered to be the initiating insult leading to downstream degeneration[25,138]. Therefore, if NAD^+ levels are maintained after axotomy and mitochondrial loss is still observed, then these two events operate in different pathways.

In order to elucidate the timing of mitochondrial loss relative to NAD^+ loss, we first wanted to confirm the protective role of NAD^+ after axotomy using Axoquant 2.0. We therefore grew cells on porous membranes and pretreated them with NAD^+. Thirty minutes later, we scraped the top of the membrane, separating the soma from the axons below, and processed the filters for tubulin immunostaining six hours later (Figure 3.8A). We then drew traces of axon density with respect to distance from the center of the explant (Figure 3.8B and 3.8C). Here we confirm that supplementing axons with NAD^+ significantly protects axons from degeneration after transection[17-19,25].

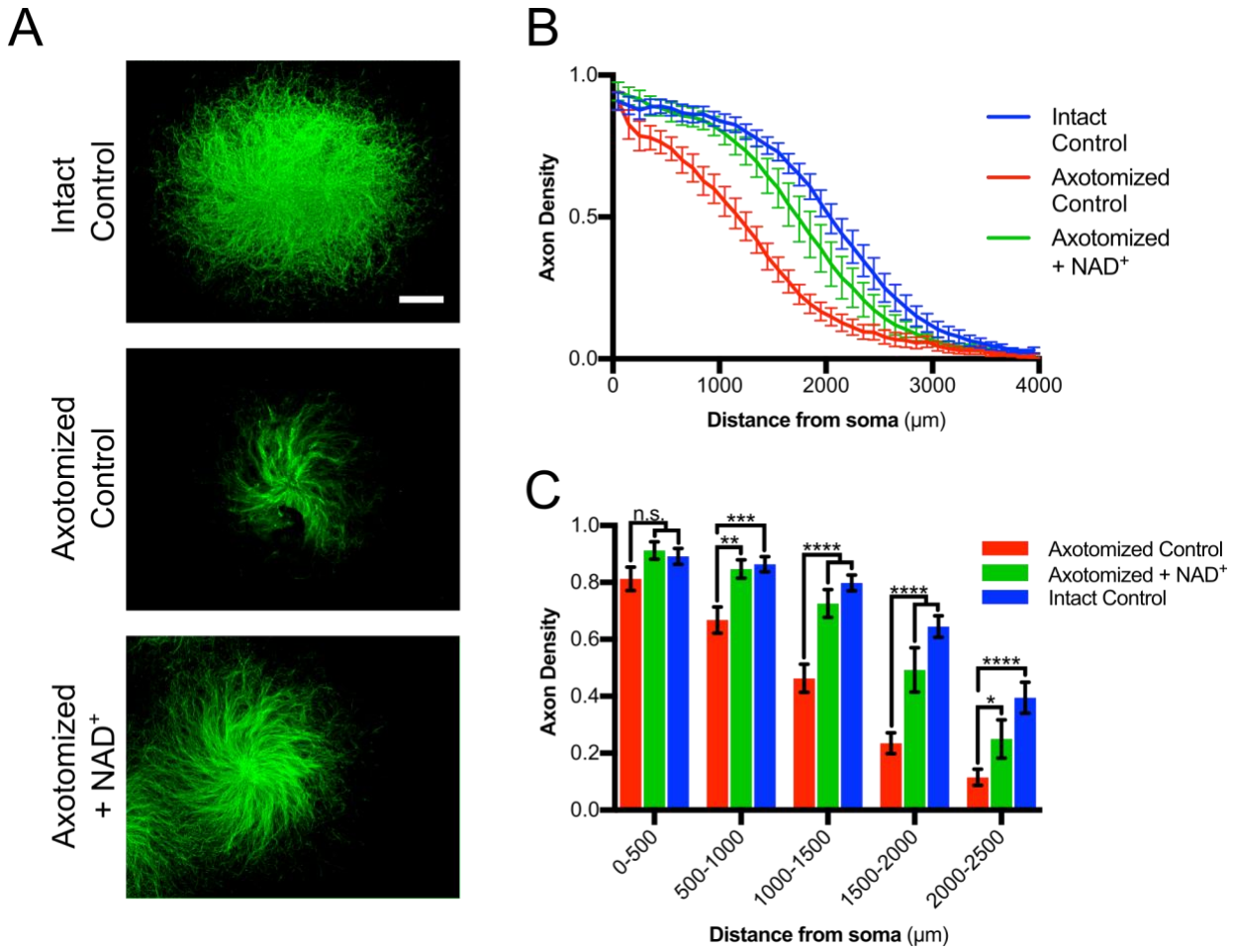

Figure 3.8. NAD$^+$ supplementation reduces axotomy-induced axonal degeneration. DRG neurons cultured on porous filters were either left intact (Intact Control) or scraped on the side with cell soma in untreated media (Axotomized Control) or in the presence of NAD$^+$ (Axotomized + NAD$^+$). Filters were fixed after 6 hours of treatment and the axon sides were processed for tubulin immunostaining and imaged (A; scale indicates 1 mm). Axon density was assessed in 100 μm bins to generate a curve (B) or in 500 μm bins for statistical analysis (C). Data from n = 7 different embryos per condition are presented (means ± S.E.M.). ****P<0.0001, ***P<0.001, **P<0.01, *P<0.05 relative to Axotomized Control (two-factor ANOVA with repeated measures on distance from soma, $F_{distance}$ (4, 72) = 169.4, P<0.0001, $F_{treatment}$ (2, 18) = 16.33, P<0.0001, followed by Dunnett's post-hoc analysis). Statistical analysis was completed on the entire curve (0 – 4000 μm from soma) however only 0 – 2500 μm from soma are presented in C.

NAD^+-mediated axon protection during WD has already been established[17-19,25] however, to our knowledge, NAD^+ supplementation has never been shown to reduce calcium influx after axotomy. We therefore hypothesized that maintaining NAD^+ levels after axotomy would prevent late stage calcium rise. To evaluate this, we pretreated DRGs with NAD^+, axotomized axons using a scalpel blade and imaged with Fluo-4 three hours later (Figure 3.9A). We observe that, at three hours after axotomy, calcium rise is completely abolished by NAD^+ supplementation (Figure 3.9B).

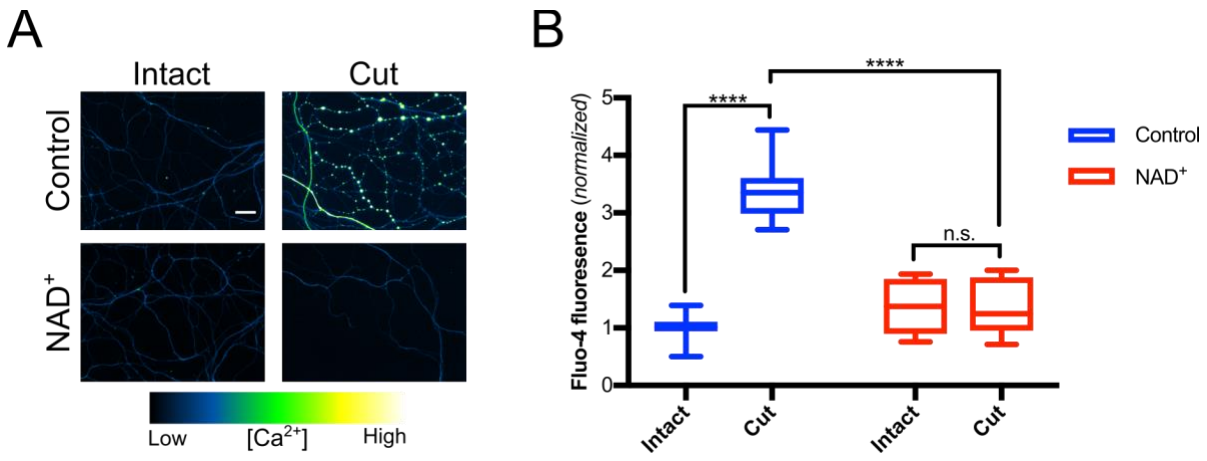

Figure 3.9. NAD^+ abolishes axotomy-induced calcium influx. Cultured DRG neurons were either transected or left intact in the presence of untreated media (Control) or NAD^+-supplemented media (NAD^+). Neurons were loaded with the fluorescent Ca^{2+} sensor dye fluo-4 and imaged (See Materials and Methods) (A; scale bar indicates 25 μm). Intra-axonal $[Ca^{2+}]$ was assessed through fluorescence microscopy by determining fluo-4 intensity (B). Data from control DRGs of n = 10 embryos and NAD^+-treated DRGs of n = 7 embryos are presented (boxplots indicate median, 25%, 75% percentile and min/max). ****P<0.0001 (two-factor ANOVA, $F_{axotomy}$ (1, 30) = 58.42, P<0.0001, $F_{treatment}$ (1, 30) = 31.22, P<0.0001, followed by Tukey's post-hoc comparison).

With the role of NAD^+ in axotomy-induced axon degeneration and calcium rise established, we now investigated the effect of NAD^+, as well as ROS scavenging, on axotomy-induced mitochondrial loss. We hypothesize that mitochondrial loss occurs downstream of the drop in NAD^+ levels and upstream of intra-axonal ROS accumulation. Therefore NAD^+ supplementation, but not ROS scavenging, should protect mitochondria from depolarization in transected axons. To address this possibility, we pretreated DRGs with either NAD^+ or NAC and axotomized using a scalpel blade. We then imaged axons loaded with Calcein-AM, an axonal marker, and TMRE, a marker of mitochondrial potential (Figure 3.10A) 3.5 hours after transection. In parallel, to obtain a readout of mitochondrial abundance in axons, we divided the area occupied by TMRE (functional mitochondrial area) by the area occupied by Calcein (axonal area) for each image (Figure 3.10B). We confirm that 3.5 hours post-axotomy, mitochondria are significantly depolarized[108]. We also show that NAD^+ supplementation rescues mitochondrial potential whereas scavenging ROS by NAC does not prevent mitochondrial depolarization after axotomy (Figure 3.10B). This places mitochondrial depolarization downstream of NAD^+ loss but upstream of axoplasmic ROS accumulation after the lag phase in WD.

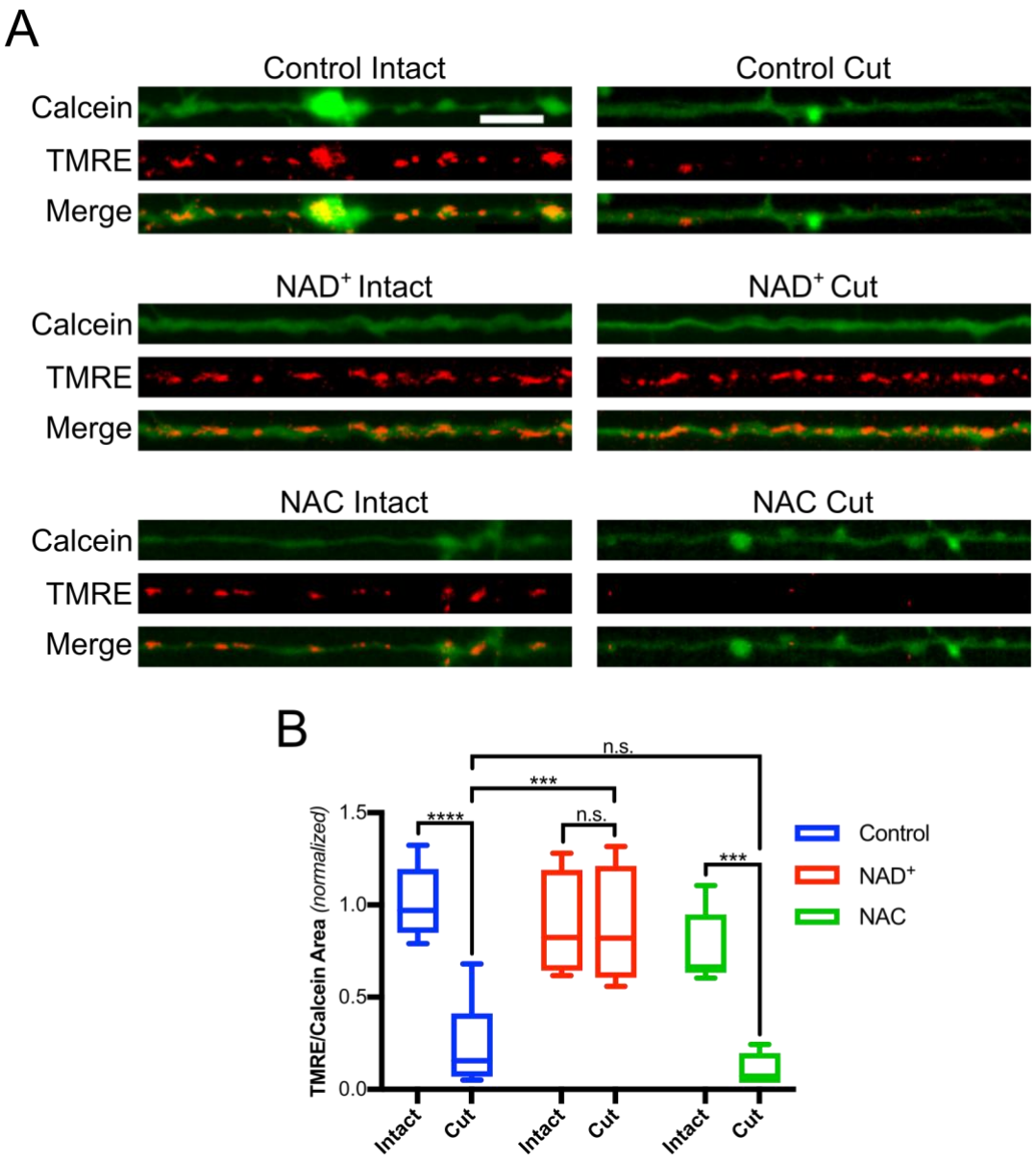

Figure 3.10. Axotomy causes widespread mitochondrial depolarization that is prevented by NAD+ but not by ROS scavenging. Cultured DRG neurons were either transected or left intact in untreated media (Control), NAD^+-supplemented media (NAD^+) or NAC-supplemented media (NAC). Neurons were loaded with the mitochondrial dye tetramethylrhodamine (TMRE) and a neuronal marker dye Calcein. Cells were imaged 3 hours after transection (scale bar indicates 10 μm). Representative axons were cropped and straightened in A. Cross-sectional area occupied by functional mitochondria (TMRE signal) was divided by total axonal area (Calcein signal) in each field to obtain a readout of mitochondrial abundance (B). Data from control DRGs of n = 10 embryos, NAC-treated DRGs of n = 5 embryos and NAD^+-treated DRGs of n = 4 embryos are presented (boxplots indicate median, 25%, 75% percentile and min/max). ****P<0.0001,

***P<0.001 (two-factor ANOVA, $F_{axotomy}$ (1, 32) = 38.84, P<0.0001, $F_{treatment}$ (2, 32) = 9.172, P=0.0007 followed by Tukey's post-hoc comparison).

3.2.3. Elucidate the effect of mitochondrial depolarization in axonal degeneration

In order to evaluate the effect of mitochondrial loss, we induced mitochondrial depolarization in DRGs using CCCP, a protonophore of the inner mitochondrial membrane that is widely used to study the effects of altered mitochondrial potential on cellular viability[139]. We hypothesized that widespread mitochondrial depolarization would mimic the insult of axotomy and therefore cause axon degeneration that requires calcium and ROS. To evaluate this, we pretreated cells with NAC, EGTA (which is a potent calcium chelator), or unsupplemented control media and then applied CCCP. After five hours we processed the DRGs for tubulin immunostaining (Figure 3.11A), recorded axon density and generated traces with respect to distance from the center of the explant (Figure 3.11B and 3.11C). Here we show that loss of mitochondrial potential causes significant degeneration in DRG axons. We also show that calcium chelation with EGTA or ROS scavenging with NAC significantly reduces CCCP-induced axonal degeneration. This would suggest that axonal degeneration after mitochondrial loss is at least in part due to calcium- and ROS-mediated activity and not simply loss of energetic function.

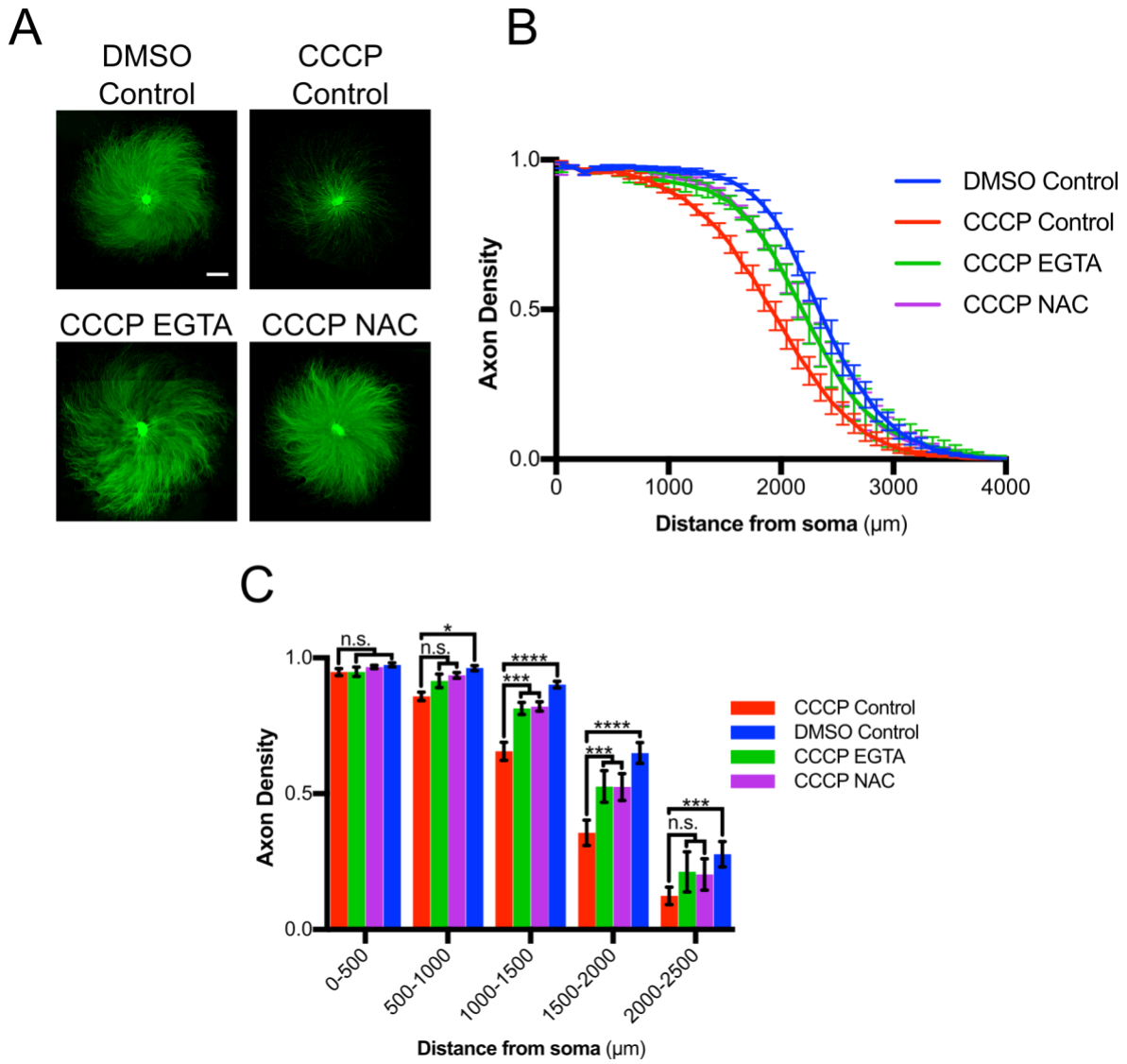

Figure 3.11. CCCP causes axonal cytoskeleton fragmentation and degeneration that is ROS- and calcium-dependent. Cultured DRG neurons were treated with either DMSO (DMSO Control) or with carbonyl cyanide m-chlorophenyl hydrazine (CCCP) in the presence of EGTA-supplemented (CCCP EGTA), NAC-supplemented (CCCP NAC) or untreated media (CCCP control). Filters were fixed after 5 hours of treatment and were processed for tubulin immunostaining and imaged (A; scale indicates 1 mm). Axon density was assessed in 100 µm bins to generate a curve (B) or in 500 µm bins for statistical analysis (C). Data from DMSO control as well as CCCP control DRGs of n = 9 embryos and CCCP + EGTA-treated as well as CCCP + NAC-treated DRGs of n = 8 embryos are presented (means ± S.E.M.). ****P<0.0001, ***P<0.001, *P<0.05 relative to CCCP Control (two-factor ANOVA with repeated measures on distance from soma, $F_{distance}$ (4, 120) = 418.2, P<0.0001, $F_{treatment}$ (3, 30) = 10.78, P<0.0001,

followed by Dunnett's post-hoc analysis). Statistical analysis was completed on the entire curve (0 – 4000 μm from soma) however only 0 – 2500 μm from soma are presented in C.

We observed that ROS and Ca^{2+} are involved in the degeneration process after axotomy as well as after mitochondrial depolarization by CCCP. Since we previously showed that TRPV1 and L-type channels are involved in WD (Figure 3.2 – 3.5), we hypothesized that CCCP-induced axon degeneration would be reduced by inhibition of TRPV1 or L-type channels as well. To assess this, we pretreated DRGs with capsazepine (CPZ) or nifedipine (Nif) and then applied CCCP. After five hours we processed the DRGs for tubulin immunostaining and imaging (Figure 3.12A-C). Here we show that TRPV1 and L-type channel inhibition significantly protect axons from degeneration after CCCP application. Taken together, these data suggest that degeneration occurring as a result of CCCP results from ROS-dependent activation of TRPV1 and L-type calcium channels.

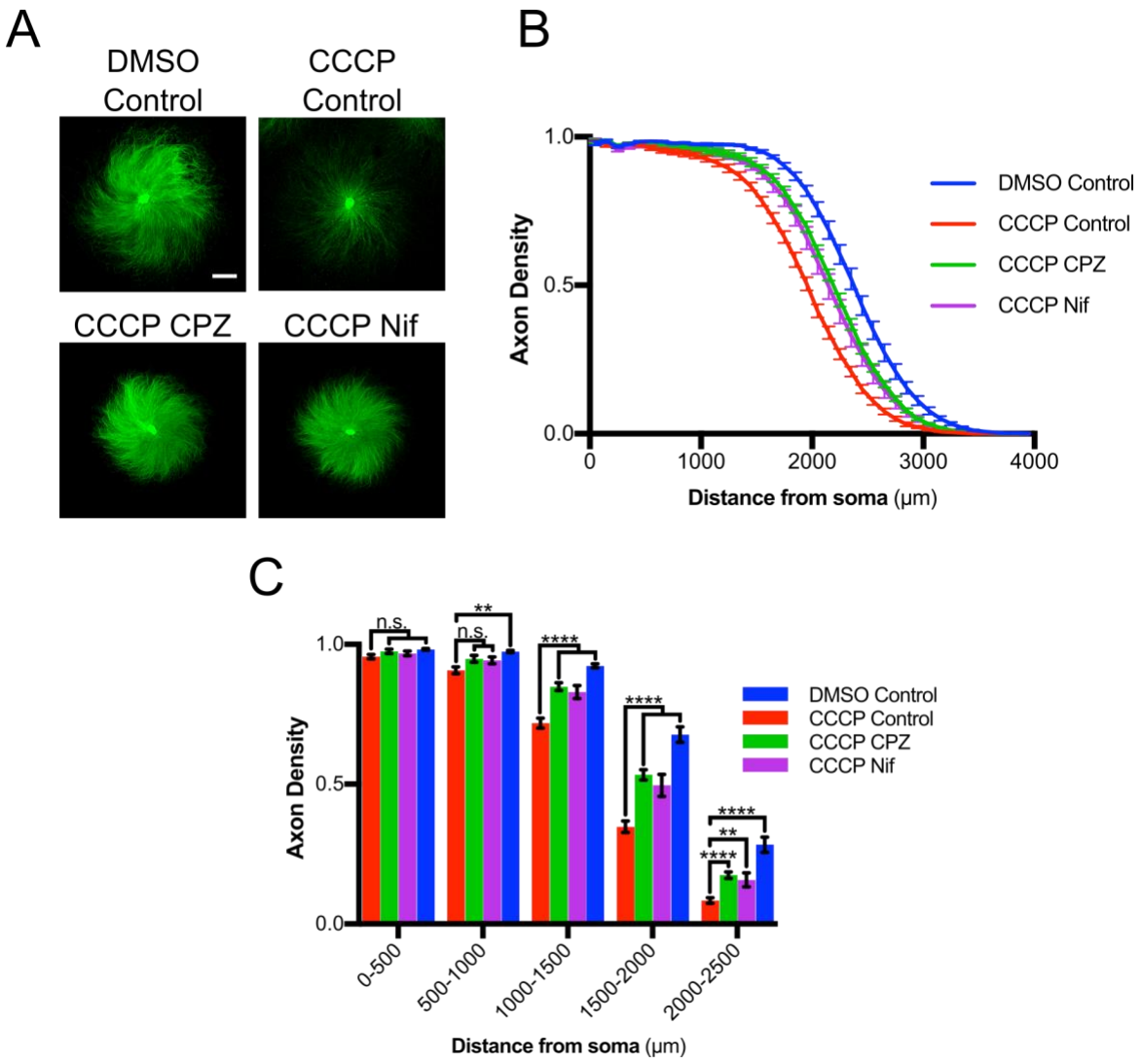

Figure 3.12. Axon degeneration from mitochondrial dysfunction is reduced by inhibition of TRPV1 and L-type channels. Cultured DRG neurons were either treated with DMSO (DMSO Control) or treated with CCCP in the presence of capsazepine (CCCP CPZ), nifedipine (CCCP Nif) or DMSO (CCCP control). Filters were fixed after 5 hours of treatment and were processed for tubulin immunostaining and imaged (A; scale indicates 1 mm). Axon density was assessed in 100 µm bins to generate a curve (B) or in 500 µm bins for statistical analysis (C). Data from DRGs of n = 9 embryos for each group are presented (means ± S.E.M.). ****P<0.0001, **P<0.01 relative to CCCP Control (two-factor ANOVA with repeated measures on distance from soma, $F_{distance}$ (4, 128) = 2317, P<0.0001, $F_{treatment}$ (3, 32) = 27.6, P<0.0001, followed by Dunnett's post-hoc analysis). Statistical analysis was completed on the entire curve (0 – 4000 µm from soma) however only 0 – 2500 µm from soma are presented in C.

3.2.4. Elucidate the effect of mitochondrial depolarization on calcium influx

To assess the effects of CCCP on axons more closely, we evaluated the acute outcome of CCCP on mitochondrial potential and calcium levels in the axon. Mitochondria act as calcium stores in the healthy cell and mitochondrial depolarization releases these stores in the cytosol[140]. However, the role of extracellular calcium in mitochondrial depolarization-induced calcium rise has not been established. We therefore incubated DRGs in Ca^{2+}-free media and loaded them with TMRE and Fluo-4 then live imaged axons while applying CCCP to the culture (Figure 3.13A). We then quantified and plotted TMRE and Fluo-4 with respect to time (Figure 3.13B and Figure 3.13C respectively).

We found that CCCP causes a rapid loss of mitochondrial potential that is sustained for the duration of the imaging period (Figure 3.13B). Furthermore, removal of calcium from the extracellular environment does not seem to affect the depolarization rate (Figure 3.13B). CCCP causes a rapid calcium rise and fall followed by a plateau phase where calcium levels are above baseline but below the level of the initial spike (Figure 3.13C; quantified in 3.13D). Interestingly, this effect is abolished in axons incubated in Ca^{2+}-free media, suggesting that the calcium rise relies on Ca^{2+} influx from the extracellular space (Figure 3.13C; quantified in 3.13D).

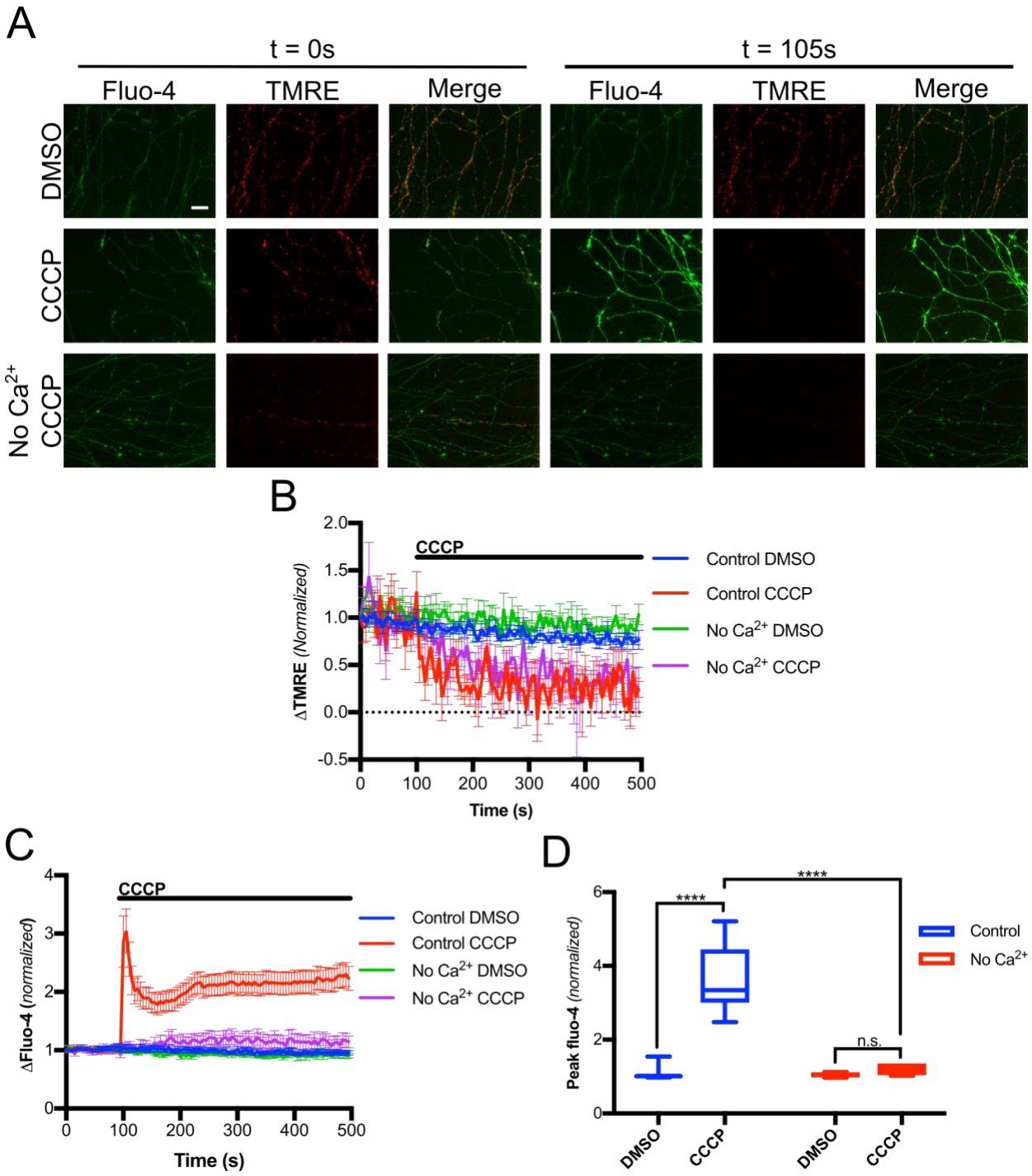

Figure 3.13. CCCP rapidly depolarizes mitochondria causing calcium influx. Cultured DRG neurons were incubated in Ca^{2+}-containing HBSS (Control) or Ca^{2+}-free HBSS (No Ca^{2+}) and were loaded with the mitochondrial dye tetramethylrhodamine (TMRE) and with the fluorescent Ca^{2+} sensor dye Fluo-4 for imaging. Cells were treated with either CCCP or DMSO during live imaging (A, scale bar indicates 25 μm) and traces of TMRE intensity (B; means ± S.E.M.) and Fluo-4

intensity (C; means ± S.E.M.) were generated for a total of t = 500s. Peak Fluo-4 values from t = 100 – 150s were extrapolated for each condition (D; boxplots indicate median, 25%, 75% percentile and min/max). Data from DRGs of n = 8 independent control experiments and n = 4 independent "No Ca^{2+}" experiments are presented. ****P<0.0001 (two-factor ANOVA, F_{CCCP} (1, 20) = 32.66, P<0.0001, $F_{treatment}$ (1, 20) = 26.97, P<0.0001, followed by Tukey's post-hoc comparison).

In light of the finding that CCCP treatment induces an axonal calcium influx, we evaluated whether this process shows a dependence on ROS. We therefore treated DRGs with NAC, loaded them with TMRE and Fluo-4 and then live-imaged axons while applying CCCP (Figure 3.14A). We observe here that pretreating cells with NAC significantly reduces the CCCP-induced calcium rise in axons (Figure 3.14B; quantified in 3.14C). Furthermore, the plateau level after the initial calcium spike in NAC-treated axons appears indistinguishable from the baseline. This suggests that ROS plays a central role in the calcium rise induced by mitochondrial depolarization.

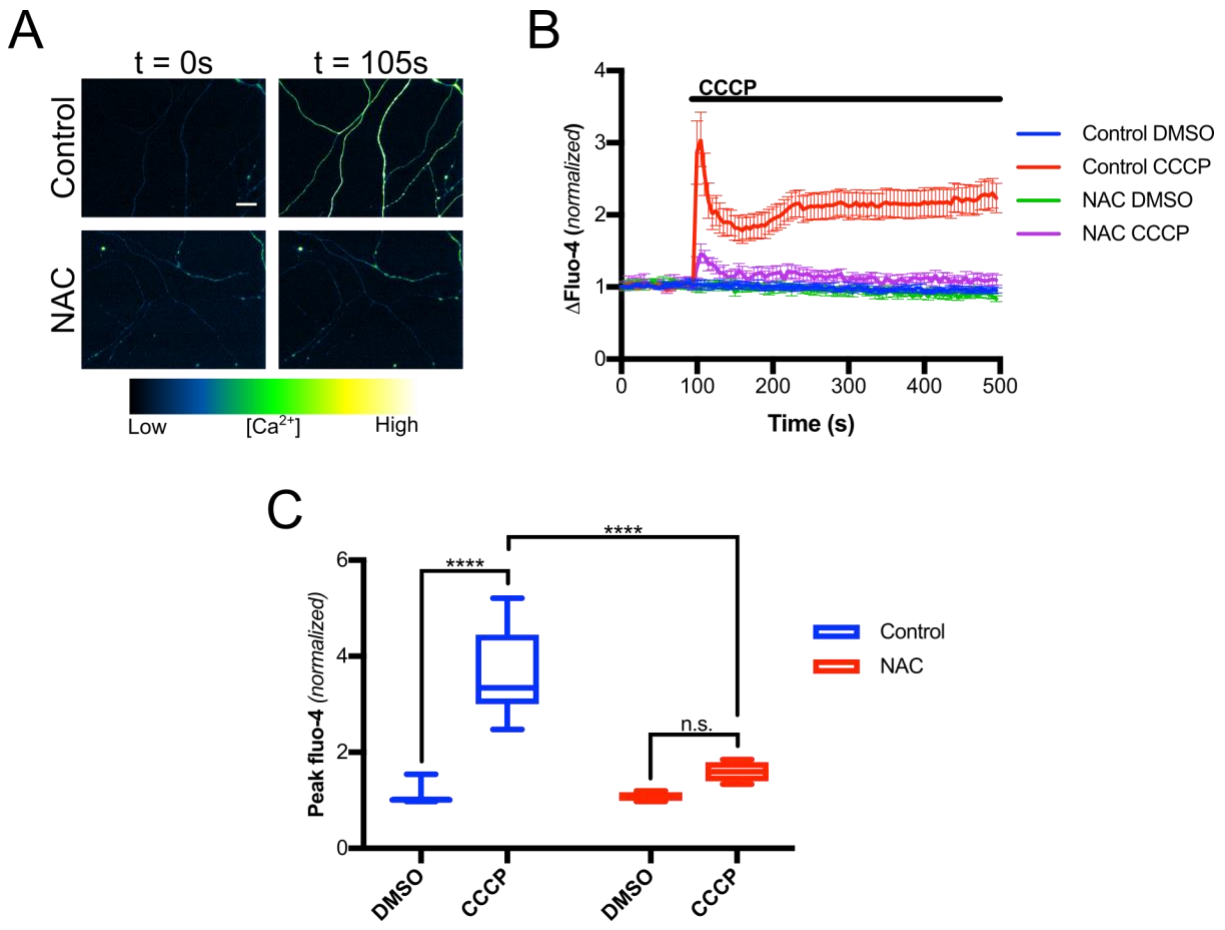

Figure 3.14. ROS is required for calcium influx following mitochondrial depolarization. Cultured DRG neurons were incubated in untreated HBSS (Control) or NAC-containing HBSS (NAC) and were loaded with a dye that fluoresces in functional mitochondria TMRE and with the fluorescent Ca^{2+} sensor dye fluo-4 for imaging. Cells were treated with either CCCP or DMSO during live imaging (A, scale bar indicates 25 μm) and traces of TMRE intensity (not shown) and Fluo-4 intensity (B; means ± S.E.M.) were generated for a total of t = 500s. Peak Fluo-4 values from t = 100 – 150s were extrapolated for each condition (C; boxplots indicate median, 25%, 75% percentile and min/max). Data from DRGs of n = 8 independent control experiments and 4 independent NAC experiments are presented. ****P<0.0001 (two-factor ANOVA, F_{CCCP} (1, 20) = 41.73, P<0.0001, $F_{treatment}$ (1, 20) = 18.37, P=0.0004, followed by Tukey's post-hoc comparison).

Since CCCP-induced calcium rise appeared to operate similarly to after axotomy, in that they both require ROS and extracellular Ca^{2+}, we next evaluated the role of TRPV1 and L-type

channels in this process. We treated DRGs with CPZ or nifedipine, loaded them with TMRE and Fluo-4 and then live-imaged axons while applying CCCP (Figure 3.14A). We show here that axons pretreated with CPZ display a significantly lower calcium peak, immediately after mitochondrial depolarization, though still significantly higher than the untreated CPZ control (Figure 3.15B). Furthermore, the calcium plateau in CPZ-treated axons is at a level indistinguishable from the CCCP control (Figure 3.15C). In nifedipine-treated axons, CCCP does not induce a significant immediate calcium rise (Figure 3.15A) and this is followed by a lower plateau. This implicates TRPV1 and L-type channels, the same channels that play a role in axotomy, as being involved in the calcium rise that occurs after mitochondrial depolarization.

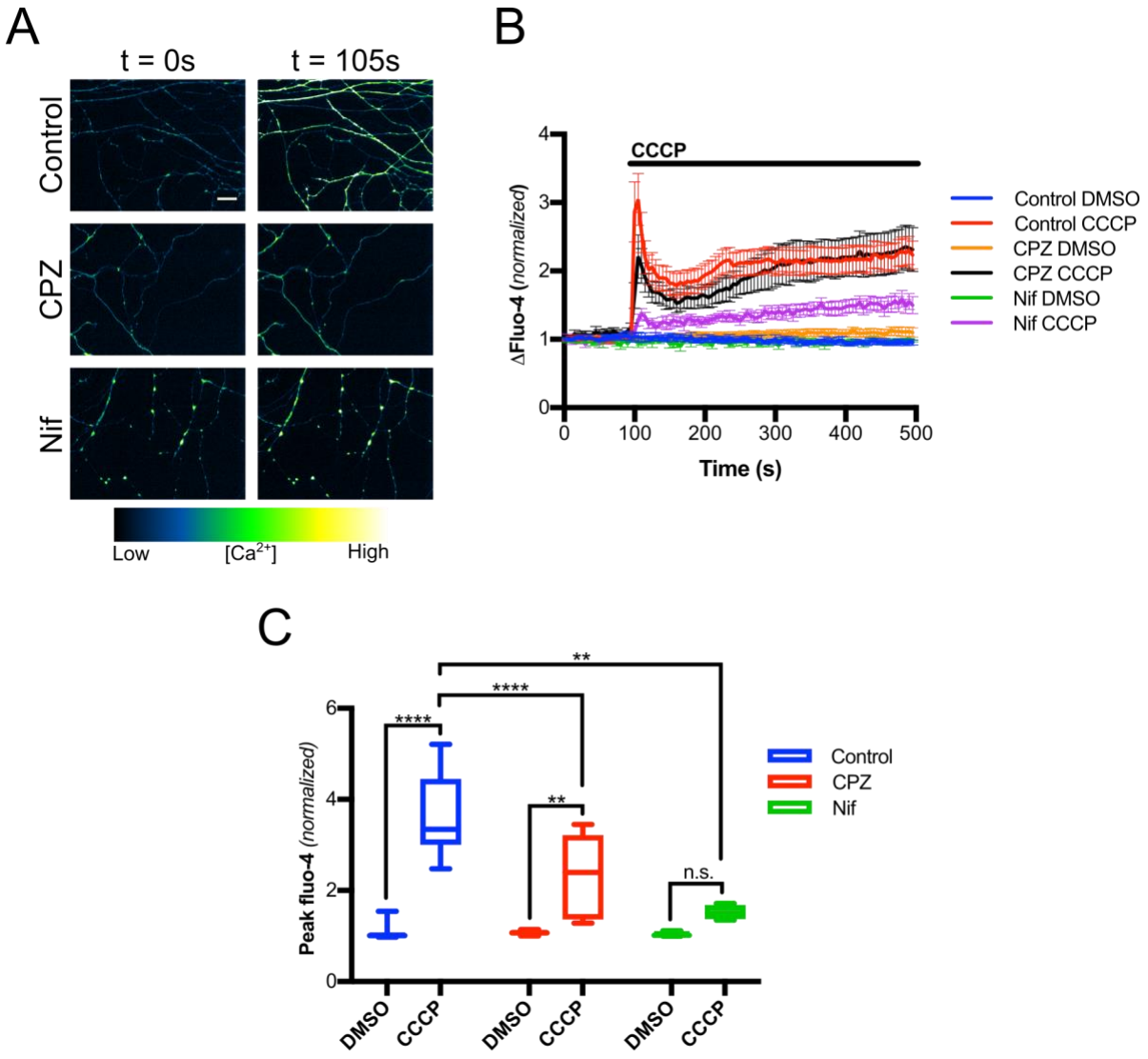

Figure 3.15. Pharmacological inhibition of TRPV1 and L-type channels reduces calcium influx following mitochondrial depolarization. Cultured DRG neurons were incubated in HBSS containing DMSO (Control), capsazepine (CPZ) or nifedipine (Nif) and were loaded with the mitochondrial dye tetramethylrhodamine (TMRE) and with the fluorescent Ca^{2+} sensor dye Fluo-4 for imaging. Cells were treated with either CCCP or DMSO during live imaging (A, scale bar indicates 25 µm) and traces of TMRE intensity (not shown) and Fluo-4 intensity (B; means ± S.E.M.) were generated for a total of t = 500s. Peak Fluo-4 values from t = 100 – 150s were extrapolated for each condition (C; boxplots indicate median, 25%, 75% percentile and min/max). Data from DRGs of n = 8 independent control experiments, n = 6 independent CPZ-treated experiments or 4 independent Nif-treated experiments are presented. ****P<0.0001, **P<0.01 (two-factor ANOVA, F_{CCCP} (1, 22) = 46.34, P<0.0001, $F_{treatment}$ (2, 22) = 8.891, P=0.0015, followed by Tukey's post-hoc comparison).

In light of the observed effect of TRPV1 inhibition on CCCP-induced calcium rise, we next evaluated the role of TRPV1 by genetic knockout. We plated *Trpv1*$^{+/+}$ or *Trpv1*$^{-/-}$ DRGs, loaded them with TMRE and Fluo-4 and live-imaged them while applying CCCP followed by a final application of capsaicin (Cap), a potent and specific agonist of TRPV1, in order to validate the expression, or lack thereof, of TRPV1 in the axons being imaged (Figure 3.16A). We show here that genetic knockout of *Trpv1* significantly reduces calcium rise in axons after CCCP treatment (Figure 3.16B; quantified in 3.16C). Thus, TRPV1 is a significant target of activation following mitochondrial depolarization.

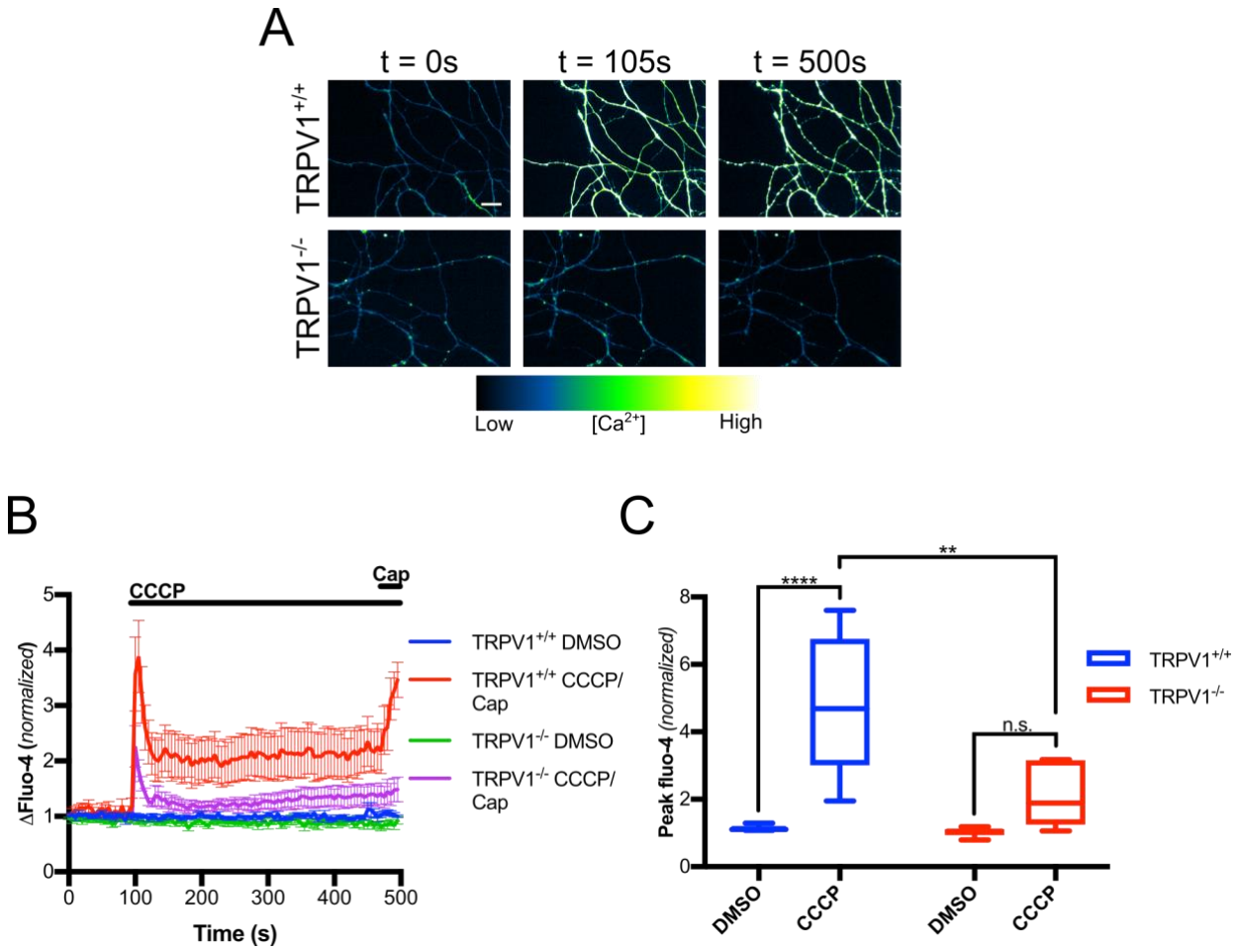

Figure 3.16. Mitochondrial depolarization causes calcium influx through TRPV1. Cultured DRG neurons from mixed-genotype litters of *Trpv1* knockout mice were loaded with a dye that fluoresces in functional mitochondria TMRE and with the fluorescent Ca^{2+} sensor dye fluo-4 for imaging. Cells were treated with either CCCP or DMSO during live imaging and were then treated with capsaicin (Cap) or DMSO at the end (t = 475 – 500s) (A, scale bar indicates 25 µm). Traces of TMRE intensity (not shown) and Fluo-4 intensity (B; means ± S.E.M.) were generated for a total of t = 500s. Peak Fluo-4 values from t = 100 – 150s were extrapolated for each condition (C; boxplots indicate median, 25%, 75% percentile and min/max). Data from DRGs of n = 6 independent experiments per condition are presented. ****P<0.0001, **P<0.01 (two-factor ANOVA, F_{CCCP} (1, 20) = 25.96, P<0.0001, $F_{treatment}$ (1, 20) = 9.342, P=0.0062, followed by Tukey's post-hoc comparison).

3.2.5 Investigate the role of cysteine 157 on TRPV1 ROS-sensitization

One of the main mechanisms of ROS-induced TRPV1 sensitization is through modification of key reactive cysteine residues on the cytosolic side of the channel[71-73]. One of the primary amino acids known to be involved in this process is cysteine 157. We therefore set out to evaluate the importance of this cysteine in CCCP-induced TRPV1 activation. We developed a set of recombinant imaging tools made up of a red genetically-encoded calcium indicator for optical imaging (R-GECO)[141] fused to wildtype TRPV1 or a TRPV1 mutant lacking cysteine 157 (C157A). HEK293T cells were infected with a modified HSV carrying a vector harbouring wildtype (Figure 3.17) or C157A TRPV1-R-GECO (Figure 3.18). Cells were live-imaged for a total of 6 minutes, with CCCP being applied at 2 minutes and capsaicin (Cap) being applied at 4 minutes. The intensity of each cell was recorded and averaged (Figure 3.17B, 3.18A). We observe that TRPV1-R-GECO reports activation from both CCCP (Figure 3.17C) and capsaicin (Figure 3.17B). We also show that wildtype TRPV1-R-GECO shows a significantly higher calcium response to CCCP compared to C157A TRPV1-R-GECO (Figure 3.18B - C). The number of wildtype TRPV1-R-GECO cells that responded to CCCP (121 out 473 cells; 25.6%) was also higher than the number of C157A TRPV1-R-GECO (29 out of 255 cells; 11.4%). This suggests that mitochondrial depolarization activates TRPV1 via the modification of cysteine 157 and validates the key role played by ROS in this process. Notably, both constructs display a robust response to capsaicin, suggesting that the C157A mutation doesn't abolish the function of the channel altogether (Figure 3.18A).

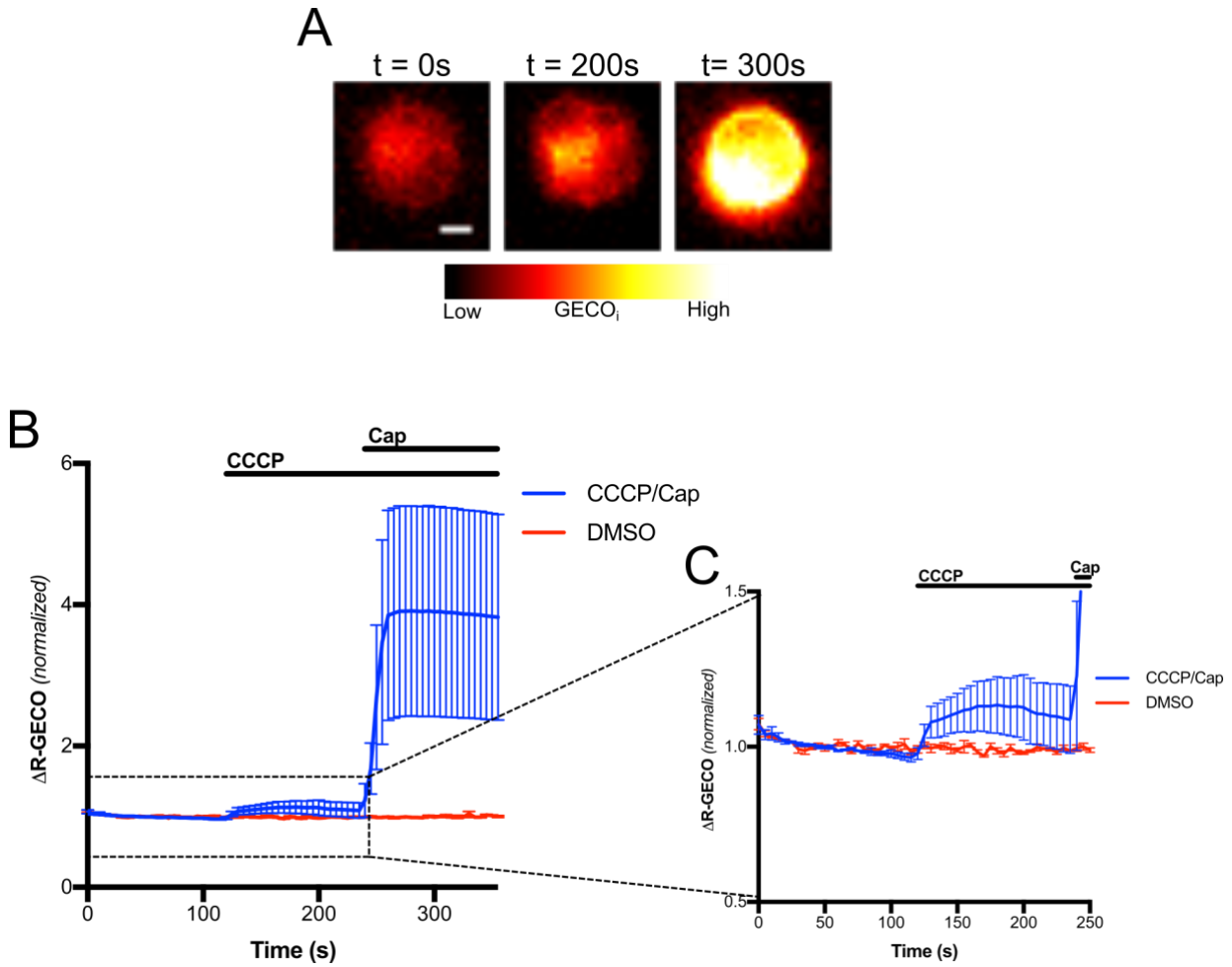

Figure 3.17. TRPV1-R-GECO detects CCCP- and capsaicin-induced calcium flux at or near TRPV1. Cultured HEK293T cells were infected with HSV containing a vector for the fusion protein TRPV1-R-GECO. After 48 hours, cells were treated with CCCP or DMSO and then capsaicin (Cap) or DMSO during live imaging (A; scale bar indicates 5 μm). Traces of R-GECO intensity in individual cells were generated and averaged for both conditions (B; zoomed in C). Data from n = 4 independent experiments per condition, each including over 400 TRPV1-R-GECO-positive cells, are presented (means ± S.E.M.).

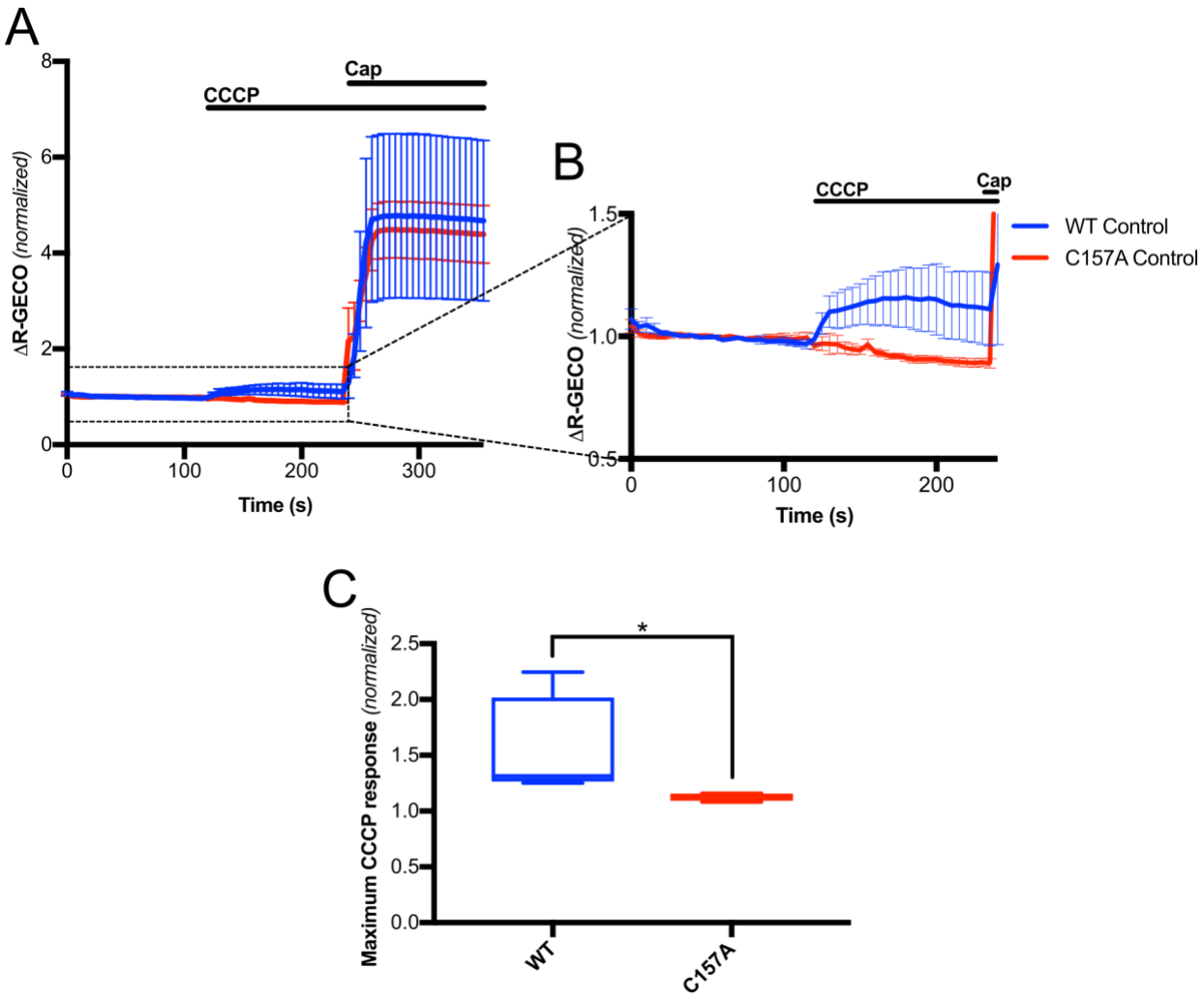

Figure 3.18. CCCP-induced TRPV1 activation is reduced by the C157A mutation. Cultured HEK293T cells were infected with HSV containing a vector for fusion protein TRPV1-R-GECO (WT) or the same protein but with mutated TRPV1 (C157A). After 48 hours, cells were treated with CCCP and then capsaicin (Cap) during live imaging. Traces of R-GECO intensity in individual cells were generated for each condition (A; zoomed in B). The maximum R-GECO intensity during the two minutes after CCCP application (t = 120 – 240s) was extrapolated from the data in panel A for each condition (C; boxplots indicate median, 25%, 75% percentile and min/max). Data from n = 4 independent WT experiments, containing 473 cells, and n = 4 independent C157A experiments, containing 255 cells, are presented (means ± S.E.M.). *P<0.05 (two-tailed Mann-Whitney U test, U = 0, P<0.0286).

Chapter 4: Discussion

4.1 The Role of TRPV1 in Wallerian Degeneration

The central role of calcium in Wallerian degeneration has been well substantiated[39,43,45]. After transection, there is an immediate calcium influx that occurs near the cut site followed by a lag phase and then a second wave of calcium occurring over the entire distal axon[43]. This later axoplasmic calcium rise is needed to cause cytoskeletal depolymerization and fragmentation largely through the activation of calpain proteases[46-48]. Furthermore, the extracellular environment is the main source of second stage Ca^{2+} rise[113]. To date, the only calcium channels that have been clearly demonstrated to be required for normal axon degeneration are L-type channels and the Na^{+}/Ca^{2+} exchanger (NCX) but there are likely other channels that have yet to be identified[39,142]. In the present study, we show for the first time that TRPV1 channels also mediate calcium flux during WD.

First, we confirmed that the distal portion of cut axons are rich in calcium by imaging transected murine DRG axons using the dark-to-light Ca^{2+}-sensing dye Fluo-4-AM three hours after axotomy. We then confirmed that removal of extracellular Ca^{2+} from the system one hour after axotomy blocks this late-stage rise. Waiting one hour to remove extracellular calcium allowed for any influx of Ca^{2+} immediately following axotomy and therefore only interrupted the delayed Ca^{2+} rise. These observations suggest the existence of two independent waves of calcium in WD[43,45].

We next addressed the lack of identified calcium channels involved in WD by testing the involvement of TRPV1, a calcium channel that is involved in axon degeneration under a number of different contexts (Johnstone et al, in preparation)[68]. Transected DRG axons were pretreated

with the TRPV1 inhibitor capsazepine (CPZ) and Ca^{2+} levels were imaged with Fluo-4 three hours later. We included DRGs pretreated with nifedipine, an inhibitor of L-type channels, to serve as a positive control. We found that both inhibitors significantly reduced calcium rise, confirming the role of L-type channels while establishing the involvement of TRPV1.

Reduced calcium flux by calcium chelation leads to downstream axonal protection[39,41]. Since TRPV1 inhibitor CPZ reduced calcium influx in transected axons, we hypothesized that CPZ would protect axons from degeneration. Indeed, we found significant protection six hours after axotomy in both CPZ-treated and nifedipine-treated axons, confirming the protective effect of L-type channel inhibition and showing for the first time that TRPV1 inhibition protects transected axons from degeneration. Interestingly, there is evidence suggesting an interplay between TRPV1 and L-type channels, as both CPZ and nifedipine have been shown to protect cortical neurons from degeneration induced by the specific TRPV1 activator, capsaicin[143]. Furthermore, capsaicin-induced hypersensitivity and nociceptive behaviour in murine behavioural assays were markedly reduced by local pre-treatment with nifedipine[144]. Furthermore, axotomy has been shown to increase axon excitability by modifying the membrane potential[145,146], presenting a case for activation of the voltage-gated L-type channels downstream of an initial ion flux. Our results suggest that voltage-gated Ca^{2+} channels can be activated downstream of TRPV1-mediated influx of calcium.

To confirm that TRPV1 is involved in WD, we used DRG cultures from *Trpv1* knockout mice. We observed that three hours after axotomy, $Trpv1^{-/-}$ axons had reduced calcium levels compared to $Trpv1^{+/+}$ axons. Furthermore, $Trpv1^{-/-}$ DRGs that we grew on porous membranes were protected from degeneration, relative to DRGs from $Trpv1^{+/+}$ littermates, six hours after axotomy. Taken together, these results indicate that axotomy induces calcium influx through TRPV1 late in

the process of WD. Furthermore, TRPV1 activation leads to downstream cytoskeletal fragmentation within axons during WD.

4.2 The Mechanism of Calcium Channel Activation in Wallerian Degeneration

The mechanism of initiating the calcium cascade after the lag phase of WD is unknown[43,132]. Until now, the only calcium channels known to be involved, L-type channels and Na^+-Ca^{2+} exchangers, are typically activated by axonal voltage changes and the Na^+/Ca^{2+} electrochemical gradient changes respectively[147,148]. Oxidative stress and elevated intracellular calcium have been causally associated in a number of healthy and disease states in neurons[88,89,149-151]. ROS accumulation and calcium rise both play crucial roles in distal axons during WD however the contribution of ROS to the late calcium influx has not been tested[39,82,84,113,152].

In light of our observation that TRPV1, a ROS-sensitive calcium channel[69,70], contributes to calcium rise and axon degeneration during WD, we therefore hypothesized that ROS are upstream activators of calcium influx in this context and that Nox complexes, which are active during WD[82], are the source of ROS. First, we found that the antioxidant NAC abolished calcium rise in cut axons, suggesting that intra-axonal ROS is necessary for calcium influx during the execution phase of WD.

It has been found that Nox complex inhibition reduces ROS accumulation and axon degeneration during WD[82]. Furthermore, Nox complexes are the primary source of ROS in developmental axon degeneration, which is also a TRPV1-dependent process (Johnstone et al, in preparation). We therefore hypothesized that inhibiting Nox complex activity in transected axons would reduce calcium influx. To test this, we used three established pharmacological Nox complex

inhibitors: VAS2870, apocynin and DPI. VAS2870 is a pan-NADPH oxidase subunit inhibitor that prevents formation of the active Nox complex[153], apocynin inhibits Nox complex core activator assembly[154] and DPI prevents NADPH from binding to the activated Nox complex[155]. Some of these inhibitors have been observed to have some small off-target effects such as ROS scavenging and inhibition of some proteins in the electron transport chain (ETC)[156] therefore any takeaways from results testing Nox complex inhibition should be consistent across all three treatments in order to control for these off-target effects. We pretreated DRGs with either VAS2870, apocynin or DPI, cut the axons and imaged three hours later with Fluo-4. Interestingly, we found that none of the Nox complex inhibitors reduced calcium influx in cut axons, suggesting that Nox complexes are not the source of ROS that initiates late stage Ca^{2+} rise after axotomy.

It is important to note that although Nox complexes do not appear to induce Ca^{2+} rise, there is still likely a prodegenerative role of these ROS-producing enzymes. Inhibition of Nox complex activity significantly protects axons experiencing WD and this occurs through activation of the ubiquitin-proteasome system (UPS)(Figure 1.2)[82]. In this context, ROS from the Nox complex activates the epidermal growth factor receptor (EGFR) which leads to phosphorylation of the E3 ubiquitin ligase zinc and ring finger 1 (ZNRF1). ZNRF1 causes proteasomal degradation of AKT. AKT normally inactivates glycogen synthase kinase-3β (GSK3β) in axons therefore AKT degradation causes an increase in active GSK3β. This leads to deactivation of collapsin response mediator protein 2 (CRMP2), a tubulin-bound protein that mediates normal axonal cytoskeleton dynamics[157,158]. Inactivated CRMP2 no longer binds to tubulin and therefore leads to loss of cytoskeletal integrity and axon degradation in WD. The Nox complex therefore activates the ZNRF1-AKT-GSK3β-CRMP2 pathway to promote axonal degeneration after axotomy without altering Ca^{2+} dynamics[82,159]. Interestingly, CRMP2 can also be deactivated by calpain-mediated

proteolytic cleavage[160]. Calpains are activated by Ca^{2+} in WD and they go on cause direct cytoskeletal degradation[46] however this also shows that calpains can recruit additional agents to amplify their prodegenerative effect. This also suggests a point of convergence between the Ca^{2+} pathway and the Nox complex pathway in WD.

Between 0.2% to 2.0% of all O_2 processed in the mitochondria is converted to ROS [93] and prevention of mitochondrial depolarization via inhibition of mPTP formation protects axons during WD[107]. However, some studies have argued that mitochondrial depolarization occurs as a consequence of axotomy but is not actually a necessary step in the WD pathway[113,115]. We decided to examine this by examining the effect of NAD^+ supplementation on mitochondria after axotomy. We first confirmed the neuroprotective effect of NAD^+ in axotomized DRGs and tested whether NAD^+ supplementation would prevent calcium influx after axotomy. Indeed, DRGs that we pretreated with NAD^+ had no observable calcium rise after axons were transected, which suggests that Ca^{2+} channel activation is downstream of NAD^+ loss.

We then hypothesized that mitochondria are depolarized downstream of NAD^+ loss and that this triggers axonal ROS accumulation, therefore placing ROS downstream of mitochondrial loss. To test this, we pretreated DRGs with NAD^+ or NAC, cut the axons and imaged 3.5 hours later using a marker of active mitochondria, TMRE and the axonal marker Calcein. Even though mitochondria were observed to begin losing their potential at the same time as calcium rise, we prolong imaging by 30 minutes beyond the timepoint used for Fluo-4 to increase the sensitivity of the assay. We found that NAD^+ significantly protected mitochondria from depolarization whereas NAC did not. This supports our hypothesis that mitochondria are lost as a result of decreased NAD^+ levels but not from ROS accumulation, which therefore likely occurs after mitochondrial depolarization.

Rapid widespread loss of mitochondria likely causes cell death in the long term through a deficit of ATP. However, in axons we hypothesized that mitochondrial depolarization is part of the WD pathway and would therefore elicit axonal degeneration that would require calcium influx. To address this, we induced mitochondrial failure using CCCP, a protonophore of the IMM that uncouples oxidative phosphorylation and depolarizes mitochondria. Five hours after CCCP treatment, we found significant cytoskeletal degradation in the axons which was protected by the calcium chelator EGTA and the antioxidant NAC. Surprisingly, both CPZ and nifedipine were neuroprotective in CCCP-induced degeneration as well. This suggests that both axotomy and mitochondrial depolarization by CCCP cause axon degeneration that requires ROS and calcium flux through TRPV1 and L-type channels.

We next hypothesized that the effects of CCCP on axonal degeneration could be explained by its acute effects on intra-axonal calcium rise. When we applied CCCP to TMRE- and Fluo-4-loaded axons we observed a rapid loss of mitochondrial potential occurring simultaneously with calcium rise. Calcium levels quickly rose to a peak then fell to a plateau that was below the level of the initial spike but higher than the baseline level. Mitochondria have Ca^{2+} stores and depolarization empties these stores into the cell[140], raising the possibility that the calcium rise can come from the mitochondria themselves. However, when we removed extracellular calcium from the system, the CCCP-induced calcium rise was sharply reduced during the initial calcium peak and during the plateau phase. This suggests that mitochondrial depolarization causes an axoplasmic calcium rise that is due mainly to influx from the extracellular space, Ca^{2+} from mitochondrial stores playing only a minor role in this process.

We then hypothesized that calcium rise after CCCP treatment employs the TRPV1 and L-type channels in a ROS-dependent manner, similarly to WD. Indeed, we found that scavenging

ROS and inhibiting TRPV1 or L-type channels significantly reduces the immediate calcium peak after CCCP treatment. Interestingly, both ROS scavenging and L-type inhibition reduced the plateau Ca^{2+} levels but TRPV1 inhibition did not. This suggests that, similarly to in WD, mitochondrial depolarization causes a ROS-dependent calcium influx that employs both TRPV1 and L-type channels however, TRPV1-mediated influx may only be important in the moments immediately following mitochondrial loss.

To confirm these results, we applied CCCP to *Trpv1*$^{-/-}$ and *Trpv1*$^{+/+}$ DRGs. We observed a reduced immediate calcium rise as well as a lower plateau in the *Trpv1*$^{-/-}$ DRG axons, confirming the involvement of TRPV1 in calcium rise after mitochondrial depolarization and suggesting, in contrast to the CPZ experiments, that loss of TRPV1 activity may affect the longer term plateau Ca^{2+} levels.

Because there is a precedent of L-type activation by upstream TRPV1 in neurons[143,144], it is possible that this sequence of calcium channel activation occurs in WD as well. However, there is also a possibility that L-type channels may be activated by ROS directly. L-type channels can be regulated by redox mechanisms and oxidative stress and have even been shown to contribute to intracellular Ca^{2+} rise from H_2O_2 treatment as a result of glutathionylation of the channel[161]. This was shown in myocytes and has not been confirmed in neurons where relative L-type subunit localization and expression levels are quite different[161,162]. Furthermore, ROS-sensitive channels are expressed in sensory axons such as TRPA1[163] and TRPM8[164,165] that may also be activated by mitochondrial depolarization. The involvement of multiple channels that are sensitive to ROS in WD suggest that TRPV1 may perform a functionally redundant role. This could explain the finding that inhibition or knockout of TRPV1 only causes a reduction in calcium levels and not a complete

calcium blockade. Elucidating this order of activation as well as the level of involvement of other TRP channels in sensory axons would be prove very valuable.

ROS-mediated sensitization of TRPV1 is an important functional aspect of the channel and has been shown to contribute to a range of TRPV1-dependent phenotypes[70,166,167]. This has been shown to occur through structural alteration of TRPV1 by covalent modification of reactive cysteine residues[69]. Specifically, allicin, the oxidized molecule in garlic, has been shown to activate TRPV1 by modifying cysteine 157 (C157) while still allowing for normal activation by capsaicin[71,72]. C157 is therefore a prime candidate for ROS-mediated sensitization in response to mitochondrial depolarization and we hypothesize that TRPV1 activity after exposure to ROS will be reduced when this amino acid is altered. We developed a set of novel imaging tools to explore the direct effects of ROS on TRPV1 activation. Wild-type TRPV1 was recombinantly fused at its C-terminus to R-GECO, a genetically-encoded calcium sensor[141]. The resulting TRPV1-R-GECO protein responded to both CCCP and capsaicin when expressed in HEK293T cells. To investigate the ROS-dependency, C157 of wildtype TRPV1 was mutated to alanine (C157A) and fused to R-GECO. We found that CCCP treatment induces a significantly larger increase in cytoplasmic Ca^{2+} in cells expressing wildtype TRPV1-R-GECO compared to cells expressing the C157A mutant whereas both constructs respond identically to capsaicin. This suggests that mitochondrial depolarization causes TRPV1 activation in part through modification of cysteine 157. We chose HEK293T cells to test CCCP challenge on these constructs because of their high infection penetrance because this cell line does not normally express TRPV1[168]. Furthermore, this cell line does not experience calcium rise in response to oxidative stress by H_2O_2[169].

4.3 An Updated Model of ROS-dependent Ca^{2+} Rise Incorporating TRPV1 During WD

The prodegenerative role of ROS in WD has been shown in multiple studies[81-84] but has never been connected to calcium influx. The ROS-sensitive TRPV1 channel is highly expressed in DRG axons[60] and can cause degeneration in both mature and developmental contexts (Johnstone et al, in preparation)[68] but its involvement in degenerating axons during WD has not been evaluated.

I have integrated the findings presented in this thesis with evidence from the literature to develop a model outlining the mechanism of late-stage calcium channel activation in WD (Figure 4.1). I propose that after axotomy, loss of NAD^+ leads to mitochondrial depolarization. This releases ROS through prolonged mPTP formation which then covalently modifies reactive cysteines on ROS-sensitive channels, such as C157 on TRPV1, either directly or through contact with oxidized lipids. It is possible that L-type channels in this setting may also be activated here by ROS modification but this has not been shown in neurons. ROS sensitization from mitochondria causes channel opening and Ca^{2+} influx which alters the excitability of the axon by changing the membrane potential[145,146]. This axonal voltage change activates voltage-gated L-type channels which increases the magnitude of the calcium cascade and causes a positive feedback loop of voltage change to L-type activation. The calcium rise also overloads any remaining functional mitochondria, depolarizing them and triggering more ROS release into the cytosol, which creates another positive feedback loop of mitochondrial loss to ROS release to calcium rise. Ultimately, these factors converge to create a massive calcium increase in the axon which leads to axonal degeneration largely through calpain-mediated cytoskeletal degradation.

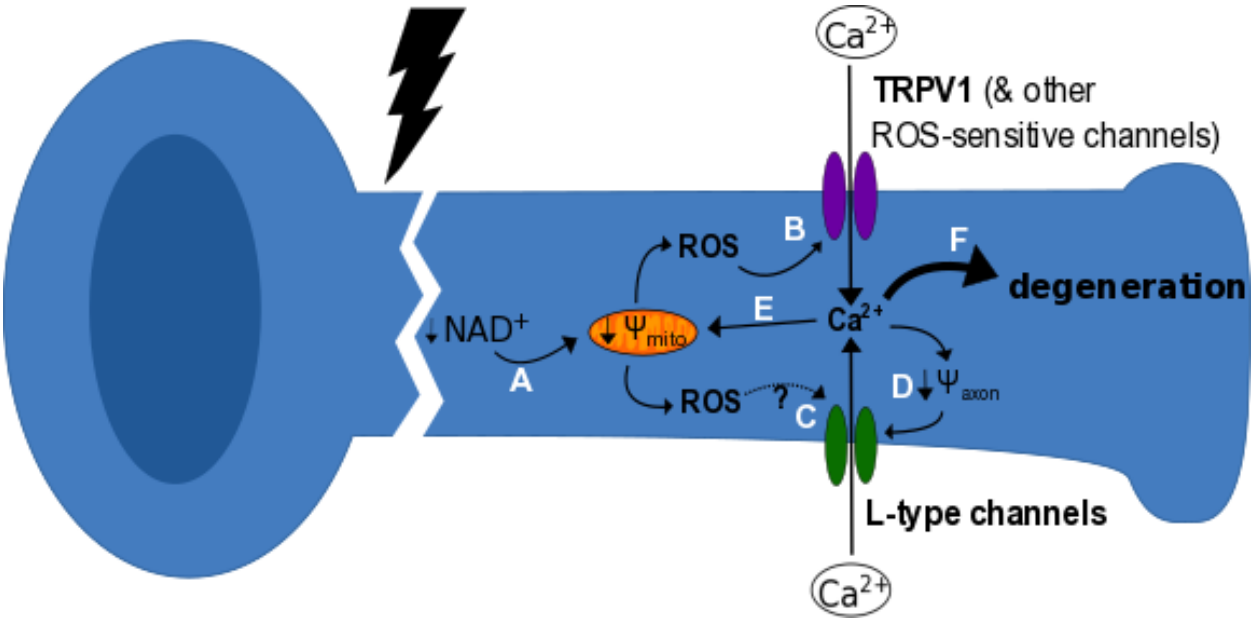

Figure 4.1. An updated model of late-stage calcium rise during WD. Loss of NAD^+ leads to mitochondrial depolarization (A). This triggers a release of ROS which goes on to activate TRPV1 (B) and possibly L-type channels (C) causing calcium influx. This causes increased axonal excitability by altered membrane voltage[145,146] (D), leading to activation of L-type channels. Calcium influx also triggers a more profound mitochondrial depolarization event (E). Ultimately, multiple positive feedback loops lead to massive calcium rise and downstream degeneration (F). NAD^+ = nicotinamide adenine dinucleotide, ROS = reactive oxygen species, TRPV1 = transient receptor potential cation channel vanilloid 1

This model maintains that NAD^+ supplementation protects transected axons. We confirm this and show that NAD^+ also abolishes Ca^{2+} influx after axotomy. The protective role of NAD^+ is well known and its downstream effect on calcium flux has been implied but has never been tested[105]. Indeed, overexpressing WldS abolishes axotomy-induced Ca^{2+} rise. This appears in contrast to the NMN hypothesis which argues that accumulation of the NAD^+ precursor NMN acts

as the primary degenerative initiator as opposed to loss of NAD^{+}[112]. Furthermore, pharmacological inhibition and genetic reduction of NMN levels abolish axonal Ca^{2+} rise during WD[113]. The interplay and dynamic interaction of these two molecules with WD machinery such as SARM1, NMNAT and the DLK MAPK cascade remains incompletely understood. It was however recently found that SARM1 overexpression or enhanced SARM1 NADase activity in healthy HEK293T cells inhibited mitochondrial respiration and reduced mitochondrial ATP levels[170]. This same study also found that SARM1 can be activated in a ROS-dependent fashion, suggesting yet another positive feedback loop in the proposed model. This, along with a reduction in NMNAT2 culminates in a rapid depletion of NAD^{+}[19].

We show that NAD^{+} supplementation but not ROS scavenging protects mitochondria after axotomy. This is supported since maintained NAD^{+} levels through WldS overexpression prevent mitochondrial loss and preserve a healthy mitochondrial phenotype[105,106,108]. Furthermore, ROS levels rise in the mitochondria after axotomy however WldS overexpression prevents this[81,82]. Along with our results, this is indicative of ROS accumulation resulting from instead of causing mitochondrial dysfunction in WD.

The model suggests that Ca^{2+} influx is initiated by ROS that comes primarily from the mitochondria as opposed to elsewhere. Others have found that ROS produced from the Nox complex causes axon death in WD however this occurs through activation of the EGFR-ZNRF1 pathway in a Ca^{2+}-independent fashion[82,159]. Due to the short-lived nature of ROS, it is possible for it to have different roles based on the relative location of its production, whether from the Nox complex or the mitochondria in this case[79]. As mentioned above, mitochondrial ROS production is also shown to increase after axotomy and mitochondrial dysfunction leads to Ca^{2+} influx and axon death[75,81]. Since the EGFR-ZNRF1 axis in WD ends with CRMP2 inactivation and

cytoskeletal instability and the Ca^{2+} influx cascade ultimately causes calpain activation and cytoskeletal fragmentation, the functions of the two sources of ROS may converge to impair axon structure[39,48,157,158].

The model suggests that, in addition to L-type channels and the sodium-calcium exchanger, TRPV1 and potentially other ROS-sensitive channels are involved in Ca^{2+} influx during WD. This presents a new connection between mitochondrial dysfunction and axon death in WD through ROS-induced Ca^{2+} rise. Interestingly, TRPV1 activation from CCCP has previously been shown in vagal neurons however this study was done using a $Trpv1^{-/-}$, $Trpa1^{-/-}$ double null background therefore the contribution of TRPV1 alone could not be determined[109]. Mitochondrial depolarization also activates the sodium-calcium exchanger however this channel only partially accounts for the observed Ca^{2+} rise and is not activated by oxidative insult alone[142]. Therefore, it is possible that this accounts for the small Ca^{2+} rise in NAC-treated axons when exposed to CCCP (Figure 3.14B). This could mean that mitochondrial depolarization activates Ca^{2+} channels using two distinct mechanisms.

The C157A mutation in TRPV1 was previously discovered to completely block Ca^{2+} influx in the channel when induced by allicin[71]. Interestingly, allicin has previously been shown to cause oxidative stress and Ca^{2+} dysregulation in cells[171]. It is also known to react with thiol groups on proteins[172]; in this way, it shares a commonality with ROS[73]. Cysteine 157 has been associated with ROS-dependent channel modification however mutant channel activity in response to mitochondrial depolarization has never been tested[69].

WD and developmental degeneration by neurotrophic factor deprivation have notable similarities as well as some interesting differences. In both modes of axon degeneration, ROS

accumulation leads to TRPV1 activation which initiates a calcium cascade leading to downstream calpain activation and cytoskeletal degradation. However, in NGF deprivation, the source of ROS is the Nox complex, which is activated by PKC whereas after axotomy, mitochondria act as the primary source of ROS, at least at the stage where calcium influx is initiated. The different sources of ROS in these two contexts can be attributed to the differences in prodegenerative insults: WD is initiated by a physical trauma, eventually leading to NAD^+ loss, whereas NGF deprivation-mediated degeneration triggers a complex prodegenerative signaling pathway initiated by TrkA[173].

Another important difference is the downstream effects of calcium in these two contexts[173]. Both modes of degeneration lead to calpain activation but NGF deprivation also relies on activation of the intrinsic pathway of apoptosis[174]. Neurons lacking key apoptotic proteins Bax and Bak are protected from degeneration by NGF deprivation[175] but not from WD[176]. Furthermore, activation of the effector caspase-3 is necessary for degeneration after NGF deprivation[177] but is dispensable in WD[178]. This suggests that WD relies largely on calpain-mediated axon fragmentation whereas fragmentation during NGF deprivation is driven by the apoptotic machinery. It appears that these two methods of subcellular axon death are initiated by diverse stimuli which end up converging at calcium rise but then diverging once again during execution.

Chapter 5: Conclusion

5.1 Research Objectives Addressed

Objective 1: To address the first research objectives, we used the Ca^{2+} sensory dye Fluo-4-AM in intact and transected DRG axons to analyze calcium levels during WD. To evaluate axonal degeneration, we grew DRGs on porous membranes which allowed axons to pass through the membrane onto the other side. Axotomy was achieved by scraping the face of the membrane containing cell soma. To quantify degeneration, cells were immunostained for tubulin and analyzed using Axoquant 2.0[131]. Using pharmacological inhibition by CPZ and genetic knockout models, we found that TRPV1 is involved in late-stage calcium influx after axotomy and that this contributes to axonal degeneration.

Objective 2: Using Fluo-4, we showed that late-stage calcium influx occurs downstream of NAD^+ loss. Again using Fluo-4 along with wildtype and C157A TRPV1-R-GECO constructs we found that ROS is necessary for calcium influx during WD and we suggest that it acts by sensitizing calcium channels via modification of reactive cysteines. We also found that ROS does not come from the Nox complex in this case. Using CCCP, we showed that mitochondrial depolarization, an event found to be crucial for normal degeneration in WD[107], triggers ROS-dependent calcium influx through TRPV1 and L-type channels, which are shown to be involved in WD. This CCCP-induced calcium influx also leads to downstream axon degeneration. We therefore suggested that mitochondria are the source of ROS responsible for initiating calcium influx. We went on to develop an updated model outlining the mechanism of late-stage calcium influx during WD (Figure 4.1).

5.2 Limitations of the Research

One of the main limitations of this study is the choice of cells. Embryonic murine dorsal root ganglia are an effective model for displaying the effects of Wallerian degeneration and have been used in multiple studies in this area[27,32,43,75,121]. The way in which their axons grow out of the ganglia allows for simple physical separation of axons from soma in thousands of cells at once. With that being said, embryonic neurons are still in the developmental stage and therefore operate in some ways that are significantly different from their mature counterparts[179,180]. For example, embryonic DRGs are dependent on NGF for survival however mature DRGs are not[181]. These differences may alter various intra-axonal dynamics therefore experiments should be confirmed with DRGs from adult mice.

Cells that are cultured *in vitro* are isolated from the environment of interest and no longer interact with all of the other nearby cells and environmental cues present in the organism. For example, there is a significant role being played by microglia and other immune cells during Wallerian degeneration as they release inflammatory agents[182] and remove axon fragments and debris to clear the way for regenerating axons[183]. Furthermore, DRGs are cultured with FDU which prevents mitotic overgrowth of cultures by dividing cells such as fibroblasts and glia. DRG cells no longer divide at this stage of development and are therefore not affected by FDU; however, the incorporation of this compound in culture further differentiates this environment from that of the organism *in vivo*. For this reason, the phenomena being investigated in this thesis are those that occur within the axons themselves and not those that involve supporting cells. Examination of events incorporating other cells and agents of the extracellular milieu would be best done *in vivo* or, at the very least, using *in vitro* cocultures.

The HEK293T cell is an immortalized human embryonic kidney cell line that is used for its ease of viral infection and predictable growth rate. These cells also display many properties characteristic of immature neurons[116]. Despite this, these cells are quite different from the axons of DRGs and it is for this reason that the only takeaway from the results of these experiments should be the responses wildtype and C157A TRPV1 to CCCP. The interplay between mitochondrial depolarization and calcium influx in HEK293T cells shows that residue C157 can play a significant role in CCCP-dependent TRPV1 activation but whether this residue is targeted in axons undergoing WD remains unknown.

The Ca^{2+} sensor dye Fluo-4 fluoresces green after excitation at 488 nm after being bound to Ca^{2+} however it remains dark when unbound therefore it is not considered to be a ratiometric dye[184]. This means that areas of high fluorescence could also be the result of axonal overlap, leading to amplification of the Fluo-4 signal despite moderate calcium levels. For this reason, images in Fluo-4 experiments were taken at the periphery on the axonal growth area, where there is minimal axon overlap.

Nifedipine and CPZ both effectively block the calcium channels to which they are targeted however claims on the relative role of TRPV1 and L-type channels in WD or mitochondrial depolarization should not be made due to possible differences in affinity and/or mechanisms of action between the two inhibitors. They are therefore only used to show whether the calcium channels have a role in a given process or not.

5.3 Future Directions of Research

This thesis shows for the first time that TRPV1, a ROS-sensitive channel, is involved in calcium influx leading to axon degradation during WD. There are other ROS-sensitive channels, such as TRPA1[163] and TRPM8[164], that are expressed in sensory axons and it is possible that these channels may be activated during WD. Therefore, it is imperative that they be tested, using specific pharmacological inhibitors and null animals, for their contribution to calcium flux and cytoskeletal degradation. Furthermore, it has been shown that late-stage calcium rise in transected axons causes depolarization[145,146] however the contribution of the suite of calcium channels involved in this process to axonal voltage change has not been shown. Assessing the contribution of L-type, NCX and TRPV1 channels to the changes in the potential of the axonal membrane will further elucidate the order in which these channels are activated during WD.

Our findings support the notion that mitochondrial depolarization is an important step leading to axon degradation in WD[107,150] by showing that mitochondrial depolarization releases ROS which activates prodegenerative calcium channels. However, the mechanism by which axotomy leads mitochondrial depolarization is unknown. A decrease in the NAD^+:NADH ratio, which is a classic condition of WD[19,32], has been shown to cause RIRR in mitochondria[96,98] but this has not been demonstrated in the context of axotomy. One study suggests that mitochondria are depolarized due to calcium overload from the endoplasmic reticulum (ER)[152] however this does not address how decreased NAD^+ levels would lead to high Ca^{2+} in the ER. Testing the activity of the inositol triphosphate receptor (IP_3R) and ryanodine receptors (RyR), two dominant ER-bound calcium channels[185], in transected WldS and $SARM1^{-/-}$ axons will prove beneficial to determine the importance of ER Ca^{2+}.

Lastly, our findings on the involvement of TRPV1 in WD were supported both pharmacologically and genetically. However, all of our experiments were performed *in vitro*. Experiments using an *in vivo* model of axotomy, such as sciatic nerve transection, in wildtype and *Trpv1*$^{-/-}$ mice are important to solidify the role of TRPV1 in this process.

5.4 Significance of Findings

This thesis shows that ROS is a crucial element that initiates calcium influx during the execution phase of WD and implicates TRPV1 as a mediator of this process. Previous studies have examined the degenerative roles of calcium channels and oxidative stress during WD however, to the best of my knowledge, they have never been causally associated. The subcellular components of WD are not only relevant when an axon is cut from its soma, as the *WldS* gene has been shown to be neuroprotective in disease models of glaucoma[12], Parkinson's disease[13] and motor neuron disease[14]. Furthermore, NMNAT overexpression reduces neurodegeneration in mouse and *Drosophila* models of tauopathy[186,187]. TRPV1 is specifically targeted by many pharmaceuticals due to its involvement in pain[188] therefore there may already be potential treatments at the clinical level that can be used for reducing WD damage in humans.

The field of Wallerian degeneration is being intensely studied. The discovery of the WldS mouse was made in 1989[10] and the role of SARM1 in WD was not identified until 2012[26]. These recent findings have led to many new questions with answers that appear just on the horizon. It is our hope that the findings presented in this thesis will fill knowledge gaps that soon lead to the development of a fully comprehensive model of WD and that this model will open new targets for treatment of the many conditions characterized by WD-like axon loss.

References

1 Freeman, M. R. Signaling mechanisms regulating Wallerian degeneration. *Curr Opin Neurobiol* **0**, 224-231, doi:10.1016/j.conb.2014.05.001 (2014).

2 Cashman, C. R. & Hoke, A. Mechanisms of distal axonal degeneration in peripheral neuropathies. *Neurosci Lett* **596**, 33-50, doi:10.1016/j.neulet.2015.01.048 (2015).

3 Albers, J. W. & Pop-Busui, R. Diabetic neuropathy: mechanisms, emerging treatments, and subtypes. *Curr Neurol Neurosci Rep* **14**, 473, doi:10.1007/s11910-014-0473-5 (2014).

4 Kanaan, N. M. *et al.* Axonal degeneration in Alzheimer's disease: when signaling abnormalities meet the axonal transport system. *Exp Neurol* **246**, 44-53, doi:10.1016/j.expneurol.2012.06.003 (2013).

5 Burke, R. E. & O'Malley, K. Axon degeneration in Parkinson's disease. *Exp Neurol* **246**, 72-83, doi:10.1016/j.expneurol.2012.01.011 (2013).

6 Fischer-Hayes, L. R., Brotherton, T. & Glass, J. D. Axonal degeneration in the peripheral nervous system: implications for the pathogenesis of amyotrophic lateral sclerosis. *Exp Neurol* **246**, 6-13, doi:10.1016/j.expneurol.2013.05.001 (2013).

7 Criste, G., Trapp, B. & Dutta, R. Axonal loss in multiple sclerosis: causes and mechanisms. *Handb Clin Neurol* **122**, 101-113, doi:10.1016/b978-0-444-52001-2.00005-4 (2014).

8 Johnson, V. E., Stewart, W. & Smith, D. H. Axonal pathology in traumatic brain injury. *Exp Neurol* **246**, 35-43, doi:10.1016/j.expneurol.2012.01.013 (2013).

9 Waller, A. Experiments on the Section of the Glossopharyngeal and Hypoglossal Nerves of the Frog, and Observations of the Alterations Produced Thereby in the Structure of Their Primitive Fibres. *Philos. Trans. R. Soc. London* **140**, 423-429 (1850).

10 Lunn, E. R., Perry, V. H., Brown, M. C., Rosen, H. & Gordon, S. Absence of Wallerian Degeneration does not Hinder Regeneration in Peripheral Nerve. *Eur J Neurosci* **1**, 27-33 (1989).

11 Tsao, J. W., Brown, M. C., Carden, M. J., McLean, W. G. & Perry, V. H. Loss of the compound action potential: an electrophysiological, biochemical and morphological study of early events in axonal degeneration in the C57BL/Ola mouse. *Eur J Neurosci* **6**, 516-524 (1994).

12 Beirowski, B., Babetto, E., Coleman, M. P. & Martin, K. R. The WldS gene delays axonal but not somatic degeneration in a rat glaucoma model. *Eur J Neurosci* **28**, 1166-1179, doi:10.1111/j.1460-9568.2008.06426.x (2008).

13 Hasbani, D. M. & O'Malley, K. L. Wld(S) mice are protected against the Parkinsonian mimetic MPTP. *Exp Neurol* **202**, 93-99, doi:10.1016/j.expneurol.2006.05.017 (2006).

14 Ferri, A., Sanes, J. R., Coleman, M. P., Cunningham, J. M. & Kato, A. C. Inhibiting axon degeneration and synapse loss attenuates apoptosis and disease progression in a mouse model of motoneuron disease. *Curr Biol* **13**, 669-673 (2003).

15 Conforti, L. *et al.* A Ufd2/D4Cole1e chimeric protein and overexpression of Rbp7 in the slow Wallerian degeneration (WldS) mouse. *Proc Natl Acad Sci U S A* **97**, 11377-11382, doi:10.1073/pnas.97.21.11377 (2000).

16 Sasaki, Y., Vohra, B. P., Baloh, R. H. & Milbrandt, J. Transgenic mice expressing the Nmnat1 protein manifest robust delay in axonal degeneration in vivo. *J Neurosci* **29**, 6526-6534, doi:10.1523/jneurosci.1429-09.2009 (2009).

17 Sasaki, Y. & Milbrandt, J. Axonal degeneration is blocked by nicotinamide mononucleotide adenylyltransferase (Nmnat) protein transduction into transected axons. *J Biol Chem* **285**, 41211-41215, doi:10.1074/jbc.C110.193904 (2010).

18 Avery, M. A., Sheehan, A. E., Kerr, K. S., Wang, J. & Freeman, M. R. Wld S requires Nmnat1 enzymatic activity and N16-VCP interactions to suppress Wallerian degeneration. *J Cell Biol* **184**, 501-513, doi:10.1083/jcb.200808042 (2009).

19 Gilley, J. & Coleman, M. P. Endogenous Nmnat2 is an essential survival factor for maintenance of healthy axons. *PLoS Biol* **8**, e1000300, doi:10.1371/journal.pbio.1000300 (2010).

20 Belenky, P., Bogan, K. L. & Brenner, C. NAD+ metabolism in health and disease. *Trends Biochem Sci* **32**, 12-19, doi:10.1016/j.tibs.2006.11.006 (2007).

21 Graziani, G. & Szabo, C. Clinical perspectives of PARP inhibitors. *Pharmacol Res* **52**, 109-118, doi:10.1016/j.phrs.2005.02.013 (2005).

22 Guse, A. H. Regulation of calcium signaling by the second messenger cyclic adenosine diphosphoribose (cADPR). *Curr Mol Med* **4**, 239-248 (2004).

23 Mack, T. G. *et al.* Wallerian degeneration of injured axons and synapses is delayed by a Ube4b/Nmnat chimeric gene. *Nat Neurosci* **4**, 1199-1206, doi:10.1038/nn770 (2001).

24 Sasaki, Y., Vohra, B. P., Lund, F. E. & Milbrandt, J. Nicotinamide mononucleotide adenylyl transferase-mediated axonal protection requires enzymatic activity but not increased levels of neuronal nicotinamide adenine dinucleotide. *J Neurosci* **29**, 5525-5535, doi:10.1523/jneurosci.5469-08.2009 (2009).

25 Wang, J. *et al.* in *J Cell Biol* Vol. 170 349-355 (2005).

26 Osterloh, J. M. *et al.* dSarm/Sarm1 is required for activation of an injury-induced axon death pathway. *Science* **337**, 481-484, doi:10.1126/science.1223899 (2012).

27 Gerdts, J., Summers, D. W., Sasaki, Y., DiAntonio, A. & Milbrandt, J. in *J Neurosci* Vol. 33 13569-13580 (2013).

28 Kim, Y. *et al.* MyD88-5 links mitochondria, microtubules, and JNK3 in neurons and regulates neuronal survival. *J Exp Med* **204**, 2063-2074, doi:10.1084/jem.20070868 (2007).

29 Mukherjee, P., Woods, T. A., Moore, R. A. & Peterson, K. E. Activation of the innate signaling molecule MAVS by bunyavirus infection upregulates the adaptor protein SARM1, leading to neuronal death. *Immunity* **38**, 705-716, doi:10.1016/j.immuni.2013.02.013 (2013).

30 Couillault, C. *et al.* TLR-independent control of innate immunity in Caenorhabditis elegans by the TIR domain adaptor protein TIR-1, an ortholog of human SARM. *Nat Immunol* **5**, 488-494, doi:10.1038/ni1060 (2004).

31 Akhouayri, I., Turc, C., Royet, J. & Charroux, B. Toll-8/Tollo negatively regulates antimicrobial response in the Drosophila respiratory epithelium. *PLoS Pathog* **7**, e1002319, doi:10.1371/journal.ppat.1002319 (2011).

32 Essuman, K. *et al.* The SARM1 Toll/Interleukin-1 Receptor Domain Possesses Intrinsic NAD+ Cleavage Activity that Promotes Pathological Axonal Degeneration. *Neuron* **93**, 1334-1343.e1335, doi:10.1016/j.neuron.2017.02.022 (2017).

33 Gilley, J., Ribchester, R. R. & Coleman, M. P. Sarm1 Deletion, but Not WldS, Confers Lifelong Rescue in a Mouse Model of Severe Axonopathy. *Cell Rep* **21**, 10-16, doi:10.1016/j.celrep.2017.09.027 (2017).

34 Miller, B. R. *et al.* A dual leucine kinase-dependent axon self-destruction program promotes Wallerian degeneration. *Nat Neurosci* **12**, 387-389, doi:10.1038/nn.2290 (2009).

35 Cavalli, V., Kujala, P., Klumperman, J. & Goldstein, L. S. Sunday Driver links axonal transport to damage signaling. *J Cell Biol* **168**, 775-787, doi:10.1083/jcb.200410136 (2005).

36 Yang, J. *et al.* Pathological axonal death through a MAPK cascade that triggers a local energy deficit. *Cell* **160**, 161-176, doi:10.1016/j.cell.2014.11.053 (2015).

37 Shin, J. E. *et al.* SCG10 is a JNK target in the axonal degeneration pathway. *Proc Natl Acad Sci U S A* **109**, E3696-3705, doi:10.1073/pnas.1216204109 (2012).

38 Walker, L. J. *et al.* in *eLife* Vol. 6 (2017).

39 George, E. B., Glass, J. D. & Griffin, J. W. Axotomy-induced axonal degeneration is mediated by calcium influx through ion-specific channels. *J Neurosci* **15**, 6445-6452 (1995).

40 Conforti, L., Gilley, J. & Coleman, M. P. Wallerian degeneration: an emerging axon death pathway linking injury and disease. *Nature Reviews Neuroscience* **15**, 394-409, doi:doi:10.1038/nrn3680 (2014).

41 Schlaepfer, W. W. & Bunge, R. P. Effects of calcium ion concentration on the degeneration of amputated axons in tissue culture. *J Cell Biol* **59**, 456-470 (1973).

42 Nakai, J., Ohkura, M. & Imoto, K. A high signal-to-noise Ca(2+) probe composed of a single green fluorescent protein. *Nat Biotechnol* **19**, 137-141, doi:10.1038/84397 (2001).

43 Vargas, M. E., Yamagishi, Y., Tessier-Lavigne, M. & Sagasti, A. Live Imaging of Calcium Dynamics during Axon Degeneration Reveals Two Functionally Distinct Phases of Calcium Influx. *J Neurosci* **35**, 15026-15038, doi:10.1523/jneurosci.2484-15.2015 (2015).

44 Breckwoldt, M. O. *et al.* Multiparametric optical analysis of mitochondrial redox signals during neuronal physiology and pathology in vivo. *Nat Med* **20**, 555-560, doi:10.1038/nm.3520 (2014).

45 Adalbert, R. *et al.* Intra-axonal calcium changes after axotomy in wild-type and slow Wallerian degeneration axons. *Neuroscience* **225**, 44-54, doi:10.1016/j.neuroscience.2012.08.056 (2012).

46 Ma, M. *et al.* Calpains mediate axonal cytoskeleton disintegration during Wallerian degeneration. *Neurobiol Dis* **56**, 34-46, doi:10.1016/j.nbd.2013.03.009 (2013).

47 Yang, J. *et al.* Regulation of axon degeneration after injury and in development by the endogenous calpain inhibitor calpastatin. *Neuron* **80**, 1175-1189, doi:10.1016/j.neuron.2013.08.034 (2013).

48 Bernier, B., Castejon, S., Culver, D. G. & Glass, J. D. Axonal neurofilaments are resistant to calpain-mediated degradation in the WLD(S) mouse. *Neuroreport* **10**, 1423-1426 (1999).

49 Shen, H., Hyrc, K. L. & Goldberg, M. P. Maintaining energy homeostasis is an essential component of Wld(S)-mediated axon protection. *Neurobiol Dis* **59**, 69-79, doi:10.1016/j.nbd.2013.07.007 (2013).

50 Cui, M. *et al.* TRPV1 receptors in the CNS play a key role in broad-spectrum analgesia of TRPV1 antagonists. *J Neurosci* **26**, 9385-9393, doi:10.1523/jneurosci.1246-06.2006 (2006).

51 Clapham, D. E. TRP channels as cellular sensors. *Nature* **426**, 517-524, doi:10.1038/nature02196 (2003).

52 Plant, T. D. TRPs in mechanosensing and volume regulation. *Handb Exp Pharmacol* **223**, 743-766, doi:10.1007/978-3-319-05161-1_2 (2014).

53 Berrout, J., Jin, M. & O'Neil, R. G. Critical role of TRPP2 and TRPC1 channels in stretch-induced injury of blood-brain barrier endothelial cells. *Brain Res* **1436**, 1-12, doi:10.1016/j.brainres.2011.11.044 (2012).

54 Zhang, W., Yan, Z., Jan, L. Y. & Jan, Y. N. Sound response mediated by the TRP channels NOMPC, NANCHUNG, and INACTIVE in chordotonal organs of Drosophila larvae. *Proc Natl Acad Sci U S A* **110**, 13612-13617, doi:10.1073/pnas.1312477110 (2013).

55 Roper, S. D. TRPs in taste and chemesthesis. *Handb Exp Pharmacol* **223**, 827-871, doi:10.1007/978-3-319-05161-1_5 (2014).

56 Hoffmann, T. *et al.* TRPA1 and TRPV1 are differentially involved in heat nociception of mice. *Eur J Pain* **17**, 1472-1482, doi:10.1002/j.1532-2149.2013.00331.x (2013).

57 Tan, C. H. & McNaughton, P. A. The TRPM2 ion channel is required for sensitivity to warmth. *Nature* **536**, 460-463, doi:10.1038/nature19074 (2016).

58 Darre, L. & Domene, C. Binding of Capsaicin to the TRPV1 Ion Channel. *Mol Pharm* **12**, 4454-4465, doi:10.1021/acs.molpharmaceut.5b00641 (2015).

59 Caterina, M. J. *et al.* The capsaicin receptor: a heat-activated ion channel in the pain pathway. *Nature* **389**, 816-824, doi:10.1038/39807 (1997).

60 Bevan, S., Quallo, T. & Andersson, D. A. TRPV1. *Handb Exp Pharmacol* **222**, 207-245, doi:10.1007/978-3-642-54215-2_9 (2014).

61 Macpherson, L. J. *et al.* The pungency of garlic: activation of TRPA1 and TRPV1 in response to allicin. *Curr Biol* **15**, 929-934, doi:10.1016/j.cub.2005.04.018 (2005).

62 Everaerts, W. *et al.* The capsaicin receptor TRPV1 is a crucial mediator of the noxious effects of mustard oil. *Curr Biol* **21**, 316-321, doi:10.1016/j.cub.2011.01.031 (2011).

63 Moriyama, T. *et al.* Sensitization of TRPV1 by EP1 and IP reveals peripheral nociceptive mechanism of prostaglandins. *Mol Pain* **1**, 3, doi:10.1186/1744-8069-1-3 (2005).

64 Lapointe, T. K. *et al.* TRPV1 sensitization mediates postinflammatory visceral pain following acute colitis. *Am J Physiol Gastrointest Liver Physiol* **309**, G87-99, doi:10.1152/ajpgi.00421.2014 (2015).

65 Koplas, P. A., Rosenberg, R. L. & Oxford, G. S. The role of calcium in the desensitization of capsaicin responses in rat dorsal root ganglion neurons. *J Neurosci* **17**, 3525-3537 (1997).

66 Jhaveri, M. D., Elmes, S. J., Kendall, D. A. & Chapman, V. Inhibition of peripheral vanilloid TRPV1 receptors reduces noxious heat-evoked responses of dorsal horn neurons in naive, carrageenan-inflamed and neuropathic rats. *Eur J Neurosci* **22**, 361-370, doi:10.1111/j.1460-9568.2005.04227.x (2005).

67 Derry, S., Sven-Rice, A., Cole, P., Tan, T. & Moore, R. A. Topical capsaicin (high concentration) for chronic neuropathic pain in adults. *Cochrane Database Syst Rev*, Cd007393, doi:10.1002/14651858.CD007393.pub3 (2013).

68 Wang, S. *et al.* Ca2+ and calpain mediate capsaicin-induced ablation of axonal terminals expressing transient receptor potential vanilloid 1. *J Biol Chem* **292**, 8291-8303, doi:10.1074/jbc.M117.778290 (2017).

69 Chuang, H. H. & Lin, S. Oxidative challenges sensitize the capsaicin receptor by covalent cysteine modification. *Proc Natl Acad Sci U S A* **106**, 20097-20102, doi:10.1073/pnas.0902675106 (2009).

70 Keeble, J. E. *et al.* Hydrogen peroxide is a novel mediator of inflammatory hyperalgesia, acting via transient receptor potential vanilloid 1-dependent and independent mechanisms. *Pain* **141**, 135-142, doi:10.1016/j.pain.2008.10.025 (2009).

71 Salazar, H. *et al.* A single N-terminal cysteine in TRPV1 determines activation by pungent compounds from onion and garlic. *Nat Neurosci* **11**, 255-261, doi:10.1038/nn2056 (2008).

72 Salazar, H. *et al.* Structural determinants of gating in the TRPV1 channel. *Nat Struct Mol Biol* **16**, 704-710, doi:10.1038/nsmb.1633 (2009).

73 Ogawa, N. *et al.* Functional and Structural Divergence in Human TRPV1 Channel Subunits by Oxidative Cysteine Modification. *J Biol Chem* **291**, 4197-4210, doi:10.1074/jbc.M115.700278 (2016).

74 Hargreaves, K. M. & Ruparel, S. Role of Oxidized Lipids and TRP Channels in Orofacial Pain and Inflammation. *J Dent Res* **95**, 1117-1123, doi:10.1177/0022034516653751 (2016).

75 Summers, D. W., DiAntonio, A. & Milbrandt, J. Mitochondrial dysfunction induces Sarm1-dependent cell death in sensory neurons. *J Neurosci* **34**, 9338-9350, doi:10.1523/jneurosci.0877-14.2014 (2014).

76 Ren, F. *et al.* Blockade of transient receptor potential cation channel subfamily V member 1 promotes regeneration after sciatic nerve injury. *Neural Regen Res* **10**, 1324-1331, doi:10.4103/1673-5374.162770 (2015).

77 Jankowski, M. P., Soneji, D. J., Ekmann, K. M., Anderson, C. E. & Koerber, H. R. Dynamic changes in heat transducing channel TRPV1 expression regulate mechanically insensitive, heat sensitive C-fiber recruitment after axotomy and regeneration. *J Neurosci* **32**, 17869-17873, doi:10.1523/jneurosci.3148-12.2012 (2012).

78 Grivennikova, V. G. & Vinogradov, A. D. Mitochondrial production of reactive oxygen species. *Biochemistry (Mosc)* **78**, 1490-1511, doi:10.1134/s0006297913130087 (2013).

79 Rapoport, R., Hanukoglu, I. & Sklan, D. A fluorimetric assay for hydrogen peroxide, suitable for NAD(P)H-dependent superoxide generating redox systems. *Anal Biochem* **218**, 309-313 (1994).

80 Schieber, M. & Chandel, N. S. ROS function in redox signaling and oxidative stress. *Curr Biol* **24**, R453-462, doi:10.1016/j.cub.2014.03.034 (2014).

81 O'Donnell, K. C., Vargas, M. E. & Sagasti, A. WldS and PGC-1alpha regulate mitochondrial transport and oxidation state after axonal injury. *J Neurosci* **33**, 14778-14790, doi:10.1523/jneurosci.1331-13.2013 (2013).

82 Wakatsuki, S., Furuno, A., Ohshima, M. & Araki, T. Oxidative stress-dependent phosphorylation activates ZNRF1 to induce neuronal/axonal degeneration. *J Cell Biol* **211**, 881-896, doi:10.1083/jcb.201506102 (2015).

83 Press, C. & Milbrandt, J. Nmnat delays axonal degeneration caused by mitochondrial and oxidative stress. *J Neurosci* **28**, 4861-4871, doi:10.1523/jneurosci.0525-08.2008 (2008).

84 Welin, D., Novikova, L. N., Wiberg, M., Kellerth, J. O. & Novikov, L. N. Effects of N-acetyl-cysteine on the survival and regeneration of sural sensory neurons in adult rats. *Brain Res* **1287**, 58-66, doi:10.1016/j.brainres.2009.06.038 (2009).

85 Frati, A. *et al.* Diffuse Axonal Injury and Oxidative Stress: A Comprehensive Review. *Int J Mol Sci* **18**, doi:10.3390/ijms18122600 (2017).

86 Brandes, R. P., Weissmann, N. & Schroder, K. Nox family NADPH oxidases: Molecular mechanisms of activation. *Free Radic Biol Med* **76**, 208-226, doi:10.1016/j.freeradbiomed.2014.07.046 (2014).

87 Winterbourn, C. C., Kettle, A. J. & Hampton, M. B. Reactive Oxygen Species and Neutrophil Function. *Annu Rev Biochem* **85**, 765-792, doi:10.1146/annurev-biochem-060815-014442 (2016).

88 Wilson, C. *et al.* A Feed-Forward Mechanism Involving the NOX Complex and RyR-Mediated Ca2+ Release During Axonal Specification. *J Neurosci* **36**, 11107-11119, doi:10.1523/jneurosci.1455-16.2016 (2016).

89 Maher, P. & Schubert, D. Signaling by reactive oxygen species in the nervous system. *Cell Mol Life Sci* **57**, 1287-1305 (2000).

90 Cox, J. A., Jeng, A. Y., Sharkey, N. A., Blumberg, P. M. & Tauber, A. I. Activation of the human neutrophil nicotinamide adenine dinucleotide phosphate (NADPH)-oxidase by protein kinase C. *J Clin Invest* **76**, 1932-1938 (1985).

91 Ibi, M. *et al.* Reactive oxygen species derived from NOX1/NADPH oxidase enhance inflammatory pain. *J Neurosci* **28**, 9486-9494, doi:10.1523/jneurosci.1857-08.2008 (2008).

92 Li, X. *et al.* in *J Hematol Oncol* Vol. 6 19 (2013).

93 Madamanchi, N. R. & Runge, M. S. Mitochondrial dysfunction in atherosclerosis. *Circ Res* **100**, 460-473, doi:10.1161/01.res.0000258450.44413.96 (2007).

94 Droge, W. Free radicals in the physiological control of cell function. *Physiol Rev* **82**, 47-95, doi:10.1152/physrev.00018.2001 (2002).

95 Korge, P. *et al.* Protective role of transient pore openings in calcium handling by cardiac mitochondria. *J Biol Chem* **286**, 34851-34857, doi:10.1074/jbc.M111.239921 (2011).

96 Murphy, M. in *Biochem J* Vol. 417 1-13 (2009).

97 Zorov, D. B., Juhaszova, M. & Sollott, S. J. in *Physiol Rev* Vol. 94 909-950 (2014).

98 Zorov, D. B., Filburn, C. R., Klotz, L. O., Zweier, J. L. & Sollott, S. J. Reactive oxygen species (ROS)-induced ROS release: a new phenomenon accompanying induction of the mitochondrial permeability transition in cardiac myocytes. *J Exp Med* **192**, 1001-1014 (2000).

99 Zorov, D. B., Juhaszova, M. & Sollott, S. J. Mitochondrial ROS-induced ROS release: an update and review. *Biochim Biophys Acta* **1757**, 509-517, doi:10.1016/j.bbabio.2006.04.029 (2006).

100 Brady, N. R., Hamacher-Brady, A., Westerhoff, H. V. & Gottlieb, R. A. A wave of reactive oxygen species (ROS)-induced ROS release in a sea of excitable mitochondria. *Antioxid Redox Signal* **8**, 1651-1665, doi:10.1089/ars.2006.8.1651 (2006).

101 Aon, M. A., Cortassa, S. & O'Rourke, B. Mitochondrial Oscillations in Physiology and Pathophysiology. *Adv Exp Med Biol* **641**, 98-117 (2008).

102 Orrenius, S., Gogvadze, V. & Zhivotovsky, B. Calcium and mitochondria in the regulation of cell death. *Biochem Biophys Res Commun* **460**, 72-81, doi:10.1016/j.bbrc.2015.01.137 (2015).

103 Deniaud, A. *et al.* Endoplasmic reticulum stress induces calcium-dependent permeability transition, mitochondrial outer membrane permeabilization and apoptosis. *Oncogene* **27**, 285-299, doi:10.1038/sj.onc.1210638 (2008).

104 Duchen, M. R. Mitochondria and Ca(2+)in cell physiology and pathophysiology. *Cell Calcium* **28**, 339-348, doi:10.1054/ceca.2000.0170 (2000).

105 Avery, M. A. *et al.* WldS prevents axon degeneration through increased mitochondrial flux and enhanced mitochondrial Ca2+ buffering. *Curr Biol* **22**, 596-600, doi:10.1016/j.cub.2012.02.043 (2012).

106 Godzik, K. & Coleman, M. P. The axon-protective WLD(S) protein partially rescues mitochondrial respiration and glycolysis after axonal injury. *J Mol Neurosci* **55**, 865-871, doi:10.1007/s12031-014-0440-2 (2015).

107 Barrientos, S. A. *et al.* Axonal degeneration is mediated by the mitochondrial permeability transition pore. *J Neurosci* **31**, 966-978, doi:10.1523/jneurosci.4065-10.2011 (2011).

108 Sievers, C., Platt, N., Perry, V. H., Coleman, M. P. & Conforti, L. Neurites undergoing Wallerian degeneration show an apoptotic-like process with Annexin V positive staining and loss of mitochondrial membrane potential. *Neurosci Res* **46**, 161-169 (2003).

109 Stanford, K. R. & Taylor-Clark, T. E. Mitochondrial modulation-induced activation of vagal sensory neuronal subsets by antimycin A, but not CCCP or rotenone, correlates with mitochondrial superoxide production. *PLoS One* **13**, e0197106, doi:10.1371/journal.pone.0197106 (2018).

110 Tokunaga, S. & Araki, T. Wallerian degeneration slow mouse neurons are protected against cell death caused by mechanisms involving mitochondrial electron transport dysfunction. *J Neurosci Res* **90**, 664-671, doi:10.1002/jnr.22792 (2012).

111 Moran, M. *et al.* Mitochondrial respiratory chain dysfunction: implications in neurodegeneration. *Free Radic Biol Med* **53**, 595-609, doi:10.1016/j.freeradbiomed.2012.05.009 (2012).

112 Di Stefano, M. *et al.* A rise in NAD precursor nicotinamide mononucleotide (NMN) after injury promotes axon degeneration. *Cell Death Differ* **22**, 731-742, doi:10.1038/cdd.2014.164 (2015).

113 Loreto, A., Di Stefano, M., Gering, M. & Conforti, L. Wallerian Degeneration Is Executed by an NMN-SARM1-Dependent Late Ca(2+) Influx but Only Modestly Influenced by Mitochondria. *Cell Rep* **13**, 2539-2552, doi:10.1016/j.celrep.2015.11.032 (2015).

114 Rawson, R. L. *et al.* Axons degenerate in the absence of mitochondria in C. elegans. *Curr Biol* **24**, 760-765, doi:10.1016/j.cub.2014.02.025 (2014).

115 Kitay, B. M., McCormack, R., Wang, Y., Tsoulfas, P. & Zhai, R. G. Mislocalization of neuronal mitochondria reveals regulation of Wallerian degeneration and NMNAT/WLD(S)-mediated axon protection independent of axonal mitochondria. *Hum Mol Genet* **22**, 1601-1614, doi:10.1093/hmg/ddt009 (2013).

116 Graham, F. L., Smiley, J., Russell, W. C. & Nairn, R. Characteristics of a human cell line transformed by DNA from human adenovirus type 5. *J Gen Virol* **36**, 59-74, doi:10.1099/0022-1317-36-1-59 (1977).

117 Shaw, G., Morse, S., Ararat, M. & Graham, F. L. Preferential transformation of human neuronal cells by human adenoviruses and the origin of HEK 293 cells. *Faseb j* **16**, 869-871, doi:10.1096/fj.01-0995fje (2002).

118 Lin, Y. C. *et al.* Genome dynamics of the human embryonic kidney 293 lineage in response to cell biology manipulations. *Nat Commun* **5**, 4767, doi:10.1038/ncomms5767 (2014).

119 Mergler, S. *et al.* Thermo-sensitive transient receptor potential vanilloid channel-1 regulates intracellular calcium and triggers chromogranin A secretion in pancreatic neuroendocrine BON-1 tumor cells. *Cell Signal* **24**, 233-246, doi:10.1016/j.cellsig.2011.09.005 (2012).

120 Zagranichnaya, T. K., Wu, X. & Villereal, M. L. Endogenous TRPC1, TRPC3, and TRPC7 proteins combine to form native store-operated channels in HEK-293 cells. *J Biol Chem* **280**, 29559-29569, doi:10.1074/jbc.M505842200 (2005).

121 Gilley, J., Orsomando, G., Nascimento-Ferreira, I. & Coleman, M. P. Absence of SARM1 rescues development and survival of NMNAT2-deficient axons. *Cell Rep* **10**, 1974-1981, doi:10.1016/j.celrep.2015.02.060 (2015).

122 Tandrup, T. Are the neurons in the dorsal root ganglion pseudounipolar? A comparison of the number of neurons and number of myelinated and unmyelinated fibres in the dorsal root. *J Comp Neurol* **357**, 341-347, doi:10.1002/cne.903570302 (1995).

123 Hung, C. Y. & Tan, C. H. TRP Channels in Nociception and Pathological Pain. *Adv Exp Med Biol* **1099**, 13-27, doi:10.1007/978-981-13-1756-9_2 (2018).

124 Caterina, M. J. *et al.* Impaired nociception and pain sensation in mice lacking the capsaicin receptor. *Science* **288**, 306-313 (2000).

125 Eichler, M. E., Dubinsky, J. M., Tong, J. & Rich, K. M. The ability of diphenylpiperazines to prevent neuronal death in dorsal root ganglion neurons in vitro after nerve growth factor deprivation and in vivo after axotomy. *J Neurochem* **62**, 2148-2157 (1994).

126 Kulbatski, I., Cook, D. J. & Tator, C. H. Calcium entry through L-type calcium channels is essential for neurite regeneration in cultured sympathetic neurons. *J Neurotrauma* **21**, 357-374, doi:10.1089/089771504322972130 (2004).

127 Calixto, A., Jara, J. S. & Court, F. A. Diapause formation and downregulation of insulin-like signaling via DAF-16/FOXO delays axonal degeneration and neuronal loss. *PLoS Genet* **8**, e1003141, doi:10.1371/journal.pgen.1003141 (2012).

128 Lin, C. S., Lee, S. H., Huang, H. S., Chen, Y. S. & Ma, M. C. H2O2 generated by NADPH oxidase 4 contributes to transient receptor potential vanilloid 1 channel-mediated mechanosensation in the rat kidney. *Am J Physiol Renal Physiol* **309**, F369-376, doi:10.1152/ajprenal.00462.2014 (2015).

129 Nesuashvili, L., Hadley, S. H., Bahia, P. K. & Taylor-Clark, T. E. Sensory nerve terminal mitochondrial dysfunction activates airway sensory nerves via transient receptor potential (TRP) channels. *Mol Pharmacol* **83**, 1007-1019, doi:10.1124/mol.112.084319 (2013).

130 Unsain, N., Heard, K. N., Higgins, J. M. & Barker, P. A. Production and isolation of axons from sensory neurons for biochemical analysis using porous filters. *J Vis Exp*, doi:10.3791/51795 (2014).

131 Johnstone, A. D. *et al.* A novel method for quantifying axon degeneration. *PLoS One* **13**, e0199570, doi:10.1371/journal.pone.0199570 (2018).

132 Fuchs, A., Rigaud, M., Sarantopoulos, C. D., Filip, P. & Hogan, Q. H. Contribution of Calcium Channel Subtypes to the Intracellular Calcium Signal in Sensory Neurons: The Effect of Injury. *Anesthesiology* **107**, 117-127, doi:10.1097/01.anes.0000267511.21864.93 (2007).

133 Terenghi, G., Hart, A. & Wiberg, M. The nerve injury and the dying neurons: diagnosis and prevention. *J Hand Surg Eur Vol* **36**, 730-734, doi:10.1177/1753193411422202 (2011).

134 Karalija, A., Novikova, L. N., Kingham, P. J., Wiberg, M. & Novikov, L. N. The effects of N-acetyl-cysteine and acetyl-L-carnitine on neural survival, neuroinflammation and regeneration following spinal cord injury. *Neuroscience* **269**, 143-151, doi:10.1016/j.neuroscience.2014.03.042 (2014).

135 Kuwabara, W. M. *et al.* NADPH oxidase-dependent production of reactive oxygen species induces endoplasmatic reticulum stress in neutrophil-like HL60 cells. *PLoS One* **10**, e0116410, doi:10.1371/journal.pone.0116410 (2015).

136 Kim, J. H. *et al.* Post-treatment of an NADPH oxidase inhibitor prevents seizure-induced neuronal death. *Brain Res* **1499**, 163-172, doi:10.1016/j.brainres.2013.01.007 (2013).

137 Wingler, K. *et al.* VAS2870 is a pan-NADPH oxidase inhibitor. *Cell Mol Life Sci* **69**, 3159-3160, doi:10.1007/s00018-012-1107-1 (2012).

138 Gerdts, J., Summers, D. W., Milbrandt, J. & DiAntonio, A. Axon self destruction: new links among SARM1, MAPKs, and NAD+ metabolism. *Neuron* **89**, 449-460, doi:10.1016/j.neuron.2015.12.023 (2016).

139 Ly, J. D., Grubb, D. R. & Lawen, A. The mitochondrial membrane potential (deltapsi(m)) in apoptosis; an update. *Apoptosis* **8**, 115-128 (2003).

140 Ichas, F., Jouaville, L. S. & Mazat, J. P. Mitochondria are excitable organelles capable of generating and conveying electrical and calcium signals. *Cell* **89**, 1145-1153 (1997).

141 Zhao, Y. *et al.* An expanded palette of genetically encoded Ca(2)(+) indicators. *Science* **333**, 1888-1891, doi:10.1126/science.1208592 (2011).

142 Persson, A. K. *et al.* Sodium channels contribute to degeneration of dorsal root ganglion neurites induced by mitochondrial dysfunction in an in vitro model of axonal injury. *J Neurosci* **33**, 19250-19261, doi:10.1523/jneurosci.2148-13.2013 (2013).

143 Shirakawa, H. *et al.* TRPV1 stimulation triggers apoptotic cell death of rat cortical neurons. *Biochem Biophys Res Commun* **377**, 1211-1215, doi:10.1016/j.bbrc.2008.10.152 (2008).

144 Castro-Junior, C. J. *et al.* Phalpha1beta toxin prevents capsaicin-induced nociceptive behavior and mechanical hypersensitivity without acting on TRPV1 channels. *Neuropharmacology* **71**, 237-246, doi:10.1016/j.neuropharm.2013.04.001 (2013).

145 Sapunar, D., Ljubkovic, M., Lirk, P., McCallum, J. B. & Hogan, Q. H. Distinct membrane effects of spinal nerve ligation on injured and adjacent dorsal root ganglion neurons in rats. *Anesthesiology* **103**, 360-376 (2005).

146 Moldovan, M., Alvarez, S. & Krarup, C. Motor axon excitability during Wallerian degeneration. *Brain* **132**, 511-523, doi:10.1093/brain/awn332 (2009).

147 Khananshvili, D. The SLC8 gene family of sodium-calcium exchangers (NCX) - structure, function, and regulation in health and disease. *Mol Aspects Med* **34**, 220-235, doi:10.1016/j.mam.2012.07.003 (2013).

148 Lipscombe, D., Helton, T. D. & Xu, W. L-type calcium channels: the low down. *J Neurophysiol* **92**, 2633-2641, doi:10.1152/jn.00486.2004 (2004).

149 Carrasco, C., Naziroglu, M., Rodriguez, A. B. & Pariente, J. A. Neuropathic Pain: Delving into the Oxidative Origin and the Possible Implication of Transient Receptor Potential Channels. *Front Physiol* **9**, 95, doi:10.3389/fphys.2018.00095 (2018).

150 Court, F. A. & Coleman, M. P. Mitochondria as a central sensor for axonal degenerative stimuli. *Trends Neurosci* **35**, 364-372, doi:10.1016/j.tins.2012.04.001 (2012).

151 Mattson, M. P. Calcium and neurodegeneration. *Aging Cell* **6**, 337-350, doi:10.1111/j.1474-9726.2007.00275.x (2007).

152 Villegas, R. *et al.* in *J Neurosci* Vol. 34 7179-7189 (2014).

153 Altenhöfer, S. *et al.* in *Cell Mol Life Sci* Vol. 69 2327-2343 (2012).

154 Stolk, J., Hiltermann, T. J., Dijkman, J. H. & Verhoeven, A. J. Characteristics of the inhibition of NADPH oxidase activation in neutrophils by apocynin, a methoxy-substituted catechol. *Am J Respir Cell Mol Biol* **11**, 95-102, doi:10.1165/ajrcmb.11.1.8018341 (1994).

155 Tammariello, S. P., Quinn, M. T. & Estus, S. NADPH oxidase contributes directly to oxidative stress and apoptosis in nerve growth factor-deprived sympathetic neurons. *J Neurosci* **20**, Rc53 (2000).

156 Altenhöfer, S., Radermacher, K. A., Kleikers, P. W., Wingler, K. & Schmidt, H. H. in *Antioxid Redox Signal* Vol. 23 406-427 (2015).

157 Arimura, N., Menager, C., Fukata, Y. & Kaibuchi, K. Role of CRMP-2 in neuronal polarity. *J Neurobiol* **58**, 34-47, doi:10.1002/neu.10269 (2004).

158 Charrier, E. *et al.* Collapsin response mediator proteins (CRMPs): involvement in nervous system development and adult neurodegenerative disorders. *Mol Neurobiol* **28**, 51-64, doi:10.1385/mn:28:1:51 (2003).

159 Wakatsuki, S., Saitoh, F. & Araki, T. ZNRF1 promotes Wallerian degeneration by degrading AKT to induce GSK3B-dependent CRMP2 phosphorylation. *Nat Cell Biol* **13**, 1415-1423, doi:10.1038/ncb2373 (2011).

160 Zhang, Z. *et al.* Calpain-mediated collapsin response mediator protein-1, -2, and -4 proteolysis after neurotoxic and traumatic brain injury. *J Neurotrauma* **24**, 460-472, doi:10.1089/neu.2006.0078 (2007).

161 Johnstone, V. P. & Hool, L. C. Glutathionylation of the L-type Ca2+ channel in oxidative stress-induced pathology of the heart. *Int J Mol Sci* **15**, 19203-19225, doi:10.3390/ijms151019203 (2014).

162 Zamponi, G. W., Striessnig, J., Koschak, A. & Dolphin, A. C. The Physiology, Pathology, and Pharmacology of Voltage-Gated Calcium Channels and Their Future Therapeutic Potential. *Pharmacol Rev* **67**, 821-870, doi:10.1124/pr.114.009654 (2015).

163 Koivisto, A. *et al.* TRPA1: a transducer and amplifier of pain and inflammation. *Basic Clin Pharmacol Toxicol* **114**, 50-55, doi:10.1111/bcpt.12138 (2014).

164 Nocchi, L., Daly, D. M., Chapple, C. & Grundy, D. Induction of oxidative stress causes functional alterations in mouse urothelium via a TRPM8-mediated mechanism: implications for aging. *Aging Cell* **13**, 540-550, doi:10.1111/acel.12208 (2014).

165 Takashima, Y., Ma, L. & McKemy, D. D. The development of peripheral cold neural circuits based on TRPM8 expression. *Neuroscience* **169**, 828-842, doi:10.1016/j.neuroscience.2010.05.039 (2010).

166 Liu, B. Y. *et al.* Role of TRPA1 and TRPV1 in the ROS-dependent sensory irritation of superior laryngeal capsaicin-sensitive afferents by cigarette smoke in anesthetized rats. *Pulm Pharmacol Ther* **26**, 364-372, doi:10.1016/j.pupt.2013.01.010 (2013).

167 Westlund, K. N., Kochukov, M. Y., Lu, Y. & McNearney, T. A. Impact of central and peripheral TRPV1 and ROS levels on proinflammatory mediators and nociceptive behavior. *Mol Pain* **6**, 46, doi:10.1186/1744-8069-6-46 (2010).

168 Nishihara, E., Hiyama, T. Y. & Noda, M. Osmosensitivity of transient receptor potential vanilloid 1 is synergistically enhanced by distinct activating stimuli such as temperature and protons. *PLoS One* **6**, e22246, doi:10.1371/journal.pone.0022246 (2011).

169 Wilkinson, J. A., Scragg, J. L., Boyle, J. P., Nilius, B. & Peers, C. H2O 2-stimulated Ca2+ influx via TRPM2 is not the sole determinant of subsequent cell death. *Pflugers Arch* **455**, 1141-1151, doi:10.1007/s00424-007-0384-2 (2008).

170 Murata, H. *et al.* JNK-mediated phosphorylation of SARM1 regulates NAD(+) cleavage activity to inhibit mitochondrial respiration. *J Biol Chem*, doi:10.1074/jbc.RA118.004578 (2018).

171 Corral, M. J. *et al.* Allicin Induces Calcium and Mitochondrial Dysregulation Causing Necrotic Death in Leishmania. *PLoS Negl Trop Dis* **10**, e0004525, doi:10.1371/journal.pntd.0004525 (2016).

172 Rabinkov, A. *et al.* The mode of action of allicin: trapping of radicals and interaction with thiol containing proteins. *Biochim Biophys Acta* **1379**, 233-244 (1998).

173 Simon, D. J. *et al.* Axon Degeneration Gated by Retrograde Activation of Somatic Pro-apoptotic Signaling. *Cell* **164**, 1031-1045, doi:10.1016/j.cell.2016.01.032 (2016).

174 Geden, M. J. & Deshmukh, M. Axon degeneration: context defines distinct pathways. *Curr Opin Neurobiol* **39**, 108-115, doi:10.1016/j.conb.2016.05.002 (2016).

175 Deckwerth, T. L. *et al.* BAX is required for neuronal death after trophic factor deprivation and during development. *Neuron* **17**, 401-411 (1996).

176 Whitmore, A. V., Lindsten, T., Raff, M. C. & Thompson, C. B. in *Cell Death Differ* Vol. 10 260-261 (2003).

177 Wright, K. M., Vaughn, A. E. & Deshmukh, M. Apoptosome dependent caspase-3 activation pathway is non-redundant and necessary for apoptosis in sympathetic neurons. *Cell Death Differ* **14**, 625-633, doi:10.1038/sj.cdd.4402024 (2007).

178 Simon, D. J. *et al.* A caspase cascade regulating developmental axon degeneration. *J Neurosci* **32**, 17540-17553, doi:10.1523/jneurosci.3012-12.2012 (2012).

179 Owen, D. E. & Egerton, J. Culture of dissociated sensory neurons from dorsal root ganglia of postnatal and adult rats. *Methods Mol Biol* **846**, 179-187, doi:10.1007/978-1-61779-536-7_16 (2012).

180 Burkey, T. H., Hingtgen, C. M. & Vasko, M. R. Isolation and culture of sensory neurons from the dorsal-root ganglia of embryonic or adult rats. *Methods Mol Med* **99**, 189-202, doi:10.1385/1-59259-770-x:189 (2004).

181 Vogelbaum, M. A., Tong, J. X. & Rich, K. M. Developmental regulation of apoptosis in dorsal root ganglion neurons. *J Neurosci* **18**, 8928-8935 (1998).

182 Gaudet, A. D., Popovich, P. G. & Ramer, M. S. Wallerian degeneration: gaining perspective on inflammatory events after peripheral nerve injury. *J Neuroinflammation* **8**, 110, doi:10.1186/1742-2094-8-110 (2011).

183 Chen, P., Piao, X. & Bonaldo, P. Role of macrophages in Wallerian degeneration and axonal regeneration after peripheral nerve injury. *Acta Neuropathol* **130**, 605-618, doi:10.1007/s00401-015-1482-4 (2015).

184 Gee, K. R. *et al.* Chemical and physiological characterization of fluo-4 Ca(2+)-indicator dyes. *Cell Calcium* **27**, 97-106, doi:10.1054/ceca.1999.0095 (2000).

185 Berridge, M. J. Inositol trisphosphate and calcium signalling. *Nature* **361**, 315-325, doi:10.1038/361315a0 (1993).

186 Rossi, F. *et al.* NAD-biosynthetic enzyme NMNAT1 reduces early behavioral impairment in the htau mouse model of tauopathy. *Behav Brain Res* **339**, 140-152, doi:10.1016/j.bbr.2017.11.030 (2018).

187 Ali, Y. O., Ruan, K. & Zhai, R. G. NMNAT suppresses tau-induced neurodegeneration by promoting clearance of hyperphosphorylated tau oligomers in a Drosophila model of tauopathy. *Hum Mol Genet* **21**, 237-250, doi:10.1093/hmg/ddr449 (2012).

188 Gunthorpe, M. J. & Szallasi, A. Peripheral TRPV1 receptors as targets for drug development: new molecules and mechanisms. *Curr Pharm Des* **14**, 32-41 (2008).

Appendices

Appendix A: Axon degeneration results showing all data bins

Experiments that employed Axoquant 2.0 calculated axon density in bins from 0 – 4000 μm from soma however axons very near the soma (0 – 500 μm) had an extremely high density and a large degree of overlap. Any significant loss of axonal abundance in this region resulted in less axon overlap but not noticeably alter the density readout of Axoquant 2.0. Axons that were a large distance from soma (2500 – 4000 μm) few and far between. This created a large variability from sample to sample since a small increase or decrease in axons could result in large deviations from the mean. This result underreported the effect size of any treatments or manipulations. Statistical analysis was still performed on the entire axon density curve however, to display a more accurate representation of effect sizes for presentations purposes, only 500 – 2500 μm from soma were included in the results section. All data, including the complete set of bins, are presented below.

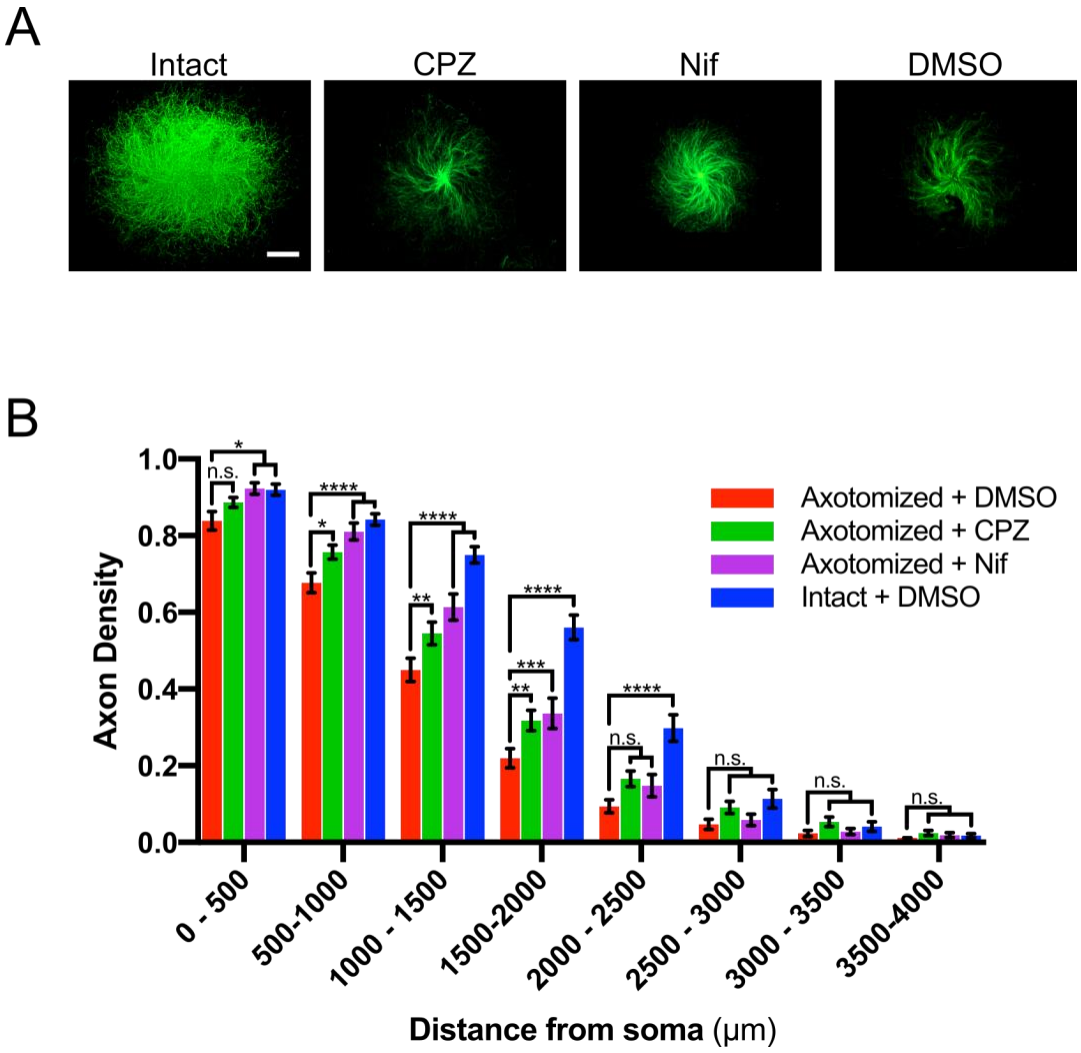

Figure A.1. Pharmacological inhibition of TRPV1 and L-type channels reduces axotomy-induced degeneration. Images (A) and complete bins (0 – 4000 µm from soma) shown in Figure 3.3 (See Results).

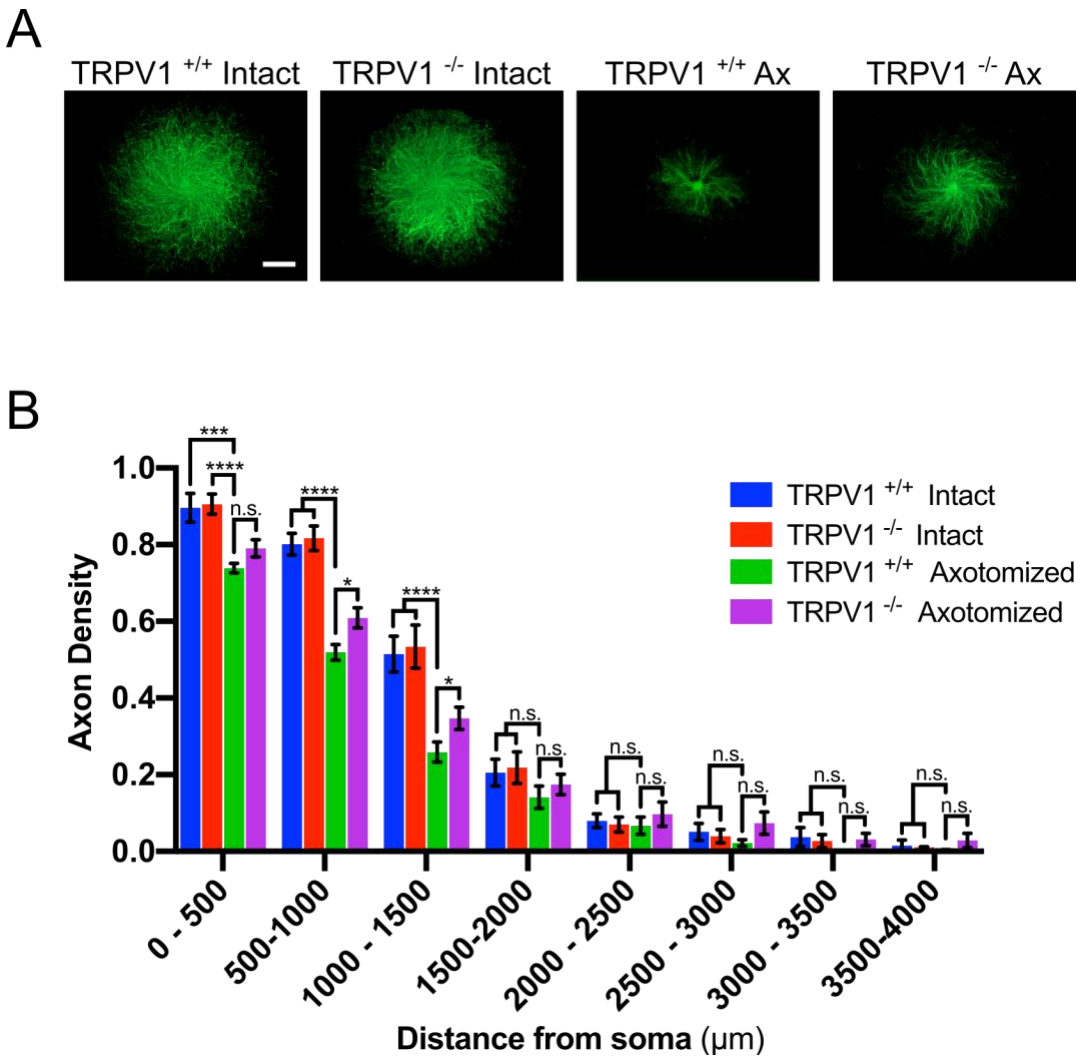

Figure A.2. *Trpv1* knockout reduces axotomy-induced degeneration. Images (A) and complete bins (0 – 4000 µm from soma) shown in Figure 3.5 (See Results).

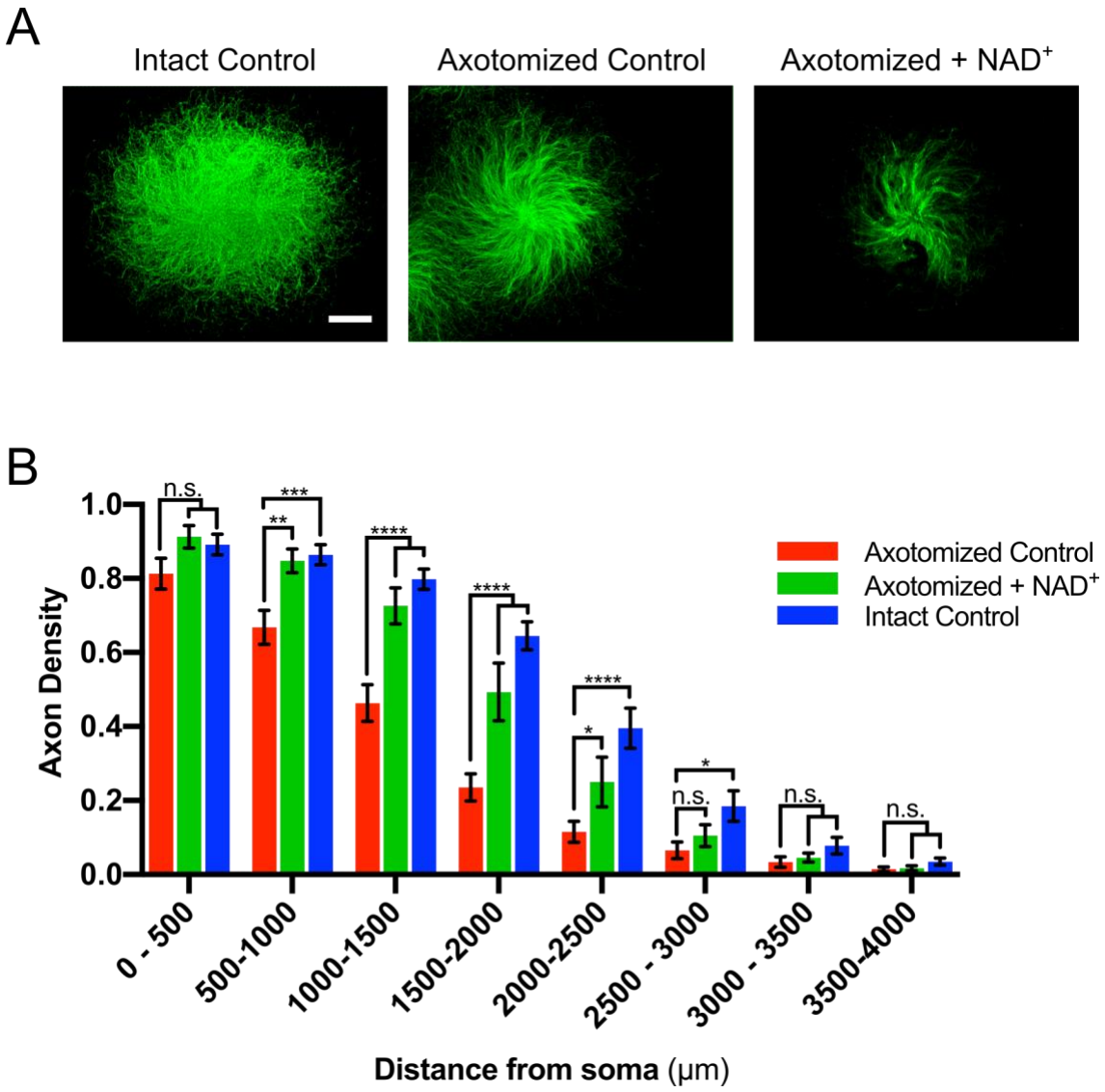

Figure A.3. NAD$^+$ supplementation reduces axotomy-induced axonal degeneration. Images (A) and complete bins (0 – 4000 μm from soma) shown in Figure 3.8 (See Results).

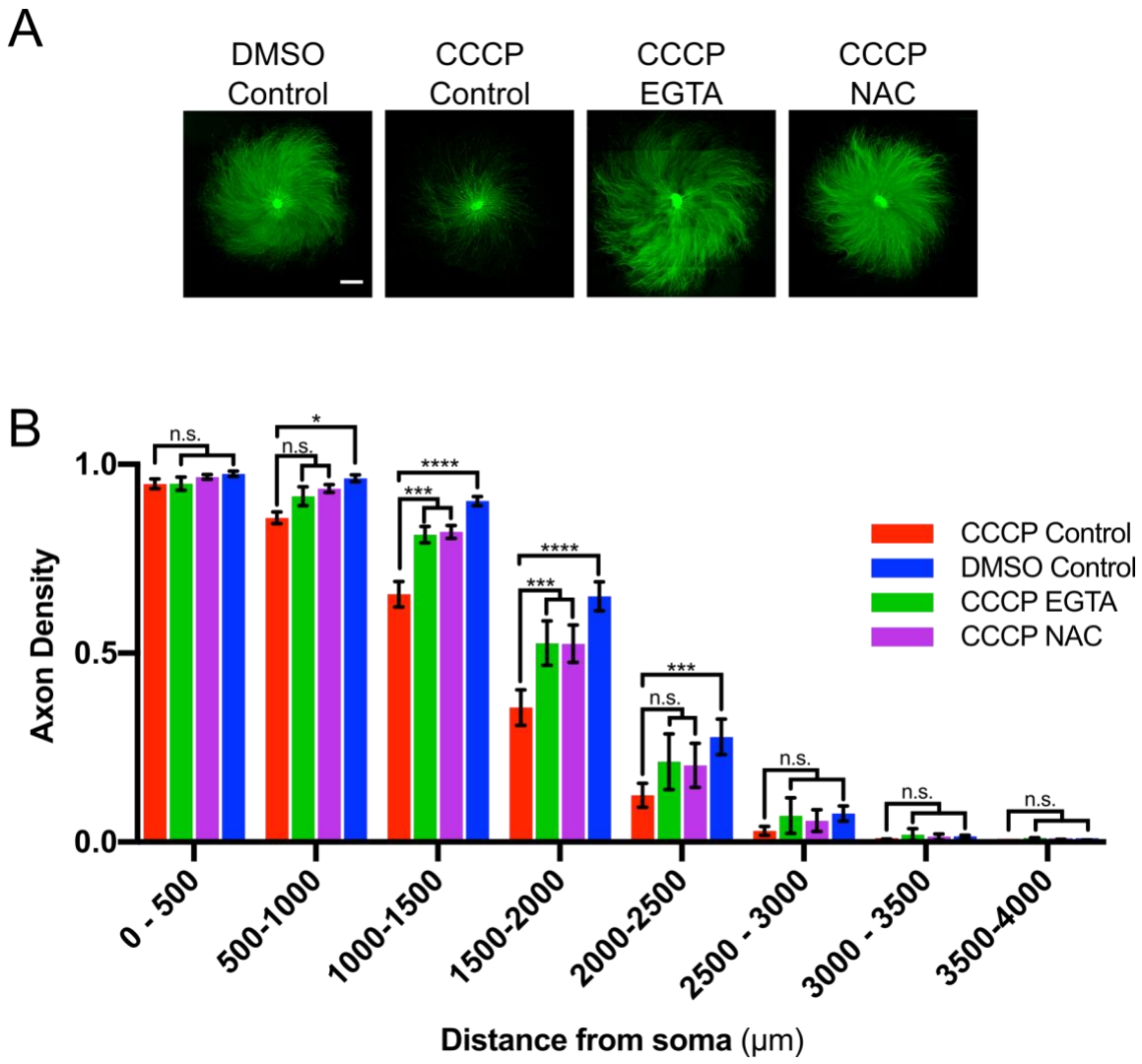

Figure A.4. CCCP causes axonal cytoskeleton fragmentation and degeneration that is ROS- and calcium-dependent. Images (A) and complete bins (0 – 4000 μm from soma) shown in Figure 3.11 (See Results).

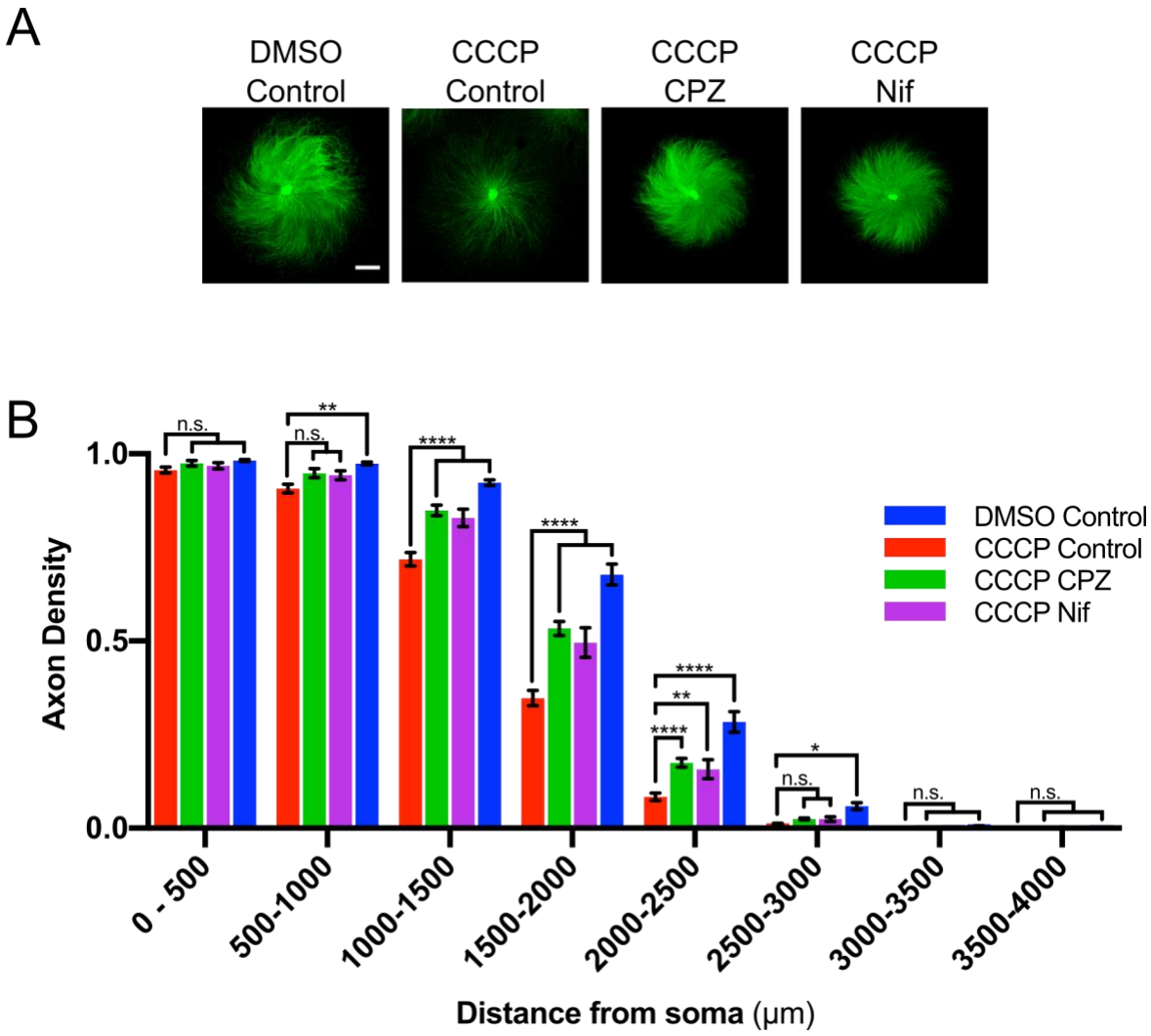

Figure A.5. Axon degeneration from mitochondrial dysfunction is reduced by inhibition of TRPV1 and L-type channels. Images (A) and complete bins (0 – 4000 μm from soma) shown in Figure 3.12 (See Results).